

The Journal of Refractory Innovations

bulletin

—
2023

18 Energy Savings and Additional Benefits of Inert Gas Stirring

33 Technical Challenges for Refractory Recycling

74 Reaction Textures in $\text{Al}_2\text{O}_3\text{-SiO}_2$ Bricks



RHI MAGNESITA



Bulletin

The Journal of Refractory Innovations

2023

Published by
Chief Editor
Executive Editors

RHI Magnesita GmbH, Vienna, Austria
Thomas Prietl

Thomas Drnek, Christoph Eglsäer, Alexander Leitner, Thomas Mathew, Gustavo Morello Maschio, Ravikumar Periyasamy, Stefan Postrach, Marcelo Dos Santos, Peter Steinkellner, Karl-Michael Zettl

Raw Materials Expert
Technical Proofreader
Lingual Proofreaders
Project Manager
Design and Typesetting

David Wappel
Clare McFarlane
Clare McFarlane, Terri Gattringer-Sabino
Michaela Hall
Universal Druckerei GmbH, Leoben, Austria

Contact

Michaela Hall
RHI Magnesita GmbH, Technology Center
Magnesitstrasse 2
8700 Leoben, Austria

E-mail

bulletin@rhimagnesita.com

Phone

+43 50213 5300

Website

rhimagnesita.com

LinkedIn

<https://www.linkedin.com/company/rhi-magnesita>

The products, processes, technologies, or tradenames in the Bulletin may be the subject of intellectual property rights held by RHI Magnesita N.V., its affiliates, or other companies.

The texts, photographs and graphic design contained in this publication are protected by copyright. Unless indicated otherwise, the related rights of use, especially the rights of reproduction, dissemination, provision and editing, are held exclusively by RHI Magnesita N.V. Usage of this publication shall only be permitted for personal information purposes. Any type of use going beyond that, especially reproduction, editing, other usage or commercial use is subject to explicit prior written approval by RHI Magnesita N.V.

Cover picture: The image depicts a tundish that plays a pivotal role in the steel continuous casting process, serving as a crucial intermediate vessel between the ladle and the mould. Its primary function is to ensure a smooth and controlled flow of molten metal into the mould, preventing turbulence and minimising impurities in the cast product. Constructed from an outer steel shell and lined with refractory materials to withstand extreme temperatures, the tundish also incorporates features such as an impact pot, as well as dams and weirs to regulate the metal flow.

RHI Magnesita Worldwide news

Europe

ANKRAL LC Series Shines Bright in Trial

RHI Magnesita's unwavering commitment to sustainability in the cement and lime industry is evident, with the aim to achieve a zero-waste product life cycle, preserve natural resources, and reduce carbon emissions. With the ANKRAL LC series, a product line has been introduced that aligns perfectly with these ambitions by incorporating recycled materials without compromising performance.

The latest addition to this portfolio is ANKRAL RS-LC, setting a new standard with the lowest carbon footprint compared to similar products, thanks to an unmatched recycling rate of 40%. In March 2023, a significant milestone was reached with its first installation at Vassiliko Cement in Cyprus, specifically in the upper transition and security zone of a modern precalciner kiln. This kiln, producing around 6200 tonnes of clinker daily with an average alternative fuel rate of approximately 65%, operates in difficult conditions typical of today's cement industry. After six months in operation, the inspection revealed ANKRAL RS-LC to be in remarkable condition, displaying only minimal signs of wear in the key lining area. These initial results underscore that sustainable refractories can seamlessly maintain product quality even in the face of modern manufacturing challenges. These exceptional results have already sparked significant interest from other cement producers, leading to a surge in new orders, and demonstrate how RHI Magnesita is at the forefront of reshaping the industry one successful innovation at a time.

Europe

MIRECO Celebrates One Year of Success

It's been an extraordinary year for MIRECO since the company's launch in November 2022 and the pioneering spirit that accompanies this joint venture has seen remarkable results. As part of celebrating this anniversary, the MIRECO team is not only reminiscing but also setting new goals for a sustainable future. In just one year MIRECO has made remarkable strides in recycling, such as achieving the target to recycle 160000 tonnes in 2023. Another milestone that has been reached is MIRECO can now include a full disclosure of its products' CO₂ footprint. This transparency forms a solid basis for sustainable decisions and developments, providing a valuable database for customers to make informed choices. MIRECO understands that in a world where sustainability is paramount, having access to such information is crucial. These achievements are also fuelling the ambitions for 2024 and with even greater enthusiasm the team is gearing up to reach new heights by aiming to recycle 200000 tonnes. This is not just a number, it's a promise to continue revolutionising recycling, sustainability, and positive environmental impact.

Worldwide

Pioneering Spinosphere Technology in the Lime Industry

With a steadfast commitment to quality, innovation, and environmental responsibility, RHI Magnesita explores new frontiers to develop refractory solutions that meet the rigorous demands of various industries. The introduction of RUBINAL VTX to the lime industry marks a significant milestone on this journey. RUBINAL VTX represents the debut of Spinosphere technology in the lime sector, following the successful implementation of the ANKRAL X series in the cement industry. Spinosphere technology is a groundbreaking approach that provides magnesia bricks with the essential microstructural flexibility while preserving excellent thermal properties. It achieves this by replacing conventional spinel grains with MgO grains surrounded by solid, spherical spinels. This innovation enables RUBINAL VTX to excel in all lining areas of lime shaft kilns subject to the harshest thermal and chemical conditions. Whether it's supporting arches or vault constructions, RUBINAL VTX not only promises exceptional performance but also contributes to a lower carbon footprint. With the first orders at hand, RHI Magnesita is seeing a strong industry interest in this remarkable solution.

China

RHI Magnesita Delivers a Presentation on CO₂ in the Refractory Industry at a Major Chinese Symposium

On October 15, RHI Magnesita's Global Head of Environment & Energy, Thomas Drnek, gave a keynote presentation on the topic "RHIM – CO₂ in the Refractory Industry" to 500 experts, academics, and entrepreneurs at one of China's top industry events, the "Annual Symposium on Refractories". Hosted by the refractories branch of the Chinese Ceramic Society and Wuhan University of Science and Technology, this year's theme was "Innovation, Leading, Green Development". The symposium focused mainly on China's "30-60" goal: Targeting to peak CO₂ emissions by 2030 and to achieve carbon neutrality by 2060. Joint discussions were also held on the topic of a green and innovative development path under the new national policy of "carbon peak and carbon neutral", aimed to promote the green, low-carbon, and high-quality development of the refractory industry.

One of just five specially invited guests, Dr Drnek introduced RHI Magnesita's 2025 sustainability targets, CO₂ report, and CO₂ reduction outcome, as well as the product carbon footprint, verified methodology for its calculation, and the future outlook. Additional plenary sessions focused on trends in material science and life cycle. A full 110 academic reports on the development frontiers of refractory materials and their related disciplines drove much of the symposium's content and discussions.

"It was a great honour and opportunity to be invited to present at the Annual Symposium on Refractories in Wuhan," said Thomas Drnek. "I personally believe this event has expanded the depth of academic exchange on the sustainability topic and will play a pivotal role in promoting the healthy development, transformation, and upgrading of the refractory materials industry."

Germany

The Female Force of the Refractory Industry

Women in research, science, and the refractory industry are thriving and on the rise. At RHI Magnesita the share of senior leadership positions held by females is 19%. With the "Women@Refractories" event at UNITECR 2023, which took place in September 2023 in Frankfurt (Germany), RHI Magnesita co-created a unique networking and exchange platform with participants

of all genders. Following a highly inspiring keynote speech by entrepreneur and investor Lea-Sophie Cramer, a panel was hosted by four female leaders from RHI Magnesita. Together with Lea-Sophie Cramer, Anja Moser-Tscharf (Managing Director of RHI Magnesita MIRECO Mitterdorf GmbH), Daniela Gavagnin (Head of Pioneer Research), Romy-Sophie Katz (Managing Director of RHI Magnesita Sensors and Technology Development), and Neha Jain (Head of Global Quality Management) clearly demonstrated that diversity is more than just a relevant business case. The panellists shared with the international audience of all genders about their different career paths and highlights, but above all the challenges and experiences as a minority in the refractory industry.

South America

Sustainable Recognition Program Promotes Recycling Initiatives in South America

As part of a regional "Sustainable Recognition Program", the top ten partner industries that provided used refractory materials for RHI Magnesita's recycling initiatives in South America were awarded a commemorative plaque. These included companies operating in the steel, cement and lime, as well as nonferrous markets. This recognition is part of RHI Magnesita's actions to promote sustainability and reduce CO₂ emissions in the supply chain, because approximately 2 tonnes of CO₂ emissions can be saved for every tonne of refractory material recycled.

Throughout 2022, RHI Magnesita collected over 40000 tonnes of used refractory products in Brazil, further strengthening the circular business model. The reclaimed material is then processed using various methods including sorting, cleaning, stabilisation, crushing, and sieving to maximise the amount of material that can be reused in new products (see page 33). Ongoing R&D activities ensure these processing technologies are constantly being improved and that the performance of refractories containing recycled material is not compromised. Currently, over 10% of South American production is derived from the company's recycling efforts, which not only reduces CO₂ emissions but also decreases landfilling.

China

Acquisition of Jinan New Emei Completed

RHI Magnesita has successfully finalised its acquisition of a majority shareholding in Jinan New Emei (China). This acquisition boosts RHI Magnesita's position in the Chinese market, diversifying its product range and expanding its customer base. RHI Magnesita now holds 65% of Jinan New Emei's shares, effective May 1, 2023. A dedicated integration team, "Taishan", has been established to ensure a smooth merger while maintaining business continuity.

This acquisition brings a state-of-the-art, highly automated plant in Laiwu (Jinan, Shandong province) into RHI Magnesita's global network, providing additional production capacities for regional customers. The integration aims to further enhance customer service and elevate the local-to-local strategy. The gradual integration of Jinan New Emei started with a celebratory event attended by colleagues, customers, suppliers, and local government representatives. RHI Magnesita expects this partnership to deliver substantial value for its customers and the company itself, reinforcing its commitment to innovation and growth in the refractory industry.

Europe

RHI Magnesita Celebrates the Acquisition of P-D Refractories, Boosting Its Position in the Process Industries

In celebrations across all acquired plants in Germany and the Czech Republic, the team of P-D Refractories was officially welcomed to the global team of RHI Magnesita. The acquisition of P-D Refractories adds to RHI Magnesita's capabilities in alumina-based refractories and strengthens its position in the process industries, particularly the glass and aluminium sectors. To commemorate this milestone and integrate P-D Refractories into the global network, official celebrations were held simultaneously at four P-D Refractories sites.

P-D Refractories is well-known for producing high-quality nonbasic bricks for various industries. The acquisition offers significant opportunities for growth and strengthening market presence, enabling RHI Magnesita to provide high-grade refractory products and solutions to an expanded customer base. This strategic move represents a significant step forward for RHI Magnesita and promises a brighter future for global process industries with improved capabilities and expertise.

Austria

Low-Cost Intelligent Rock Bolts for Mining Applications

At the 15th International ISRM Congress 2023 and 72nd Geomechanics Colloquium in Salzburg (Austria), Mislav Mikulec (RHI Magnesita's Geology & Mining Technology Department) and Wolfgang Dolsak (DSI Underground) held a presentation about digitalisation and automation in mining, titled "Development and Implementation of a Sensor-Supported Rock Bolt System for Underground Monitoring".

Alongside digitalisation in underground mining and tunnel construction, user-friendly data acquisition and processing is of paramount importance, considering the particularities of the working environment. Various conventional data measurement systems are currently in use for different applications; however, their scope is somehow isolated and not applied for large-scale monitoring of default ground support systems such as rock bolts. For underground applications, system sourcing and installation of special monitoring bolts is cost intensive and impracticable for a large-scale application. Therefore, a low-cost intelligent rock bolt assembly concept was developed during the EU-funded illuMINEation project, part of the Horizon 2020 research and innovation programme. The majority of tests were conducted in RHI Magnesita's Breitenau underground mine (Austria) which was one of the main use case partners in this project. This low-cost intelligent rock bolt assembly enables an easy application with already installed rock bolts or in combination with rock bolts featuring an integrated tendon sensor. The principal idea is to provide real-time recordings and visualisation of geotechnical and environmental measurands on a large-scale collective basis. Partnering in such innovative projects demonstrates the strong commitment of RHI Magnesita to drive innovation, digitalisation, and sustainable operations not only in the refractory sector but also in the mining industry.

Europe

ReSoURCE Project Updates Available on Different Platforms

In the Refractory Sorting Using Revolutionizing Classification Equipment (ReSoURCE) project, RHI Magnesita's scientists and partners are developing a new state-of-the-art process chain for refractory recycling, with artificial intelligence-supported multisensor sorting equipment as its core technology. This technically advanced sustainability project, which is led by RHI Magnesita, received €6 million from the European Union (EU) within the Horizon Europe programme (grant agreement number 101058310).

To maximise the impact of funding, the European Commission requests that the research area and results are communicated on a regular basis, for example to the scientific community, process industries, and broader public. Therefore, complementary platforms are being used to regularly disseminate the knowledge, including a website (<https://www.project-resource.eu/>), science blog (<https://www.project-resource.eu/blog/>), YouTube channel (https://www.youtube.com/channel/UCUP7_n9N4JHpq09uHu3e97Q), LinkedIn (<https://www.linkedin.com/company/82318877>), X-account (<https://twitter.com/2022ReSoURCE>), and scientific conferences.

These communication channels not only provide general background information about the scientific disciplines involved in ReSoURCE, but there is also the latest news about specific research areas. To provide this level of transparency, the project is employing the most up-to-date approaches in the field of scientific communication. By reporting the ongoing research openly, RHI Magnesita and its partners can keep customers and interested parties informed about current activities as well as contribute to a better understanding of science and scientific processes in general. Furthermore, it is an excellent opportunity to showcase the expertise of different talented scientists and the highly experienced consortium members.

The globally leading academic and industrial partners that have joined forces with RHI Magnesita and the EU to innovate recycling in the refractory industry are LSA – Laser Analytical Systems & Automation GmbH (<http://www.lsa-systems.de/en/>), InnoLas Laser GmbH (<https://www.innolas-laser.com/>), Norsk Elektro Optikk AS (<https://neo.no/home>), Fraunhofer ILT Institute for Laser Technology (<https://www.ilt.fraunhofer.de/en.html>), Montanuniversität Leoben (<https://www.unileoben.ac.at/>), SINTEF AS (<https://www.sintef.no/en/>), CPI Centre for Process Innovation Ltd (<https://www.uk-cpi.com/>), and Crowdhelix Ltd (<https://crowdhelix.com>).



A letter from our editor



Welcome to another exciting edition of our esteemed Bulletin journal, dedicated to the remarkable world of refractories. In the realm of materials science, refractories play a pivotal role in enabling our modern way of life, from the production of steel for our skyscrapers to the glass in our windows. These exceptional materials endure extreme temperatures and harsh environments, safeguarding vital industrial processes and technological advancements. Refractories, the unsung heroes of high-temperature industries, have held a prominent position in the annals of materials science and stand as a testament to boundless human ingenuity, enabling us to tame fire and harness its immense power for a myriad of applications. In this issue, we once again embark on a journey that highlights some of RHI Magnesita's technological achievements.

The modern world owes much of its progress to refractories, and this edition takes an in-depth look at various industries where these materials are indispensable. Steelmaking, cement production, glass manufacturing, and the petrochemical industry all depend on refractories for their relentless resistance to extreme heat and chemical attack. As we venture further into some of these domains, we will delve into the challenges facing refractory experts, the innovations that are revolutionising these industries, and the crucial role refractories play in the sustainability and environmental efforts of our time.

A significant focus of this edition is the cutting-edge research and development in refractory materials, systems, and solutions, such as inert gas stirring for the new electric arc furnaces with large melt volumes that are expected to meet the required steel production capacity at minimum CO₂ intensity during the green steel transformation period, lining wear measurements, and numerous developments to ensure sustainability in many fields of refractory applications. The refractory industry is part of the most CO₂-intensive value chains in the global economy and increasingly final customers are requesting the decarbonisation of these value chains. Therefore, final producers must report not only their direct CO₂ emissions but all CO₂ emissions inherent to their product. A product carbon footprint (PCF) provides greenhouse gas information of a product from cradle-to-gate and is an important input for customer industries to declare their products' carbon footprint accurately. RHI Magnesita is the first refractory producer to implement a PCF on the technical data sheets of nearly all its products.

Scientists and engineers are pushing the boundaries of refractory performance. New materials, such as high-performance ceramics and refractory composites, are emerging to meet the ever-increasing demands of high-temperature processes. INTERSTOP automation, robotics, and digitalisation solutions are setting standards in flow control and new products are being introduced in the steel industry. In this edition we invite you to explore our research activities that promise to redefine the capabilities and lifespan of refractories, enabling more efficient industrial processes.

Environmental sustainability is at the forefront of scientific endeavors worldwide and in this edition we address the importance of refractories in reducing energy consumption and emissions. By delving into the eco-friendly innovations and circular economy principles applied to refractories, we hope to inspire our readers to join the ongoing efforts to safeguard our planet. In conclusion, our exploration of refractories is a testament to the intersection of science, engineering, and industry. Furthermore, the durability and resilience of refractories continue to challenge the frontiers of materials science, ensuring a sustainable and innovative future for generations to come. Thank you for joining us on this journey.

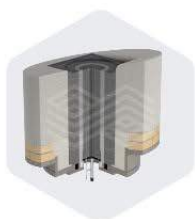
Yours sincerely

Thomas Prietl

Head of Global R&D and Innovation
RHI Magnesita

“Steelmaking, cement production, glass manufacturing, and the petrochemical industry all depend on refractories for their relentless resistance to extreme heat and chemical attack. As we venture further into some of these domains, we will delve into the challenges facing refractory experts, the innovations that are revolutionising these industries, and the crucial role refractories play in the sustainability and environmental efforts of our time.”

Contents



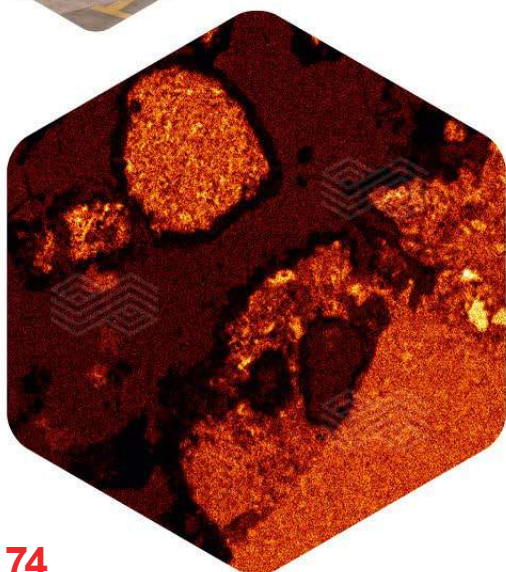
18

Energy Savings and Additional Benefits of Inert Gas Stirring



33

Technical Challenges for Refractory Recycling



74

Reaction Textures in Al₂O₃-SiO₂ Bricks

- 10 Electric Melting Furnaces for Green Steel Transformation of Integrated Steel Plants—Requirements, Challenges and Solutions from a Refractory Perspective**
- 18 Energy Savings and Additional Benefits of Inert Gas Stirring in Electric Arc Furnaces with a Focus on Green Steelmaking**
- 26 Sustainable Refractory Solutions—New Gunning Mixes Containing Circular Material**
- 33 Technical Challenges for Refractory Recycling and Innovative Processing Solutions**
- 39 Product Carbon Footprint of Refractory Products**
- 45 Sustainable Slag Engineering in the Basic Oxygen Furnace Using Circular Metallurgical Additives and Modelling Tools**
- 51 INTERSTOP Automation, Robotics and Digitalisation Solutions for Flow Control Technology**
- 57 Innovative Refractory Wear Measurement Method for Steel Ladles Using 3D Laser Scanning**
- 61 Innovative Spray Tundish Mix for Energy Savings and CO₂ Footprint Reduction**
- 66 Avoiding Asymmetric Flows Caused by Off-Centre Pouring into the Tundish: A Novel Impact Pot Design**
- 74 Reaction Textures in Al₂O₃-SiO₂ Bricks Induced by Gaseous SO_x Attack: New Insights From Mineralogy and Thermodynamic Modelling**
- 82 Trends and Advances in Blast Furnace Casthouse Technologies with a Focus on Refractory Lining Performance, Operational Safety and Decarbonisation**

Subscriptions Service and Contributions



We encourage you, our customers and interested readers, to relay your comments, feedback, and suggestions to improve the publication quality.

Email
bulletin@rhimaginesita.com

Phone
+43 50213 5300

Miriam Schnalzger, Alfred Spanring, Marcus Kirschen, Thomas Kollmann, Wagner Moulin-Silva, Johannes Wucher, Alexander Ratz, Taco Janssen and Julia Kirowitz

Electric Melting Furnaces for Green Steel Transformation of Integrated Steel Plants—Requirements, Challenges and Solutions from a Refractory Perspective

This article provides an overview of the roadmap, opportunities, and challenges of two promising process route alternatives for the green steel transformation of blast furnace–basic oxygen furnace (BF-BOF) plants. Since these integrated steel plants are characterised by CO₂ emissions nearly three times higher than mini mills—mainly driven by the blast furnace, sintering, and coking plant—this study reviews and benchmarks technology alternatives for BF-BOF plants from a refractory point of view. Additionally, examples and first research investigation results are discussed to highlight the readiness of RHI Magnesita for the green steel transformation.

Introduction

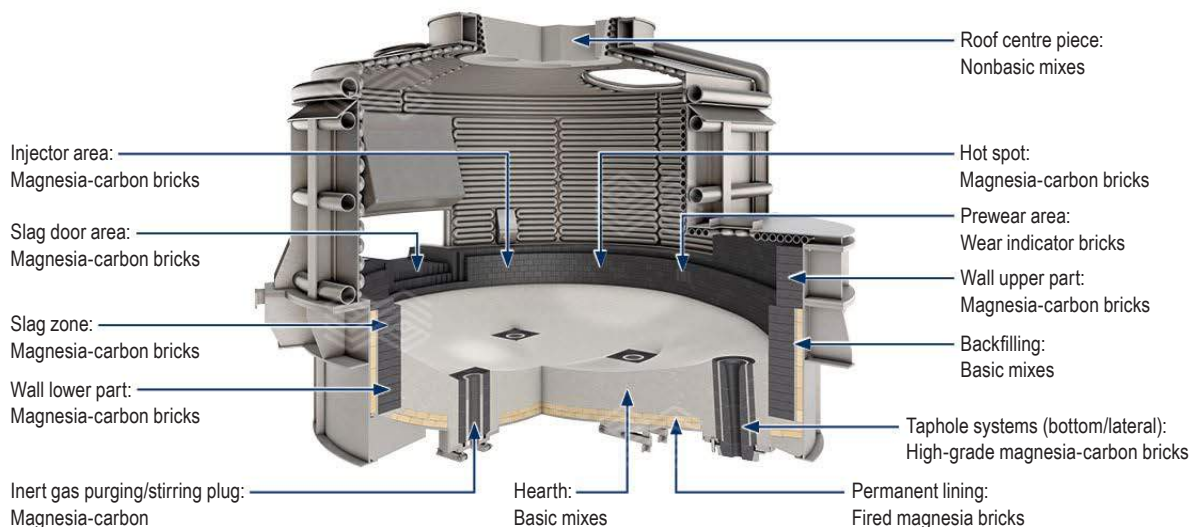
Today, the iron and steel industry is the second largest global industrial CO₂ emitter, mainly driven by blast furnace–basic oxygen furnace (BF-BOF) plants that represent 70% of worldwide steel production [1]. Consequently, BF-BOF plants are under increasing pressure to decarbonise their production facilities. Two main paths for process route alternatives are currently under evaluation: The first comprises a direct reduction (DR) unit, which is industrially proven with the current dominant use of natural gas and planned to be gradually shifted to hydrogen, combined with a continuous electric smelting furnace (ESF), followed by the basic oxygen furnace (BOF) process. The second approach is complete transformation to an electric arc furnace (EAF) plant based on direct reduced iron (DRI). However, both steelmaking technologies encounter their own challenges in terms of process and refractory solutions: The ESF technology is fully proven for the nonferrous industry, but for the steel industry a balanced refractory design and an appropriately sized unit is not yet available. In contrast, the

EAF is well-established for steelmaking, but for tapping weights exceeding 250 tonnes additional measures are required to improve process efficiency [2].

Scrap and Direct Reduced Iron Steelmaking Processes

As described above, there are two main approaches for raising the CO₂ abatement potential of steelmaking currently being discussed and evaluated: On the one hand, a DR unit combined with an ESF and continuing with the BOF process, and on the other hand, a complete transformation to an EAF mill mainly based on DRI. This section of the article discusses the differences between scrap-based and DRI-based steelmaking processes in EAF mills and addresses the impact of operating conditions on the EAF working lining. Figure 1 shows the typical refractory lining concept used for both DRI- and scrap-based EAFs [2].

Figure 1. Furnace areas and refractory products used in DRI- and scrap-charged EAFs [2].



Differences in Process Characteristics

There are several differences to be considered when comparing the production characteristics of a conventional scrap charged EAF to an EAF process based on high shares of DRI and/or hot briquetted iron (HBI). These divergences are mainly related to the electrical energy demand, chemical energy input, size of the hot heel, and metallurgical influences. Due to the remaining gangue oxides present in the DRI/HBI and varying levels of carbon, different power programs and adapted additions of lime, dolomitic lime, and doloma are required for the continuous charging of high amounts of DRI. The hot or cold DRI is charged via the fifth hole in the furnace roof. The remaining melt volume (i.e., hot heel) of a DRI-based EAF is up to 30% of the total melt volume to facilitate DRI melting. In contrast to conventional scrap-based furnaces, the DRI-EAF process operates under flat bath conditions. However, due to the absence of a scrap pile, power programs with a shorter arc length, which results in a lower arc voltage and slightly decreased efficiency of energy transfer to the steel melt, are defined. The oxide gangue present in the DRI not only decreases the metal yield of DRI charges, but also increases the risk of low slag basicity in the case of insufficient compensation of the acid gangue by flux additions. Furthermore, high levels of acid gangue content cause a significant increase in the specific amount and volume of process slags compared to the standard operation based on steel scrap, which also affects the lifetime of the refractory lining. Additionally, the electrical energy demand rises with a higher input of burned slag formers. As a result of these DRI-specific process conditions, the melting time as well as the tap-to-tap time of DRI heats can be significantly longer than for standard scrap heats [2].

Effects on the Refractory Lining Concept

Due to the above-mentioned differences, typically higher quality refractory grades and intensified maintenance, such as gunning and fettling, are applied to DRI-charged furnaces to counteract this higher strain on the refractory lining.

Figure 2 illustrates the main differences in the working lining design based on the typical magnesia-carbon brick grades in operation [2].

DRI-charged EAFs are mainly operated with high-performance grades in all furnace lining areas. Furthermore, furnace maintenance such as gunning and fettling is also usually carried out with high-grade materials. In comparison, scrap-based EAFs, both for furnace installation and for maintenance, are widely and successfully run with standard grades based on significant amounts of circular raw materials. This incorporation of circular raw materials leads to a considerable reduction in the CO₂ footprint of the individual refractory products and thereby contributes to decreased scope 3 greenhouse gas emissions at the steel plant [2].

Comparison of Specific Refractory Consumption

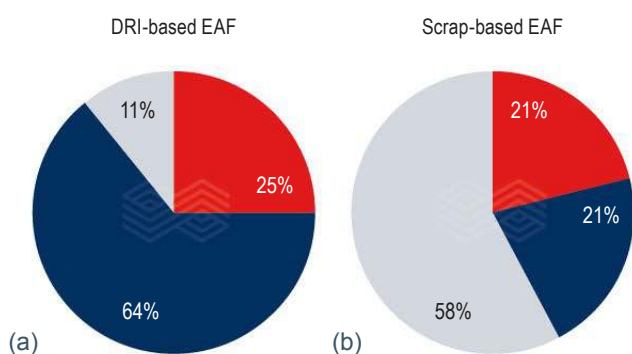
Specific refractory consumption figures (kg of refractories consumed per tonne of liquid steel produced) and EAF lifetimes of scrap-charged compared to DRI-charged EAFs can vary significantly. Typical lifetimes for EAFs are shown below, whereby the wide variation within the furnace types is a result of the maintenance philosophy adopted, which strongly influences the lifetime [2]:

- Scrap-based: 300–2000 heats.
- DRI-based: 300–700 heats.

Consequently, DRI-operated EAFs often show an overall higher consumption of refractory materials and therefore higher specific refractory consumption rates, particularly driven by maintenance mixes for gunning and fettling as well as the slag zone working lining. A comparison of the consumption figures of full-year averages for all relevant refractory products is shown in Figure 3 and Figure 4 [2]. Eccentric bottom taphole (EBT) filling mixes used to fill the taphole channel after each heat tapped are excluded from this comparison. EBT filling mix consumption ranges from 1–1.5 kg_{refractory}/t_{liquid steel} [2].

Figure 2.

MgO-C performance classes used in (a) DRI- and (b) scrap-charged EAFs [3].



- Top quality grades: Mainly based on highest quality fused magnesia (carbon/resin bonded)
- High level grades: Mainly based on fused and sintered magnesia (carbon/resin bonded)
- Standard level grades: Mainly based on fused or sintered magnesia and circular raw materials (carbon/resin bonded)

Figure 3.

Annual average specific refractory consumption figures for a scrap-charged 145-tonne EAF [4].

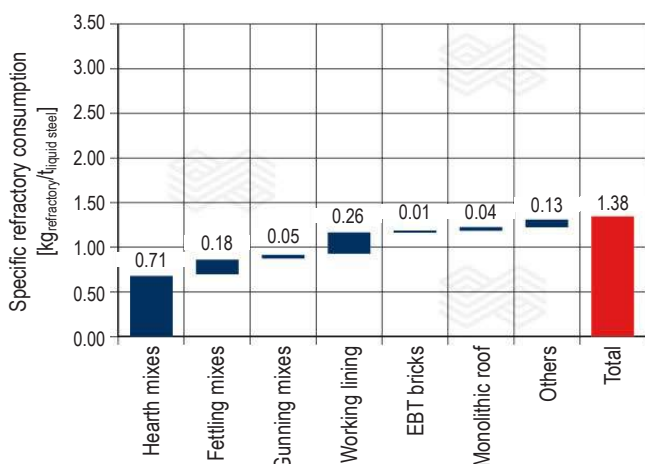
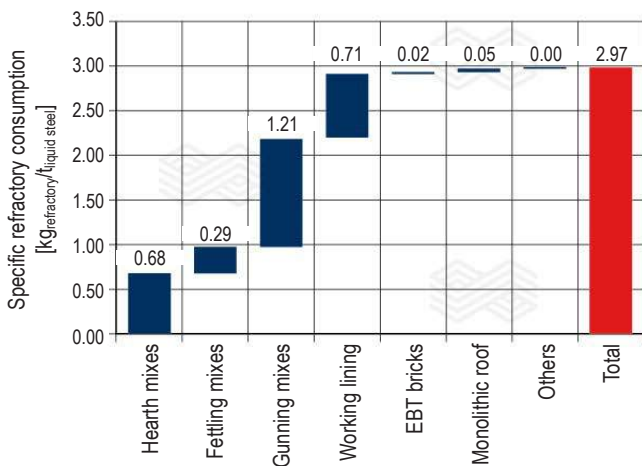


Figure 4.

Annual average specific refractory consumption figures for a DRI-charged 130-tonne EAF [4].

**Figure 5.**

Improved melt mixing by inert gas purging (RADEX DPP system) in an EAF [2].



Process Benefits of Inert Gas Purging

Modern EAF technology is based on shallow hearth designs and multiple supersonic oxygen injectors to address the inherent problem of low melt movement. With the decreasing oxygen demand of DRI charges, efficient melt mixing is even more difficult, especially in large volume EAFs that are currently being designed for integrated steel plants.

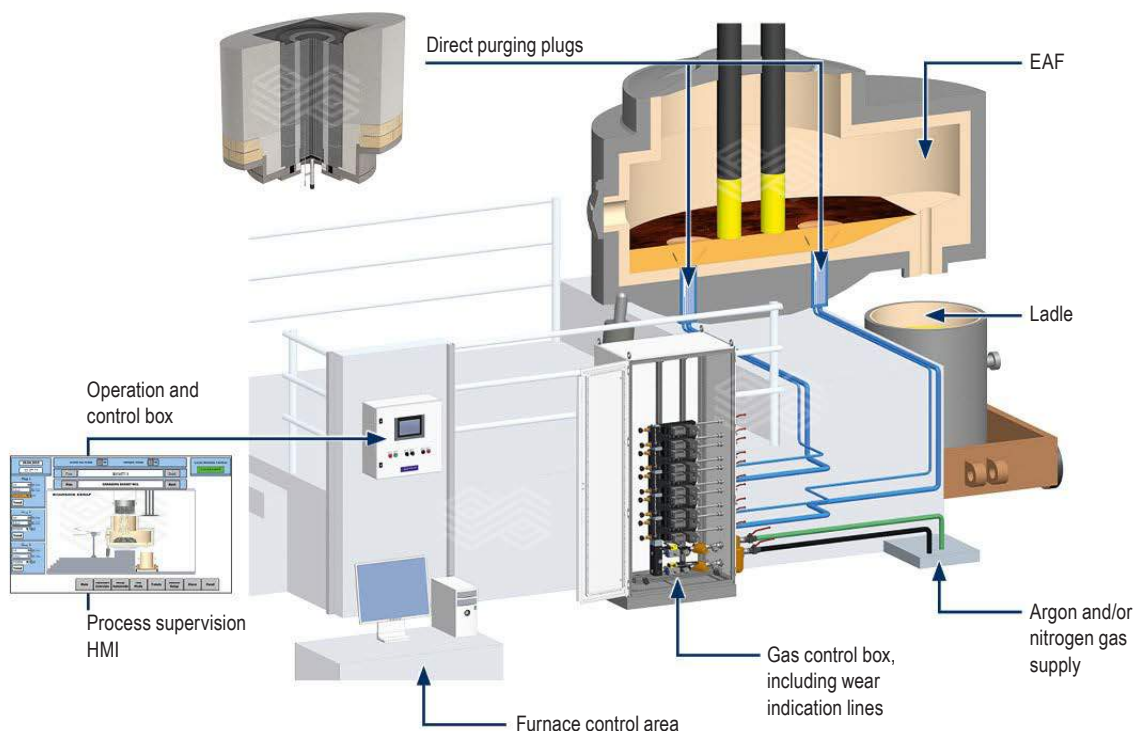
By far the most efficient movement of the entire steel melt is generated by inert gas purging (Figure 5). Developed by RHI Magnesita in the early 1980s, approximately 9% of EAFs worldwide are now equipped with gas purging systems, especially large EAFs with tapping weights above 150 tonnes and an additional 20–35% hot heel. Over the years, refractory solutions and the gas control units have been significantly improved to reach maximum safety and lifetime [2].

The gas control units from INTERSTOP are characterised by a leak-free, modular design, and minimum space requirements (Figure 6), providing very precise and fast gas flow control over a wide range of Ar and N₂ flow rates [5]. Automatic wear and leakage detection as well as customer-specified programs, data acquisition, and storage are state-of-the-art [2].

The process benefits of inert gas purging are directly related to the improved movement and mixing in the entire melt volume (see page 18). The temperature distribution is significantly more homogeneous, and decarburisation is improved, especially when charge combinations of steel scrap, DRI, or hot metal are applied. The most important process improvements for DRI charging are [5]:

Figure 6.

EAF gas purging system from INTERSTOP with a very compact design [2].



- Decreased melting time of DRI (and scrap).
- Decreased specific electrical energy demand.
- Decreased deviation between the measured steel temperature in the EAF and the ladle furnace, leading to better process control.
- Avoidance of skull formation or debris in the EAF hearth after tapping (i.e., “clean furnace”).
- Increased metal yield.
- Decreased share of over oxidised heats that leads to better process control, which is even more important for low-carbon DRI and carbon-free DRI produced in H₂-based DR units.
- Avoidance of slag slopping by retarded CO boiling in the steel melt at high or varying carbon content.

The corresponding CAPEX and OPEX of the gas purging system are easily exceeded by the process benefits, resulting in a return on investment after only a few EAF campaigns. A typical example of the observed process improvements for a 250-tonne EAF (200-tonne tapping weight), charged with more than 95% DRI, is given in Table I [2].

Alternative units for melting large volumes of DRI at low conversion costs in integrated steel plants are ESFs. They represent a well-established furnace technology in the nonferrous metallurgical industry and will now be adapted to the specific requirements of the steel industry to process low-grade DRI prior to charging it into the BOF [2].

Electric Smelting Furnaces

ESF technology is a well-known and long-established electric melting technology in the nonferrous metals industry. These melting units can be engineered using two different fundamental designs: The so-called six-in-line EAF, with its rectangular shell design, and the round ESF. Both are widely used today for melting and processing different ferroalloys such as FeNi and FeTiO₃, but also for platinum group metals (PGM), Ni, and Cu. To meet the requirements of these industry sectors and their respective processes, the scale of these ESFs is extremely large compared to state-of-the-art steel furnaces. The dimensions of a rectangular smelter typically reach 40 m in length, 15 m in width, and almost 9 m in height, while the round units can exceed 20 m in diameter and 6 m in height. However, from a refractory engineering point of view, there is a technical limit regarding the size to ensure uniform expansion during the highly demanding heat-up phase [2].

The basic question concerning the operation practice is whether the furnace will be operated in open or covered bath mode, as this makes a huge difference in terms of radiation and thermal impact on the upper sections of the furnace, especially on the roof lining. The roof lining is exposed to much higher thermal loads in combination with chemical impacts when operated in open bath mode, which must be taken into consideration when choosing the refractory material to avoid roof lining collapse and prevent the thermal application limit of the refractories being reached [2].

The general lining concepts (Figure 7) for such smelters are mainly based on high-fired, high-purity magnesia bricks in the case of ferroalloys or magnesia chrome bricks for PGM, Ni, and Cu applications, always considering the specified thermal profile of the hearth, mostly supported by bottom forced air-cooling technology. In the bath area, depending on the original equipment manufacturer (OEM) involved, different well-established cooling systems are applied. However, these different cooling systems require specific refractory solutions. That is why the given cooling design has always been the starting point for RHI Magnesita to provide the most suitable refractories in terms of both thermal as well as dimensional aspects, as this is also important to ensure safe furnace operation for the end user [2].

Depending on whether the operation mode is an open or covered bath, the refractory lining is based on either MgO or Al₂O₃. However, the type of alumina raw material used—bauxite, andalusite, or tabular alumina—is heavily influenced by the thermal impact in the respective area [2].

A further critical point is the hearth design, as this furnace region faces high lifting forces that can lead to an increased risk of floating bottom linings. Therefore, RHI Magnesita designs always consider a special and unique type of interlocking system to support the lining integrity in the hearth area. In addition, all planned furnace cooling technologies, the isotherm distribution of the refractory lining in the case of thermal expansion, as well as thermal profiles of multilayer designs considering OEM- and customer-relevant specifications are taken into account and investigated using finite element method tools during the engineering phase of the smelter refractory design [2].

In order to realise long-term stable operation of such a large furnace, the most important aspect, alongside the cooling technology, is thorough examination of the special

Table I.

Observed benefits of RADEX DPP gas purging in a 250-tonne DRI-EAF [2].

Parameter	Unit	Without gas purging (DPP)	With gas purging (DPP)	Benefit
Electrical energy	kWh/tonne	623	614	-9
Power-on time	Minute	109	108	-1.2
Temperature at ladle furnace <1560 °C	-	53%	35%	-18%
ppm oxygen <800 at tap	-	65%	67%	+2%

requirements of furnace areas that are exposed to the highest stresses. One of the most demanding areas is the interface between the bath, slag, and off-gas, as the very acidic slags combined with super-heated baths require a very tight refractory lining based on design and engineering. The detailed engineering of such linings always demands an in-depth view on the relevant expansion calculations [2].

Testing Refractory Materials for the Direct Reduced Iron Smelter

As the ESF technology is now being adapted to the steel industry, it is key to gain a deeper understanding about the chemical, thermal, and physical impact of this new steelmaking process on refractory materials. Therefore, different refractory grades, which are being considered for the slag zone area of the smelter, were tested at the Technology Center Leoben (Austria) to investigate their corrosion behaviour with a representative smelter slag. The planned smelter operation under a reducing atmosphere in combination with long settling times will ensure high yields and generate a low Fe- and FeO-content slag. Table II details the targeted smelter slag composition range, which is similar to today’s blast furnace slags and also suitable for the cement industry.

The corrosion test was performed in the high-frequency induction furnace (HF-ITO) illustrated in Figure 8, which was flushed with CO and CO₂ and filled with molten synthetic slag adjusted to the composition shown in Table II. During testing, the refractory specimens were submerged in the slag-filled crucible and rotated to evaluate not only chemical resistance, but also the hot erosion behaviour of the different grades.

Figure 8. High-frequency induction furnace for corrosion testing.

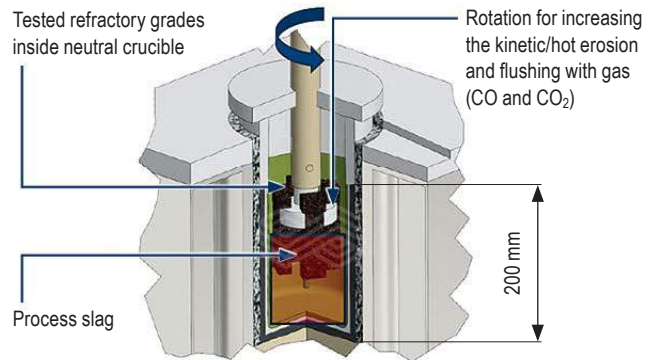


Figure 7. Well-established and proven lining concept used in rectangular ESFs for ferroalloy applications (e.g., FeNi) [2].

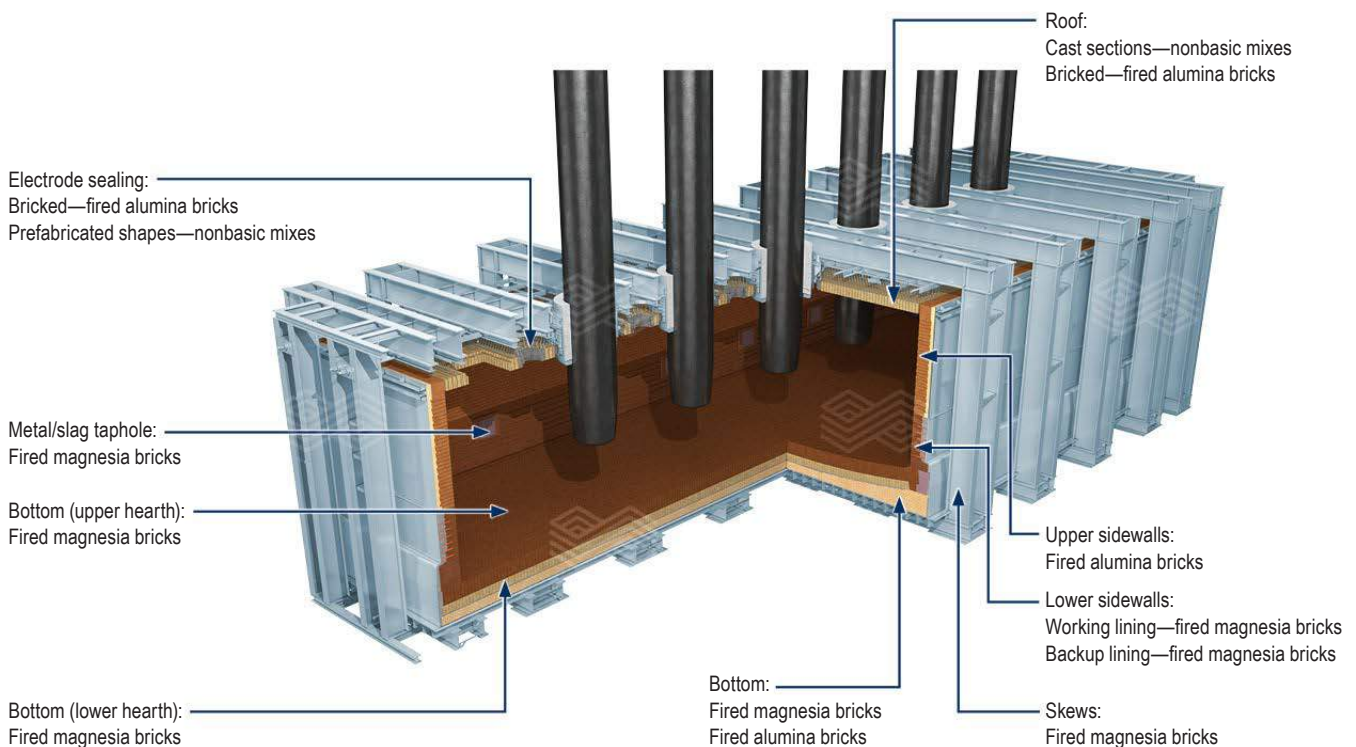


Table II. Targeted smelter slag composition range.

	CaO [wt.%]	MgO [wt.%]	Al ₂ O ₃ [wt.%]	SiO ₂ [wt.%]	MnO [wt.%]	FeO [wt.%]
Targeted slag composition	39–43	5.5–8	8.5–12	35–40	1.7–1.9	1–1.5

Table III.

Chemical composition of the specimens according to the technical data sheets.

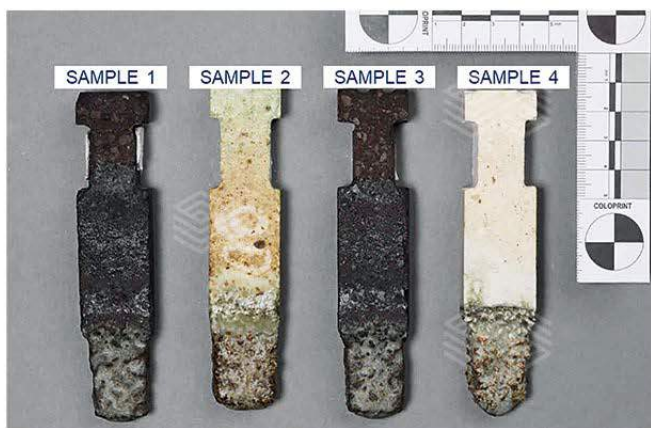
	MgO	SiO ₂	Cr ₂ O ₃	CaO	Fe ₂ O ₃	Al ₂ O ₃	ZrO ₂
	[wt.%]	[wt.%]	[wt.%]	[wt.%]	[wt.%]	[wt.%]	[wt.%]
Sample 1	57.0	0.8	21.0	0.8	12.0	7.5	0.0
Sample 2	97.0	0.6	0.0	1.9	0.2	0.1	0.0
Sample 3	46.5	0.4	27.5	0.3	9.0	12.6	0.0
Sample 4	76.0	9.0	0.0	0.7	0.3	0.0	13.5

Four basic material grades with different MgO, Cr₂O₃, and ZrO₂ contents were selected for the evaluation. The sample compositions are listed in Table III and Figure 9 depicts the specimens after the corrosion test.

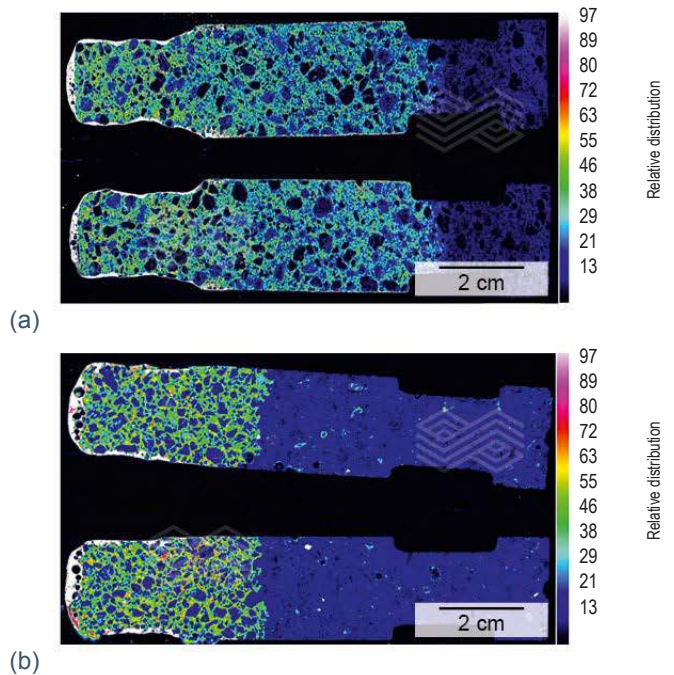
Figures 10 and 11 illustrate the micro-X-ray fluorescence results of Sample 1 and Sample 2, depicting the relative distribution of Si and Ca. The colour range demonstrates the relative amount of each element in the sample. Comparison of the images shows that both samples were coated by the CaO- and SiO₂-containing synthetic slag, indicated by the white colour seen along the specimen tip. Furthermore, it can be concluded that infiltration of Sample 1, which is based on fused magnesia and contained 21 wt.% Cr₂O₃, extended over the entire specimen and was probably caused by capillary effects. In contrast, the infiltration depth of Sample 2, which is based on sinter magnesia and no Cr₂O₃, was confined to the immersion depth of the specimen. However, the amount of infiltration seemed to be higher, as indicated by the green colour. However, this may even have a positive effect as it could potentially improve the formation of a freeze layer. In Figure 12 it is evident that the material loss of Sample 1 was higher in the immersed area.

Figure 9.

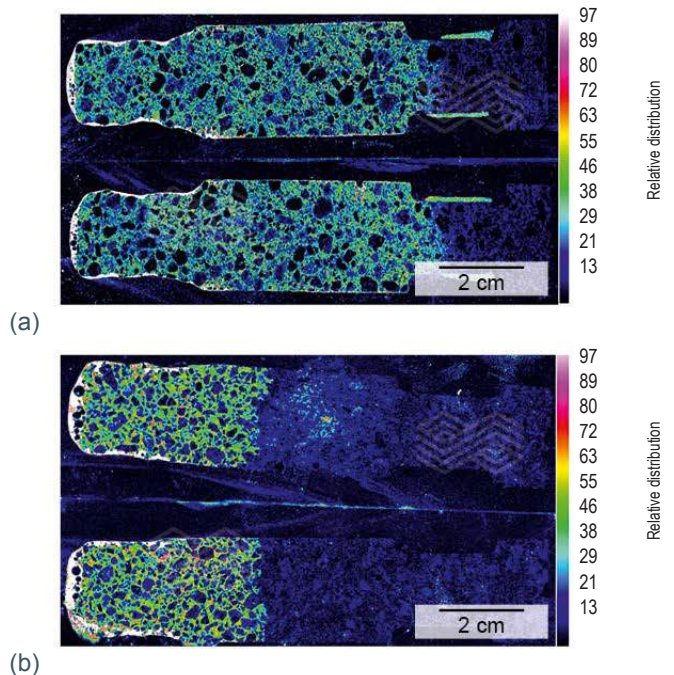
Basic refractory specimens after the corrosion test.

**Figure 10.**

Relative distribution of Ca in (a) Sample 1 and (b) Sample 2.

**Figure 11.**

Relative distribution of Si in (a) Sample 1 and (b) Sample 2.

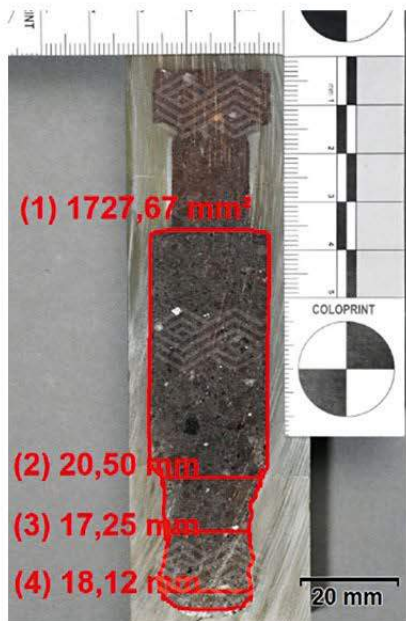


The relative distribution of Ca and Si in Sample 3, which is based on fused magnesia and 27.5 wt.% fused magnesia chromite, and Sample 4, containing MgO and ZrO₂, after an HF-ITO test are shown in Figures 13 and 14. These demonstrate Sample 3 had a similar outcome to Sample 1, namely the specimen was fully infiltrated and coated by Ca-Si slag. According to the image of Sample 4, a thicker slag layer on the tip of the specimen was formed and the results indicated a more aggressive wear compared to the other samples.

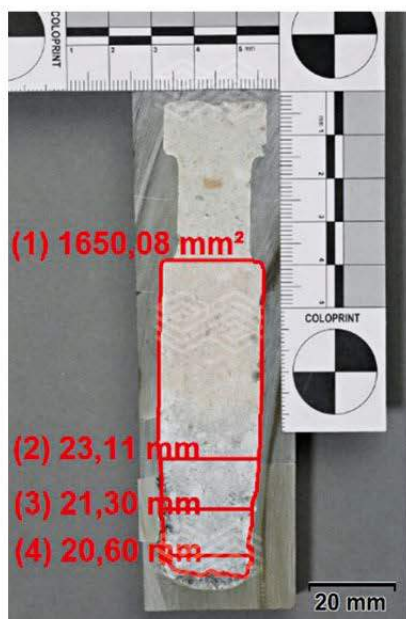
In summary, the HF-ITO tests indicate that the presence of Cr₂O₃ in the sample leads to formation of low-melting phases, which affect the infiltration resistance and result in capillary effects.

Figure 12.

Comparison of the erosion resistance of (a) Sample 1 and (b) Sample 2.



(a)



(b)

According to the results, it appears Cr₂O₃ reduction occurred; however, further mineralogical research is required to gain a deeper understanding of the chemical reactions. The results of Sample 2 look the most promising, since slag infiltration as well as material wear caused by erosion were lower compared to the other samples. Nonetheless, further mineralogical investigations are required to fully characterise refractory materials that can withstand the chemical, thermal, and physical impact present in the ESF. As a next step, RHI Magnesia will conduct HF-ITO tests with selected nonbasic materials and different synthetic slag compositions.

Figure 13.

Relative distribution of Ca in (a) Sample 3 and (b) Sample 4.

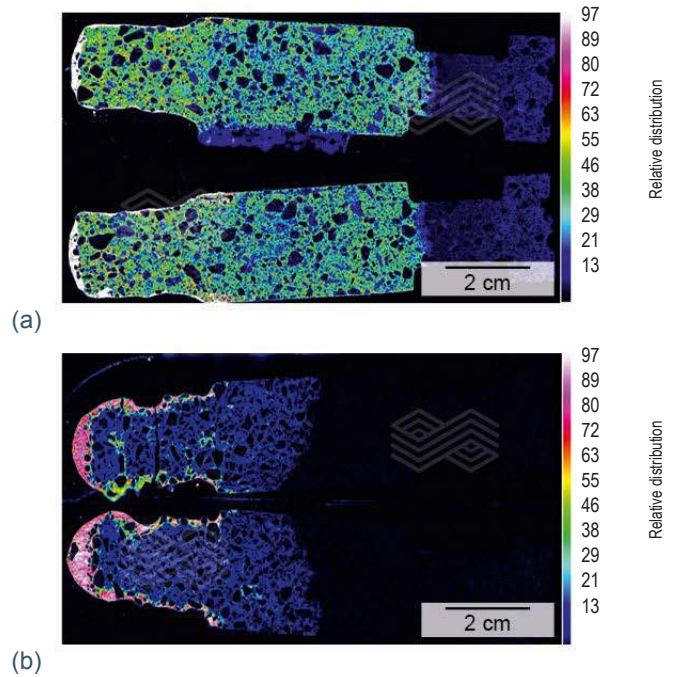
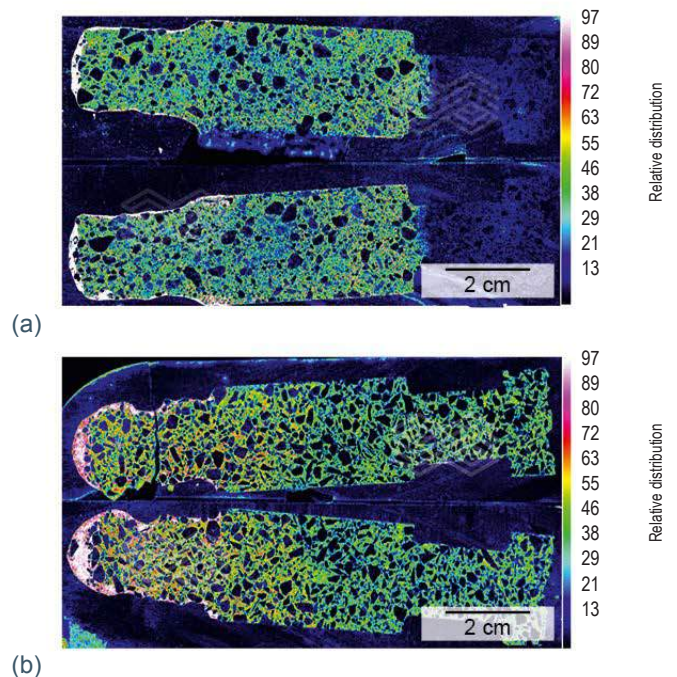


Figure 14.

Relative distribution of Si in (a) Sample 3 and (b) Sample 4.



Conclusion and Outlook

For European steel plants in particular, the abatement of CO₂ emissions is a major focus. The two described process routes can serve as technological alternatives to achieve the targeted European Union CO₂ reductions in the steel industry; however, as discussed, both options have their own benefits and challenges. The smelter technology is not yet proven for steel production but it uses the already existing infrastructure of the integrated plants, since the BOF, secondary metallurgy, casting, and rolling mill are retained. The DRI-EAF route is a well-established technology, but encounters efficiency limitations depending on the DRI quality. Undoubtedly, steel mills need to consider a vast number of aspects before deciding to implement these major process modifications.

However, as a pioneer of the refractory industry with many years' experience, RHI Magnesita aims to develop new refractory solutions to meet the requirements of the future steelmaking technologies. Investigation of the corrosion behaviour was only an initial step to better understand the chemical, mechanical, and thermal effects occurring when basic refractory materials are immersed in a smelter slag. In the framework of further R&D studies, process-adapted refractory concepts will be developed.

In addition, RHI Magnesita not only possess extensive know-how and expertise in the engineering and refractory design of mega-scale smelters, both rectangular and round, it also has numerous references in EAF applications for both scrap- and DRI-based operations. Consequently, RHI Magnesita is uniquely positioned to transfer proven concepts and learnings from one industry to another and support steel customers navigate through the green steel transformation.

References

- [1] Kildahl, H., Wang, L., Tong, L. and Ding, Y. Cost Effective Decarbonisation of Blast Furnace – Basic Oxygen Furnace Steel Production Through Thermochemical Sector Coupling. *Journal of Cleaner Production*. 2023, 389, 135963. <https://doi.org/10.1016/j.jclepro.2023.135963>
- [2] Kirowitz, J., Schnalzger, M., Janssen, T., Kirschen, M., Spanring, A., Moulin-Silva, W., Ratz, A., Kollmann, T. and Wucher, J. Electric Melting Furnaces for Green Steel Transformation of Integrated Steel Plants – Requirements, Challenges, and Solutions from a Refractory Perspective. Proceedings of the 9th European Oxygen Steelmaking Conference, Aachen, Germany, Oct. 17–22, 2022.
- [3] RHI Magnesita, 2021 RDW Shipment Data.
- [4] RHI Magnesita, 2021 Refractory Consumption Data: Europe and MENA customers.
- [5] Kirschen, M., Ehrenguber, R. and Zettl, K.-M. Latest Developments in Gas Purging Systems for BOF and EAF. Proceedings of METEC and 2nd ESTAD, Düsseldorf, Germany, June 15–19, 2015.

Authors

Miriam Schnalzger, RHI Magnesita, Vienna, Austria.
 Alfred Spanring, RHI Magnesita, Vienna, Austria.
 Marcus Kirschen, RHI Magnesita, Muelheim-Kaerlich, Germany.
 Thomas Kollmann, RHI Magnesita, Vienna, Austria.
 Wagner Moulin-Silva, RHI Magnesita, Vienna, Austria.
 Johannes Wucher, RHI Magnesita, Vienna, Austria.
 Alexander Ratz, RHI Magnesita, Vienna, Austria.
 Taco Janssen, RHI Magnesita, Bonnybridge, UK.
 Julia Kirowitz, RHI Magnesita, Vienna, Austria.
Corresponding author: Miriam Schnalzger, Miriam.Schnalzger@rhimagnesita.com



Marcus Kirschen, Uxia Dieguez, Markus Gruber, Verena Schmidt and Bernd Trummer

Energy Savings and Additional Benefits of Inert Gas Stirring in Electric Arc Furnaces with a Focus on Green Steelmaking

New electric arc furnaces (EAFs) with large melt volumes are expected to meet the required steel production capacity at minimum CO₂ intensity during the green steel transformation period. As the impact of oxygen injectors on bath mixing decreases with increasing melt volume, additional stirring technologies are required for an optimum EAF process. Inert gas stirring is an established method for improving process control, energy efficiency, metal yield, and melting time. In the following paper, the benefits of RHI Magnesita’s gas purging technology in EAFs are highlighted with a special focus on the influence of steel flow on refractory wear and hearth mix consumption. The process improvements observed are presented in industrial case studies covering EAFs fed by steel scrap, direct reduced iron, and/or hot metal. Furthermore, the gas purging benefits shown were achieved without an increase in refractory consumption, which is in contrast to competing EAF stirring technologies.

Introduction

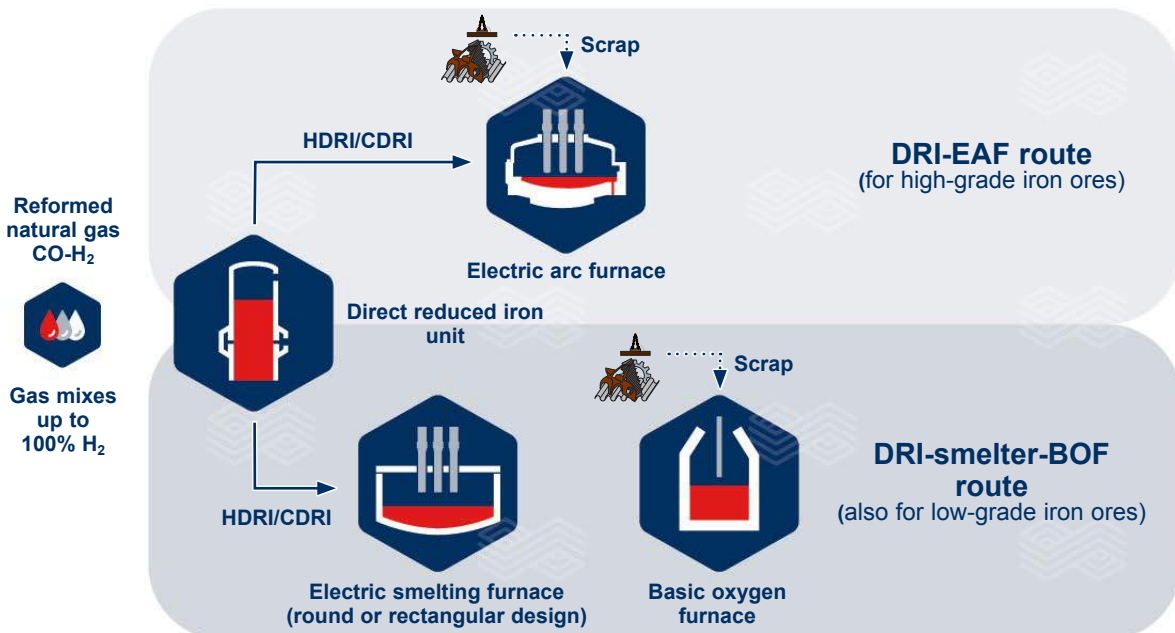
The European Green Deal initiatives define the path towards an industry-based European economy with net CO₂ emissions close to zero by 2040–2050 and all steel producing companies in Europe have provided roadmaps, initiatives, R&D consortiums, and detailed action plans to fulfil the objectives. The electric arc furnace (EAF) represents the dominant technology in green steelmaking on a European and global level with the increased use of direct reduced iron (DRI) and recycled steel scrap (Figure 1), supplemented by an optional share of hot metal (HM) during the transition period of steel plants with blast furnaces (see page 10). Decreased CO₂ emission figures are achieved by replacing coke in blast furnaces with reformed natural gas (i.e., CO and H₂) or using H₂ as a reducing agent in direct reduction plants, as well as by decreasing the CO₂ intensity

of electrical energy. However, the beneficial high flexibility of EAF steelmaking for various ferrous raw materials, varying market demands, and production volumes increase the conversion costs. This is mainly due to electrical energy costs and, to a lesser degree, increased specific refractory consumption figures.

The high production levels of typical integrated steel plants require EAFs with large melting volumes of 150 tonnes to >350 tonnes (including the hot heel). However, with an increasing EAF melt volume, the need for additional melt mixing technologies increases as the electric arcs and oxygen injectors, sources of momentum for melt mixing, are restricted to the melt surface covered with slag. The established and efficient technologies for increased melt mixing are inert gas stirring and electromagnetic stirring (EMS), a technology rarely used for the EAF until recently.

Figure 1.

Two options for green steelmaking using direct reduction: Electric arc furnace (EAF) plant based on hot and/or cold DRI (HDRI/CDRI) and a direct reduced iron (DRI) unit combined with a continuous electric smelting furnace (ESF), followed by the basic oxygen furnace (BOF) process (see page 10).



Process Improvements Through Enhanced Melt Movement in the Electric Arc Furnace

Some of the typical problems observed during the EAF daily operation are:

- Skull formation resulting in a variable melting volume due to low temperature and dead flow volumes.
- Reduced eccentric bottom tapping (EBT) opening rate due to cold spots near the EBT area.
- Unmelted input material from the slag pot decreasing metal yield.
- Hot spots located in the slag line area, which are critical for refractory wear.
- Carbon boiling especially observed when adding input materials with a high carbon content, such as pig iron, HM, or DRI.
- Low temperatures and sample reliability resulting in additional processing time during the secondary metallurgy.
- High slag zone wear rate due to a high oxidation state of the slag.
- High hearth mix wear rate due to cold spots (i.e., thermal imbalance).

Such problems mainly come from an improper thermal and chemical bath homogeneity and they directly affect the refractory performance.

In general, there are two possible sources of bath agitation or momentum to move and mix the steel melt and slag in the EAF: Electric arcs and the resulting material jets below the electrodes, and oxygen lances that induce melt flow through the impinging gas jets. However, both sources only affect the surface of the steel with restricted efficiency, due to a viscous slag layer covering the steel melt, and with increasing EAF sizes and melt volumes, as expected for the green steelmaking transformation, the impact of oxygen injectors and electrodes on bath mixing may not be enough. Therefore, in order to reduce the unbalanced thermal and chemical distribution in the furnace, it is necessary to improve bath agitation and melt homogenisation by adding other stirring sources.

Inert gas stirring is established as the most common method for improving process control, energy efficiency, metal yield, and process time in EAFs, converters, and ladles. The gas purging plugs, with a multihole design for safe gas injection into the steel melt, are the most common purging systems globally in EAFs, for example the RHI Magnesita direct purging plug (RADEX DPP) series (Figure 2). Further details regarding the technical and refractory concept of RHI Magnesita's purging plugs have been previously published [1,2]. RHI Magnesita has more than 50 references worldwide in carbon steel and stainless steel plants that currently use EAF inert gas stirring, and many of them have applied inert gas purging for decades [3–9].

In the following sections, process optimisations and improvements that have been observed in the field due to inert gas purging will be described. It is important to note that these benefits were realised even though the focus was on electricity savings.

Increased Thermal Homogeneity in the Steel Melt

Due to the improved bath movement, and thus bath mixing, the efficiency of heat transfer increases and the metallic input sources, scrap, and DRI melt faster, thereby avoiding unmelted residues and a varying furnace melt volume. Consequently, both the specific energy consumption and the power-on time of the furnace decrease (Figure 3). On the one hand, the energy savings decrease scope 2 CO₂ emissions and, on the other hand, the lower tap-to-tap time increases plant productivity. The reduction in power-on and process time also help to decrease the electrode graphite consumption.

Improved Control of Steel Tapping Temperature

The steel temperature at tapping was consecutively measured for a 75-tonne EAF before and after installing three gas purging plugs. The results showed that the standard deviation of the temperatures measured decreased from 21 °C to 7 °C with inert gas stirring. This higher temperature control at tapping leads to a better process control in the secondary metallurgy.

Figure 2.

Increased melt mixing by inert gas purging plugs in the EAF hearth.

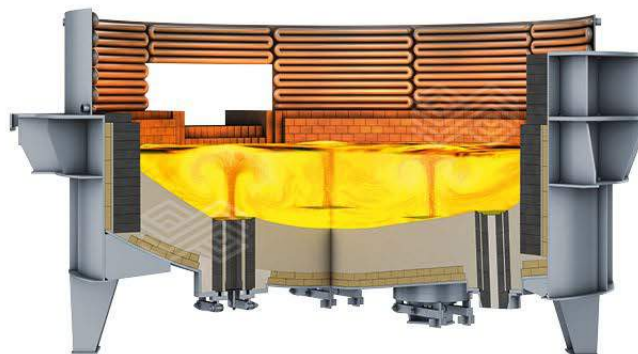
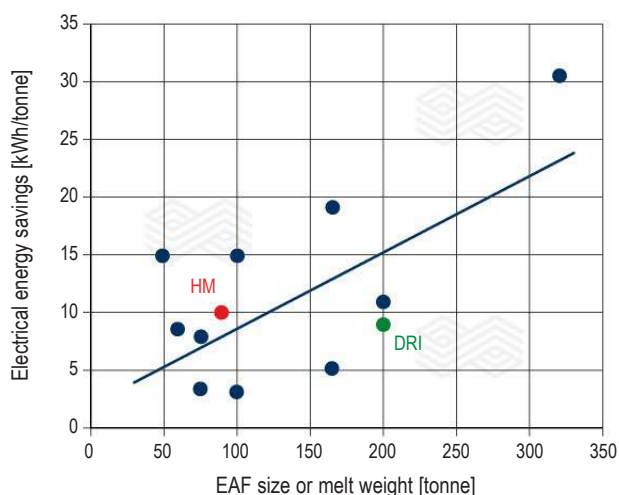


Figure 3.

Electrical energy savings with inert gas purging for different EAF sizes or melt weights: Savings in power-on time and scope 2 CO₂ emissions are proportional to the electrical energy savings. EAFs were charged with 100% steel scrap (blue), hot metal and scrap (red), or ~95% DRI (green).



Increased Chemical Homogeneity in the Steel Melt

At high chemical energy input, the instantaneous or retarded CO boiling due to the addition of high carbon-containing iron carriers, such as HM or DRI, is avoided by the continuously inserted bottom stirring gases. Furthermore, inert gas stirring significantly improves the control of FeO in the slag through an increased mass transfer between the slag and melt, as well as improved mixing of dissolved carbon and oxygen in the steel melt. The same process improvements also increase the metal yield in the case of alloyed steel production. Furthermore, dephosphorisation and the removal of nitrogen are increased with argon gas stirring. Nitrogen levels are further controlled by improved regular CO degassing.

Figure 4. Productivity increases with inert gas purging for different EAF sizes or melt weights due to improved metal yield and a lower power-on time.

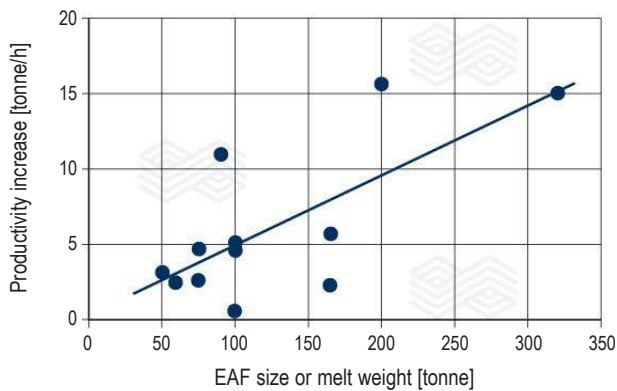
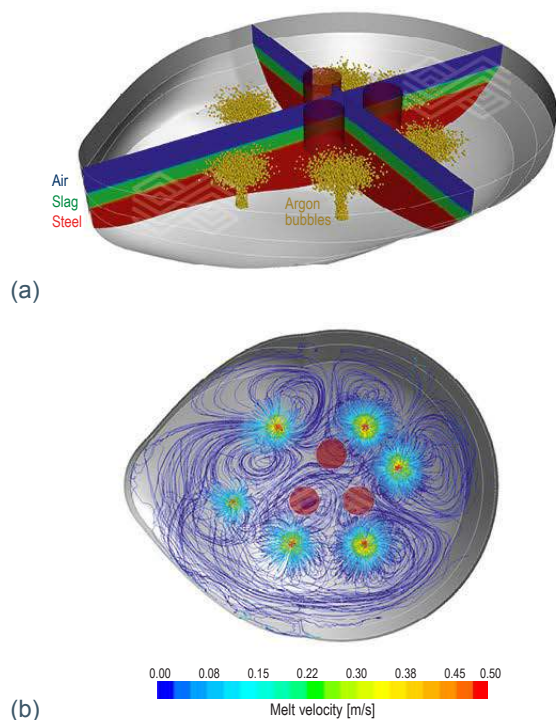


Figure 5. (a) schematic showing the 1:1 computational model of a 250-tonne EAF with the various fluid phases, six bottom purging plugs, and three electrodes and (b) streamlines of the well-agitated steel melt indicate an absence of dead volumes.



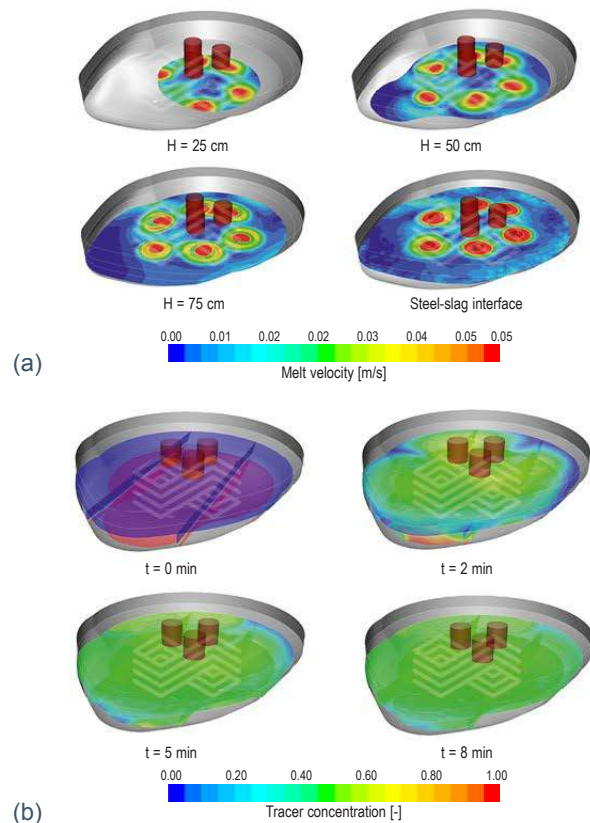
Besides achieving the customer-specific targets, metal yield improvements in the range of a few percent and lower melting times result in a systematic productivity increase of EAFs with inert gas stirring (Figure 4). In general, Figures 3 and 4 corroborate the increased performance associated with gas purging for increasing EAF melting weights.

Flow Characteristics with Inert Gas Purging Plugs

A modernly designed EAF with a 250-tonne total melt weight was simulated to visualise the steel flow due to inert gas stirring using six bottom purging plugs. Transient computational fluid dynamics (CFD) methods for a multiphase modelling approach were used, namely a volume-of-fluid model combined with a discrete particle method. The maximum volume flow rates applied were 150 litre/minute per plug or 54 m³/hour in total for six purging plugs, namely 0.216 m³/tonne for a 60 minute tap-to-tap time. However, it is important to note that the actual gas consumption would be lower than 0.2 m³/tonne as a result of process dependent and optimised flow programs.

Figure 5 shows the characteristic flow pattern developing in the steel bath after 8 minutes purging. This swirling and complex three-dimensional velocity field are indicative of good mixing efficiency within the steel bath and no dead volumes are observed. While the rising bubbles induce maximum steel velocities of up to 1 m/s, the average velocity is much slower, in the range of 10⁻² m/s. The melt velocity modelling in Figure 6a depicts effective mixing

Figure 6. Modelled steel flow in a 250-tonne EAF with six bottom purging plugs showing (a) effective mixing between the lower and upper volumes by rising steel mass flows and (b) tracer concentrations show the homogeneous mixing in the first few minutes.



between the lower and upper volumes due to rising steel mass flows and the tracer concentrations (Figure 6b) indicate homogenous mixing in the first few minutes of inert gas purging.

Wall Shear Stress Pattern and Implications on Refractory Wear

In this simulation study, the impact of increased melt movement on refractory hearth wear is directly related to the wall shear stresses from the liquid steel movement in the vicinity of the EAF hearth. Obviously, this approach only considers the erosion component and not the effect of chemical corrosion by slag. Figure 7 depicts wall shear stress levels on the hot side of an EAF hearth surface. In Figure 7a the scale is from zero to a maximum stress value of ~2 Pa, and the high stresses are clearly restricted to the plugs' hot face area (consisting of the top quality MgO-C DPPs and the surrounding MgO-C block depicted in Figure 8). In contrast, the compacted refractory hearth mix is exposed to rather low shear forces, as can be seen in Figure 7b, where the scale is refined to values below 0.2 Pa.

Influence on Hearth Mix Consumption

In addition to no increase in EAF hearth mix consumption having been observed with inert gas purging, the defined standard purging plug installation with surrounding blocks in the EAF hearth (see Figure 8) are special top-quality MgO-C products optimised for minimum wear rates and maximum lifetimes. In contrast, EMS introduces the momentum for melt movement in the lowest part of the steel melt directly on the refractory hearth in the entire area of the installed coils. The compensating mass flow in the upper melt volume results in a single roll flow regime [10]. As a result, the steel flow generated by EMS causes significantly higher shear stress patterns and erosion on the part of the EAF hearth affected. Increased hearth mix consumption after installation of an EMS system has been reported by two customers, with up to a 30% increase for one customer, and a third customer prefers a bricked MgO-C EAF hearth with EMS.

Figure 7.

Shear stress exerted by the agitated steel melt on the refractory hearth is restricted to the purging plug area. (a) full range of stress values (0–2 Pa) and (b) stress values refined to <0.2 Pa.

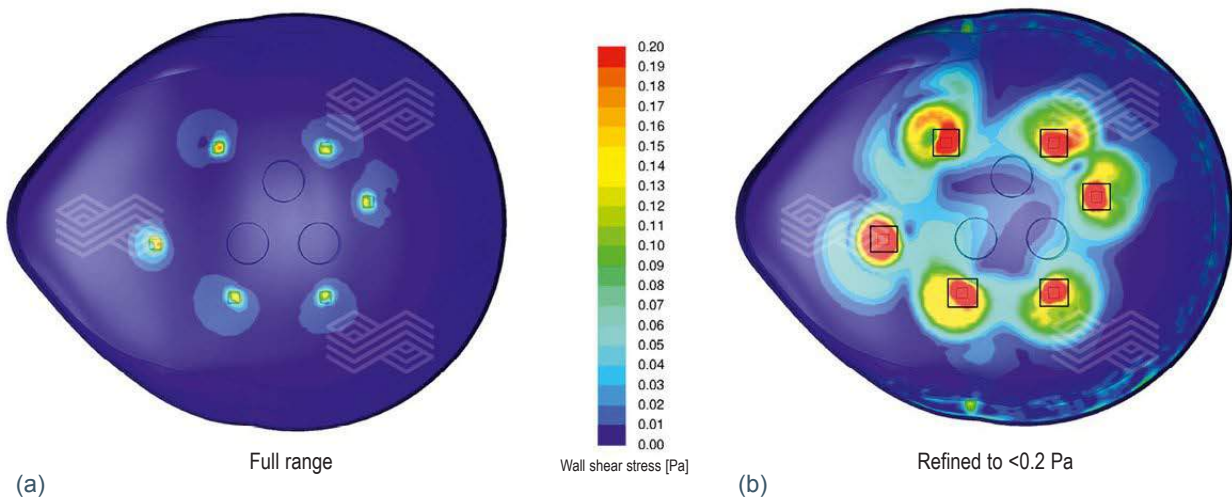
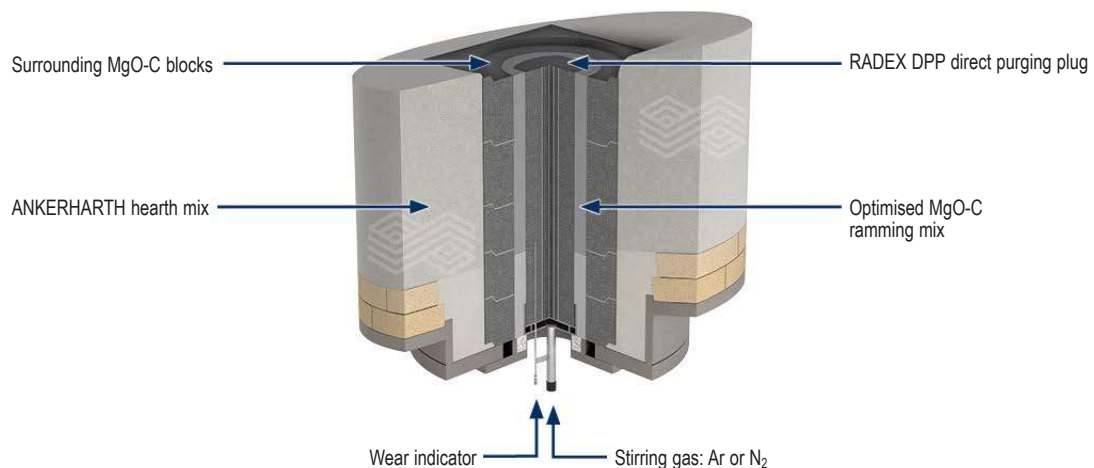


Figure 8.

Standard installation of a RADEX DPP gas purging plug with surrounding MgO-C blocks to provide maximum stability and easy exchange of the plug with minimum hearth material losses at the end of the EAF production campaign.



Modern Gas Control Units

RHI Magnesita can provide the entire gas purging system consisting of the refractory bricks and mixes, the installation procedure, process support, and the gas control unit. The gas control unit was newly developed based on decades of experience with gas purging. A typical gas control station supplying one to six RADEX DPPs in the EAF is shown in Figure 9. Each plug is controlled separately and nitrogen and/or argon is used as the purging gas. The gas flow rates can be regulated independently of the EAF control using specific EAF operating parameters or they can be incorporated into the EAF control system.

The RADEX DPP gas purging system significantly increases the availability and reliability of gas purging during the entire EAF campaign. Some of the technical advantages of the state-of-the-art gas purging systems from RHI Magnesita include:

- Modular, maintenance-friendly design (Figure 10).
- 100% leak-free system due to O-ring sealed standard blocks instead of pipes.
- Possibilities for improving the stirring efficiency.
- Option for visualisation of all input and output signals.
- Error reports with failure detection.

- Transfer of process data to customer data storage or via the Internet.
- Remote troubleshooting using a built-in modem.
- Siemens and Rockwell programmable logic controllers (PLCs) available.
- Accurate and individual flow control for multiplug purging systems.

The parameters of a RHI Magnesita gas purging system typically guaranteed are:

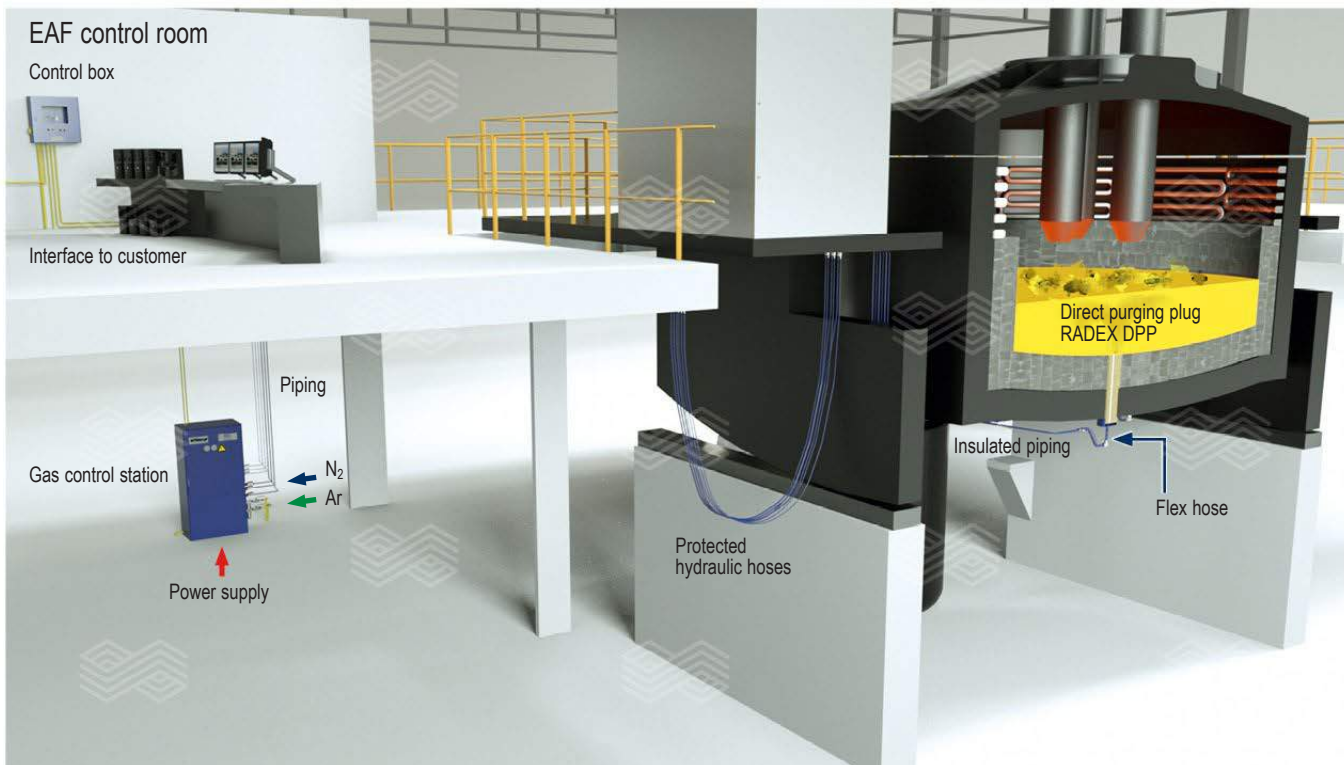
- 100% leak-free system.
- Accuracy of +/- 1.5%.
- Setting time <500 ms.

The general characteristics of the RHI Magnesita gas purging systems for EAFs and secondary metallurgy are:

- The entire gas purging technology from refractory to valve control and the purging strategy.
- One-stop project management for systems and refractories.
- Technical support by experts with process knowledge.
- Combined excellence of top suppliers, gas control systems, and refractory solutions.
- More than state-of-the-art technical solutions.

Figure 9.

Overview of INTERSTOP compact gas control station near the EAF platform.



- Fully integrated in the customers' process control systems from Level 0 to Level 2.
- Simple and cost-effective serviceability due to the modular design.
- Highly precise mass flow control and the latest generation of mass flow controllers (MFCs).
- Quick response of flow rate to set value.
- Integrated solutions from gas supply and control to purging plugs and metallurgical know-how.
- User-friendly, intuitive control panel and visualisation.
- Very compact design means a very low space requirement.
- Customer-specific software solutions.
- Exact adjustability of purging gas type and flow rate during the entire heat.
- Programmable gas flow rates for specific steel grades or production programs.
- Innovative solutions for the early detection of purging plug wear based on monitoring back pressure in the wear indication lines.

The compact design of the gas control unit, the standardised solutions for data connection to the EAF control systems, a series of purging plug solutions available for small or large EAFs, and the standard installation design of the purging plugs on the EAF steel shell provide the opportunity to revamp the inert gas stirring system of any EAF.

Conclusion and Prospects

With the upcoming transformation of the global steel industry to green steelmaking with comparable production capacities, the number of large EAF installations will increase in the

next few decades. Providing additional melt movement is crucial for a highly productive EAF process with maximum raw material conversion efficiency and minimum energy demand, especially for EAFs with a >150-tonne tap weight. The state-of-the-art technologies available for improved melt mixing are inert gas stirring and EMS. The benefits and savings in terms of energy and process time reported depend on the specific process conditions (e.g., carbon steelmaking or high-alloyed stainless steelmaking), and the carbon content of the applied raw materials (i.e., steel scrap, DRI, and/or HM), but are more or less in the same range for both approaches as a result of comparable improvements in melt mixing.

While numerous case studies have confirmed energy savings between 5–30 kWh/tonne, which increase with EAF size, a closer look at the characteristics and benefits of the two technologies provide some decisive differences between the two stirring technologies, for example the impact on hearth wear, CAPEX, and installation effort. These details are summarised in Table I, which highlights that inert gas purging provides a large series of EAF process benefits at comparably low costs and a fast return on investment within a few months.

The topics currently being investigated to further develop inert gas purging systems include:

- The use of CO₂ gas mixtures or metallurgically reactive gases as bottom purging gases.
- Automatic control algorithms.
- Fully automated performance reporting.

Figure 10.

(a) photograph and (b) schematic of the modular and compact gas control station for easy installation and maintenance.

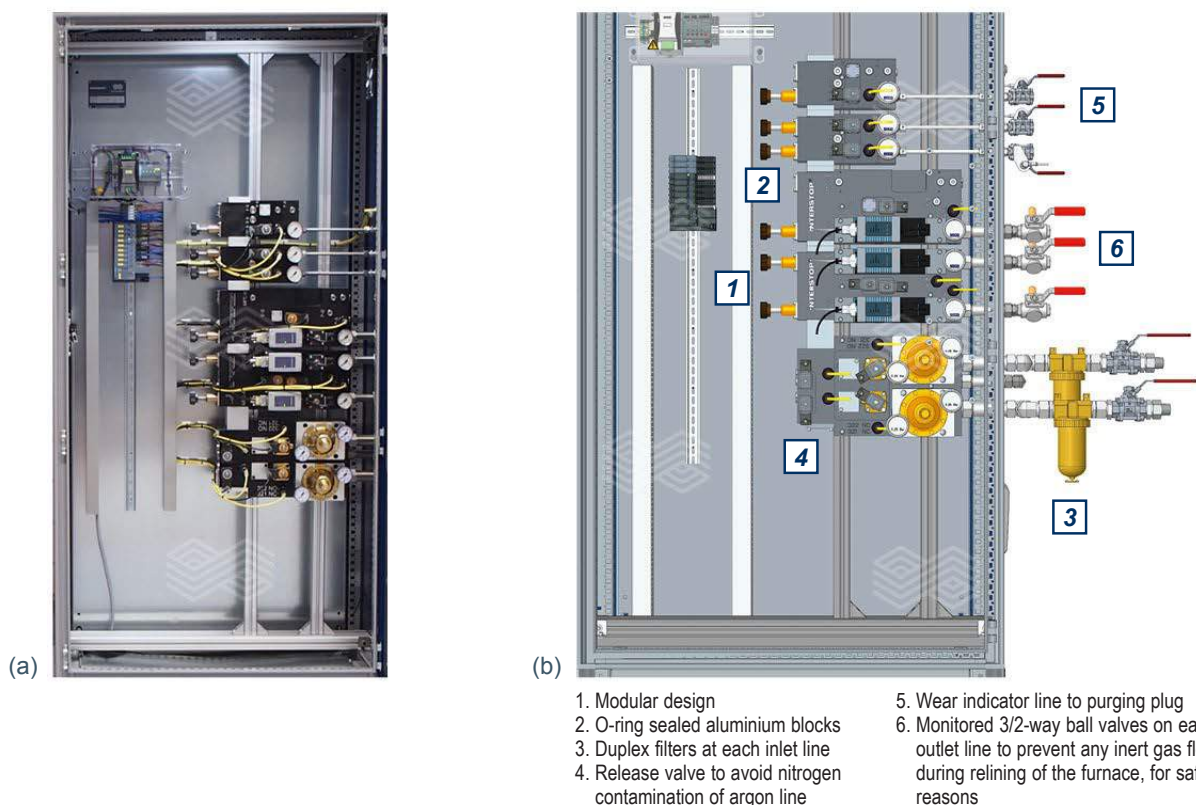


Table I.

Comparison of an inert gas purging system with electromagnetic stirring. Weighting (W): Low importance = 0 and high importance = 10. Rating (R): Unsatisfactory = 0 and very good = 4.

Criteria	Weighting	Inert gas stirring			Electromagnetic stirring		
		Rating	W x R	Rating	W x R		
Design							
Low construction effort for new EAF	7	++++	4	28	+	1	7
Low construction effort for EAF revamp	5	++++	4	20		0	0
Low influence on shell weight	6	++++	4	24	+	1	6
Number of installations	3	+++	3	9	+	1	3
Low maintenance	7	++	2	14	+++	3	21
Thermal effect							
Reduction in electrical energy [kWh/tonne]	7	++	2	14	+++	3	21
Reduction in power on	7	++	2	14	+++	3	21
Increased tap temperature control	7	+++	3	21	+++	3	21
Lower superheat	7	+++	3	21	+++	3	21
Improved EBT opening rate	7	++	2	14	+++	3	21
Reduction of scrap cave in	7	++	2	14	++	2	14
Improved melting of heavy scrap	8	++	2	16	++	2	16
Improved melting of HBI/DRI	8	++	2	16	++	2	16
Reduction of skull formation	8	++	2	16	+++	3	24
Chemical effect							
Improved bath mixing/mixing time	7	++	2	14	+++	3	21
Improved yield [%]	7	++	2	14	++	2	14
Lower FeO in slag	7	++	2	14	++	2	14
Low refractory hearth wear	7	++++	4	28	++	2	14
Improved alloy yield	8	+++	3	24	+++	3	24
Increase in decarburisation rate	8	+++	3	24	+++	3	24
Lower oxygen in steel (closer to equilibrium)	7	+++	3	21	+++	3	21
Reduced P level	8	+++	3	24	++	2	16
Reduced N level	8	+++	3	24	+	1	8
Possible CO ₂ utilisation	2	+++	3	6		0	0
OPEX							
No need for special refractories	2	++	2	4	++++	4	8
Low stirring gas consumption	2	++	2	4	++++	4	8
Low system energy consumption (kWh)	5	++++	4	20	+	1	5
CAPEX							
Low CAPEX	8	++++	4	32		0	0
Return on investment							
Fast return on investment	7	+++	3	21	+	1	7
			Total	515		Total	396

References

- [1] Kirschen, M., Ehrenguber, R., Periyasamy, R. and Zettl, K.-M. Increasing EAF Energy Efficiency and Productivity by Excellence in Bottom Gas Purging. *SEAFSI Quarterly Journal*. 2015, 44, 23–29.
- [2] Kirschen, M., Ehrenguber, R. and Zettl, K.-M. Latest Developments in Gas Purging Systems for BOF and EAF. Proceedings of METEC and 2nd ESTAD, Düsseldorf, Germany, June 15–19, 2015.
- [3] Ricci, M., Waterfall, S. and Sun, S. Optimization of Bottom Stirring in the 165-Tonne Electric Arc Furnace at ArcelorMittal Dofasco. *RHI Bulletin*. 2008, 1, 22–28.
- [4] Kazakov, S.V., Gulyaev, M.P. and Filippov, V.V. Hydrodynamics of Electric Arc Furnace Bath at Stirring with Inert Gases. Proceedings of 21st International Conference on Metallurgy and Materials, Brno, Czech Republic, May 23–25, 2012.
- [5] Dong, K., Zhu, R. and Liu, W. Bottom-Blown Stirring Technology Application in Consteel EAF. *Advanced Materials Research*. 2012, 361–363, 639–643.
- [6] Borges, R., Figueiredo Jr., A., Baitz, R., Gonzaga, E., Rocha, A., Cabral, E. and Murari, A. A New Direct Purging System for Electric Arc Furnace. Proceedings of 57th International Colloquium on Refractories, Aachen, Germany, Sept 24–25, 2014, 128–129.
- [7] Niemi, T., Vallo, K. and Kotschmar, A. Impact of Inert Gas Bottom Purging to the Energy and Production Efficiency of an EAF (in Finnish). *Materia*. 2015, 5, 34–35.
- [8] Liu, F., Zhu, R., Dong, K., Bao, X. and Fan, S. Simulation and Application of Bottom-Blowing in Electrical Arc Furnace Steelmaking Process. *ISIJ International*. 2015, 55, 2365–2373.
- [9] Yang, Z., Yang, L., Cheng, T., Chen, F., Zheng, F., Wang, S. and Guo, Y. Fluid Flow Characteristic of EAF Molten Steel with Different Bottom-Blowing Gas Flow Rate Distributions. *ISIJ International*. 2020, 60, 1957–1967.
- [10] De Santis, M., Marx, K., Pierre, R., Kleimt, B., De Miranda, U., Schrader, T., Garcia, J. and Eriksson J.E. SimuEAF. Research Fund for Coal and Steel project, Final Report no. EUR 30444-EN, 2020.

Reprint permission

Reprinted with permission from the ESTAD Proceedings. Originally presented at 6th European Steel Application Days, Düsseldorf, Germany, June 14, 2023

Authors

Marcus Kirschen, RHI Magnesita, Mülheim-Kärlich, Germany.

Uxia Dieguez, RHI Magnesita, Vienna, Austria.

Markus Gruber, RHI Magnesita, Leoben, Austria.

Verena Schmidt, RHI Magnesita Switzerland AG, Hünenberg, Switzerland.

Bernd Trummer, RHI Magnesita, Vienna, Austria.

Corresponding author: Marcus Kirschen, Marcus.Kirschen@rhimagnesita.com



Julia Kirowitz, Ronald Lanzenberger, Bernd Petritz, Laura Rechberger and Uxia Dieguez

Sustainable Refractory Solutions—New Gunning Mixes Containing Circular Material

Closing the loop of raw material flows through a circular economy and thereby finding sustainable refractory solutions is one fundamental strategic pillar of RHI Magnesita. In the last years, a major effort has been undertaken to translate this approach into gunning mixes. The main challenge was to implement a significant amount of circular raw materials, while keeping the main properties of the gunning mixes on the same level, for example the refractory performance, adhesive properties, and machinery handling. By following these criteria in a systematic development process, it has been possible to create a new sustainable gunning mix portfolio with a reduced product carbon footprint of up to 85%. In an intense and comprehensive trial phase in the main steel producing units, namely electric arc furnaces, basic oxygen furnaces, and ladles, it was possible to fully prove this new refractory concept.

Introduction

With the targets of increasing sustainability and substantially reducing CO₂ emissions, RHI Magnesita entered into a joint venture with Horn & Co. Group, the industry leader when it comes to circular material processing. This partnership called MIRECO positions RHI Magnesita as a pioneer in circular economy solutions for the refractory industry. Both companies have been working together for many years, with RHI Magnesita having purchased the majority of its circular raw materials from Horn & Co. Group. As a result, a close and trustful relationship evolved over time, forming an ideal basis for a joint and sustainable future. This was a crucial step to pave the way towards RHI Magnesita’s ambitious global target of achieving a 15% CO₂ emissions reduction by 2025, as amongst other measures the usage of circular materials significantly impacts this area. In this article factors that influence incorporating circular refractory materials in basic gunning mixes are discussed as well as the approaches taken to develop the new sustainable product portfolio.

Product Carbon Footprint

To provide increasing customer transparency, RHI Magnesita is calculating the product carbon footprint (PCF) of its refractory products and has implemented this information on the technical data sheets (see page 39). All emerging greenhouse gases are considered in these calculations, starting with the raw material extraction, followed by transportation, production, and packaging. Furthermore, the indirect emissions from the electricity used and externally purchased raw materials are included in the calculations—namely scope 1, 2, and 3 emissions. The so-called cradle-to-gate approach adopted excludes the final transportation from RHI Magnesita’s production plants to the customer.

Once the refractory products have been shipped, this PCF can be considered as scope 3 emissions at the customer site.

This means that the emissions value RHI Magnesita delivers can serve as a basis for further calculations in for example a steel plant, which will continue to gain importance in the near future. The PCF of our products will be reevaluated and recalculated on a regular basis.

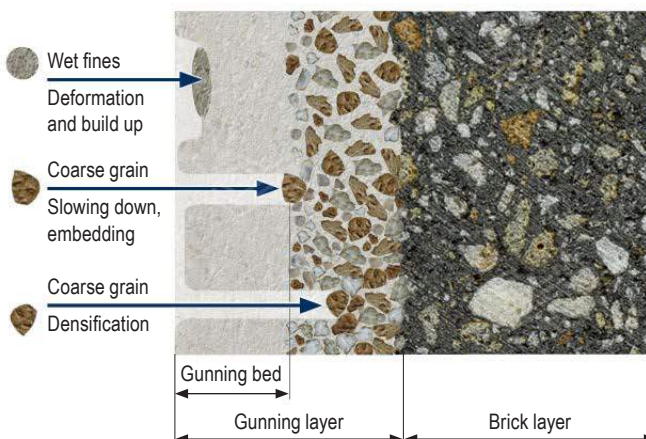
Basic Gunning Mixes and Their Fundamental Properties

In today’s steelmaking plants, basic refractory gunning mixes are essential for the efficient operation of steel producing units [1]. The optimal choice of raw materials, a well-balanced grain size distribution, and an advanced binder system are crucial for the mix performance [2].

Grain size distribution

During the development of innovative gunning mixes it is essential to focus on an optimal distribution of all the fractions, which is necessary to achieve stable processing of the blend and to keep rebound at a very low level. The distribution of various grain sizes in a gunning bed is depicted in Figure 1.

Figure 1. Formation of a gunning bed.



When adding circular raw materials to this equilibrium, all these aspects have to be considered. Hence, appropriate crushing and sieving of the used refractory material is very important to achieve the necessary balanced grain size distribution in the resulting circular raw material.

Bonding system

The binder system provides the required strength [3] until the ceramic bond formation takes place at temperatures above 1300 °C. In modern hot repair basic gunning mixes two binder systems are typical: The silicate bond and the phosphate bond.

Water soluble alkali silicates are the basis for the silicate binding system. They are moderate in terms of setting and therefore suitable for a broad range of application practices, ranging from a hand lance to semi-automated systems like the SHOOTER for basic oxygen furnace (BOF) maintenance or the TERMINATOR for electric arc furnace (EAF) repair.

Phosphates with varying acidity and degree of polymerisation are the basis for the phosphate-bonded gunning mixes. When using conventional phosphates such as sodium metasilicate, the applied gunning layer does not stabilise quickly and sufficiently [4]. However, this is necessary to ensure stiffening of the material and embedding of the coarse components. Therefore, it is crucial to choose a phosphate binder with the appropriate pH, because the more acidic the phosphate, the more strongly it reacts with the basic raw materials in the mix.

Raw material selection

One further aspect that influences the refractoriness of a basic gunning mix is the raw material selection. From 900 °C onwards, the chemical bonding phase weakens and sintering of the dead burned magnesia or the mixture of selected raw materials is mainly responsible for the strength and refractoriness. To develop high-quality gunning mixes, low-iron sintered magnesia with more than 90% MgO is often combined with alpine sintered magnesia that has a relatively high CaO/SiO₂ ratio. This high CaO/SiO₂ ratio prevents the formation of refractory-reducing, low-melting phases such as merwinite (3CaO MgO 2SiO₂) and monticellite (CaO MgO SiO₂).

Based on these basic gunning mix fundamentals, the question of how incorporating circular raw materials would influence the required properties arose.

MgO-C Circular Material in Basic Gunning Mixes

Up to now, the predominant opinion was that the wetting behaviour of circular MgO-C raw materials makes it impossible to use them in basic gunning mixes because of the negative effect on processing due to a low setting speed and initial adhesion. Therefore, a complete reexamination was required, including fundamental investigations on how circular materials could be implemented into basic gunning mixes.

The first approach to increase the gunning mix sustainability was to use leftovers that would otherwise have been landfilled. Therefore, detailed research on different material sources was performed to obtain a holistic overview of the chemical composition, including impurities. Additionally, microscopic investigations were carried out to gain information about the microstructural properties and the bonding structure, for example:

- Homogeneity of component distribution.
- Degree of ceramic bonding (e.g., fired products).
- Reactions between single minerals and components that had been exposed to high temperatures.
- Type and location of impurities.

From these investigations it could be concluded that the loss on drying (LOD) was relatively high, (i.e., up to 12%), and there was a huge variation in the main oxides such as MgO, CaO, SiO₂, and Al₂O₃, as well as the carbon content between different samples. However, the amount of heavy metals was negligible and no hexavalent chromium (Cr⁶⁺) could be detected. After these investigations, the first test specimens were prepared to enable investigations on the final product characteristics. These specimens were based on the standard silicate-bonded ANKERJET GW gunning mix series and contained either very low or low addition of two circular raw material sources and different grain fractions. Reference specimens were prepared with the standard recipe for comparison.

Physical Characteristics of the First Test Specimens

During preparation of the first test specimens with MgO-C circular material, the high LOD caused serious crack formation as expected. To avoid this issue, a temperature treatment processing step of the circular material was implemented to significantly reduce the LOD before preparing the second series of test specimens. This led to a final LOD of less than 1%, which is the general upper limit for all materials and additives used in basic gunning mixes.

The outcome of the subsequent laboratory test series was a very important milestone in the project, as it showed the physical properties of the circular material containing specimens were comparable to the standard mix (Table I).

One further important aspect during selection and processing of circular raw materials is the grain size distribution. At this early stage of the project, special care was taken to ensure that the proportion of material below 0.3 mm was as low as possible, as this fraction of the carbon-containing material can cause a negative impact on the setting behaviour during application. From these investigations it could be concluded that any detrimental effect of MgO-C circular material in various quantities on the properties of the standard mix would be negligible in practical applications.

Thermochemical Calculations of Sustainable Mixes with a Process Slag

FactSage can be used to model the interaction between a refractory material and process media, for example the phase distribution in a gunning mix layer infiltrated by slag can be calculated. Since this thermodynamic modelling approach is based on a theoretical equilibrium, the results do not consider any kinetic modelling, mass transfer, or abrasion effects.

To investigate the interaction of different gunning mixes with a typical slag, the mix compositions shown in Table II were used, namely the standard ANKERJET GW mix was compared to two mixes based on the same grade, containing a low amount of MgO-C circular material, with or without carbon. The chemical composition of a customer's EAF process slag was analysed in house and used for the calculations. The results verified the conclusion given in the previous section, namely that the presence of carbon in the system does not have any negative impact on the thermodynamic balances.

First Gunning Trials at the Training Centre in Veitsch

Prior to any customer field trials, internal gunning trials at RHI Magnesita's training centre in Veitsch (Austria) were conducted to investigate the performance during application of the circular material containing gunning mixes. Special focus during these cold gunning tests was placed on the initial adhesion and the flowability of two circular material containing alternatives of the well-established ANKERJET RTW70-20-AT gunning mix. The prepared alternatives had a similar binding system, grain size distribution, and raw material content, and differed only in the circular material addition.

Table I.

Physical properties of different ANKERJET GW based specimens containing the MgO-C circular materials A or B, compared to the standard mix. Abbreviations include cold crushing strength (CCS), bulk density (BD), and porosity (POR).

Landfill source		A	B	A	B	A	B	A	B
Addition		Very low	Very low	Low	Low	Very low	Very low	Low	Low
Grain size (mm)		0.3–1	0.3–1	0.3–1	0.3–1	1–3	1–3	1–3	1–3
CCS [N/mm ²]	20.9	22.0	35.8	16.0	23.1	12.1	24.5	17.4	21.0
BD [g/cm ³]	2.29	2.35	2.61	2.28	2.51	2.31	2.57	2.33	2.53
POR [vol%]	33.74	32.16	24.88	34.25	27.71	33.33	25.87	32.80	26.75

Table II.

Chemical composition of the ANKERJET GW mixes used for the FactSage calculations.

	Standard ANKERJET GW	ANKERJET GW + low MgO-C addition	ANKERJET GW + low MgO-C addition (no carbon)
	[wt.%]	[wt.%]	[wt.%]
MgO	82.14	80.60	83.73
SiO ₂	4.80	4.95	5.14
CaO	7.60	5.89	6.12
Fe ₂ O ₃	3.70	2.55	2.65
Al ₂ O ₃	1.20	1.71	1.78
Na ₂ O	0.56	0.56	0.56
C	0.00	3.74	0.00

Since availability of the landfill that could have served as a basis for the circular raw material was very limited at the time, standard MgO-C circular material from RHI Magnesita’s Veitsch production plant was used. The advantages of this material were that the LOD was already below 1%, and could therefore be considered as “dry”, it was available in optimised fractions, and it showed a constant chemical composition over time.

The results of these cold gunning tests showed no significant differences in the workability of all tested mixes. Especially the mix with the highest addition of MgO-C circular material showed excellent flowability and even required less water for an optimum consistency.

First Steel Plant Field Trials: Mixes Containing MgO-C Circular Material

To verify the positive outcome of the cold gunning trials and to test the performance at a customer, two circular material containing alternatives of the standard mix used by the customer were created. One of them contained a very low and one of them a low amount of circular material. The chemical compositions of the three mixes are shown in Table III.

The first trial was carried out at one of our European lead customers in an EAF with a tapping weight of approximately 100 tonnes, using a TERMINATOR with an average feeding rate of 120 kg/minute.

These tests showed a really promising performance, with the initial adhesion, rebound, and refractoriness on a comparable level to the standard mix. Especially between the two alternatives with different additions of circular material, no significant difference in the behaviour could be observed. However, to maintain the high-performance standards of RHI Magnesita’s gunning mixes, at this point in the project the binding system was further optimised to avoid any spalling, particularly when the mix was applied to a low temperature surface. Figure 2 shows the spalling observed in the first test using the original binder system.

Conclusions from the first field trial with circular material containing mixes were:

- Slight spalling occurred prior to the binder system optimisation when applied to colder surfaces.
- Application of thicker gunning layers required an improved bonding system (i.e., faster setting).
- Service life depended on the production program but was equal to the standard ANKERJET RTW70-20-AT mix.
- Workability and refractoriness were excellent.

Follow-up trials took place under the same conditions, with the previously mentioned standard and circular material containing mix alternatives, but with the optimised binding system. As shown in Figure 3, no spalling occurred with the refined concept.

Table III.

Chemical composition of the ANKERJET RTW70-20 alternatives used to evaluate the performance of circular material containing mixes in a customer’s EAF.

Alternative	Circular material addition	MgO	SiO ₂	CaO	Fe ₂ O ₃	Al ₂ O ₃	C
ANKERJET RTW70-20-AT		82.1	4.8	7.6	3.7	1.2	0.0
ANKERJET RTW70-20-VL	Very low	81.0	4.9	7.4	3.5	1.3	1.3
ANKERJET RTW70-20-L	Low	80.8	4.9	6.7	3.0	1.5	2.5

Figure 2.

Slight spalling observed during application on a low temperature surface in the first test using the original binder concept.



Figure 3.

Excellent sticking properties and no spalling observed in the second test using the optimised binder concept.



Following these very positive results, further customer trials were carried out including campaigns with up to 25 tonnes of trial material and significantly longer test phases. All tests showed at least the same refractoriness as the standard mix and it was concluded that the use of MgO-C circular material in basic gunning mixes had no negative impact on the workability.

Magnesia Spinel Circular Material in Basic Gunning Mixes

To achieve RHI Magnesita's goal of further reducing the carbon footprint of its products, another project was launched to find additional sources of circular raw materials suitable for basic gunning mixes. After considering all the important raw material factors, such as a stable chemical composition, a LOD below 1%, cost efficiency, and a secured supply chain in terms of availability and on-time shipment, it was decided to start an in-depth investigation of magnesia spinel circular material and its potential usage in refractory mixes.

Setting Test and Physical Values

The first step to investigate three different magnesia spinel types was the setting test, which determines the strength, setting behaviour, and temperature development when water is added to the gunning mix. In the initial approach, a 50/50 blend of the different magnesia spinel types with original raw materials was prepared, and the test was carried out on both a silicate- and a phosphate-bonded mixture. During these trials, there was no evidence that the magnesia spinel circular raw materials were detrimental, as all the relevant properties were within the known specifications.

Subsequently, different specimens were prepared that contained a medium and high proportion of magnesia spinel circular raw material in both silicate- and phosphate-bonded versions. To understand the processes induced by heat, the samples were exposed to different temperatures. These tests showed that the physical properties of the samples were not negatively affected when compared to the standard mixture, and although different levels of circular material addition showed different characteristics, no exclusion criteria were identified.

Steel Plant Field Trials: Mixes Containing Magnesia Spinel Circular Material

As the test results showed high potential, the next step was to carry out the first field trials in a steel plant. These trials were also performed in the EAF (tapping weight of approximately 100 tonnes) at one of our lead customers in Europe.

Five tonnes of each mix were tested, including silicate- and phosphate-bonded, medium, and high circular material containing gunning mixes. Following the experiences with the MgO-C circular material containing gunning mixes, the binding systems were optimised for the first field trials to ensure optimal material processing and adhesion.

All mixes showed excellent workability, such as primary adhesion—even on colder surfaces—and very low rebound (Figure 4). The refractoriness was validated during the test period and showed at least the same performance as the standard mix, with a tendency towards higher durability; however, this has to be verified in the future. Further trials with mixes containing high amounts of magnesia spinel circular materials were subsequently carried out in the 120-tonne EAF of another European customer and the positive results of the first tests were confirmed.

Sustainable Gunning Mix Portfolio

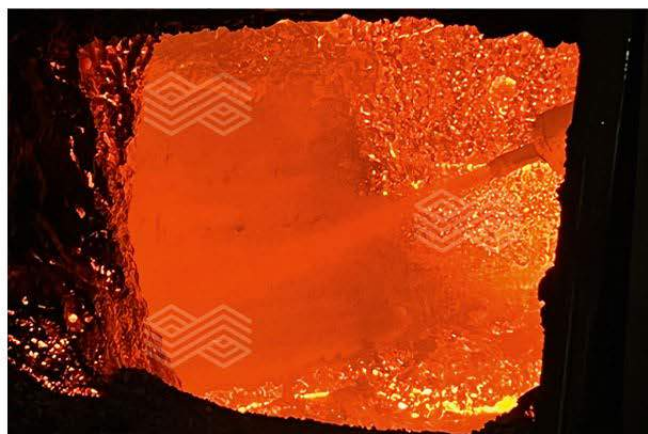
Due to the intense R&D activities, it was possible to implement completely new product types in the gunning mix portfolio, based on different amounts of MgO-C or magnesia spinel circular material. These solutions are paving the way towards a more sustainable future, by decreasing RHI Magnesita's scope 1 CO₂ equivalent (CO₂e) emissions, as well as customers' scope 3 emissions. Another aspect that increases the sustainability is being able to serve the European market with products produced in Europe—local for local—as the gunning mix product portfolio is currently available from the production plant in Veitsch.

MgO-C Circular Material Containing Gunning Mixes

To date, hundreds of tonnes of MgO-C circular material containing gunning mixes have been shipped and tested in customer applications across Europe and have proven that they can serve as a sustainable alternative to our standard gunning mixes without any performance decrease during application. Therefore, many customers are already using these products as their new standard gunning mix.

Figure 4.

Gunning mix with a high content of magnesia spinel circular material during application in an EAF.



In the current product portfolio, the higher amount of MgO-C circular material addition has been implemented, as the field trials showed equivalent performance to the standard mixes. With this well-established portfolio (Table IV), all European top selling gunning mix brands are covered.

Magnesia Spinel Circular Material Containing Gunning Mixes

After the positive laboratory tests and field trials, a product portfolio of magnesia spinel circular material containing gunning mixes has been implemented (Table V). With this portfolio, RHI Magnesita can provide customers with basic gunning mixes that have a drastically reduced PCF of up to -85% compared to the equivalent standard mix. Currently, the portfolio covers the high-performance silicate- and phosphate-bonded standard gunning mixes; however, due to the high sustainability potential and positive field trials, the portfolio will be extended.

Potential CO₂e Savings by Using Sustainable Gunning Mixes

The decreased PCF of RHI Magnesita's sustainable gunning mixes has a direct impact on the scope 3 emissions of the customers' steel plant. This means that by switching from a standard basic gunning mix to one of the above-mentioned developments, a customer's scope 3 emissions can be significantly reduced.

Table IV.

Sustainable gunning mix portfolio based on MgO-C circular material.

Grade	Application	Circular raw material content	Average PCF reduction	Description
ANKERJET YP12-AT	Standard gunning	Low	- 11%	Phosphate-bonded, high-performance gunning mix
ANKERJET YW12-AT	Standard gunning	Low		Silicate-bonded, high-performance gunning mix
ANKERJET YRW72-AT	Standard gunning	Low		Silicate-bonded, standard-performance gunning mix
ANKERJET YRW12-AT	Standard gunning	Low		Silicate-bonded, medium-performance gunning mix
ANKERJET YRP12-AT	Standard gunning	Low		Phosphate-bonded, medium-performance gunning mix
ANKERJET YKW72-AT	BOF mouth and ladle lip ring gunning	Low		Silicate-bonded ladle lip ring/BOF mouth gunning mix

Table V.

Sustainable gunning mix portfolio based on magnesia spinel circular material.

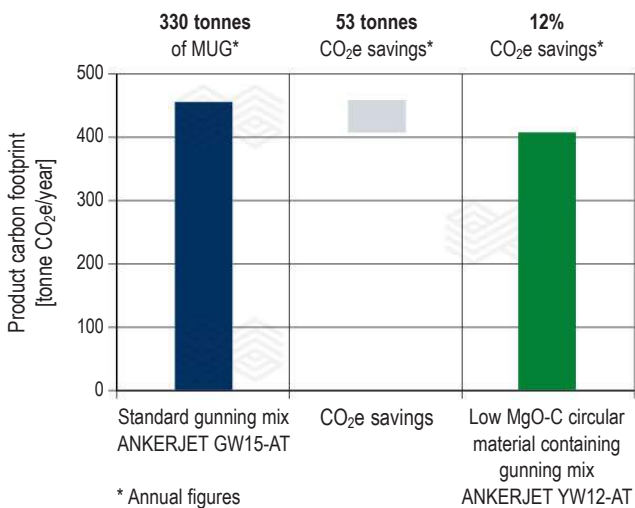
Grade	Application	Circular raw material content	PCF reduction	Description
ANKERJET XW15-AT	Standard gunning	Medium	-40%	Silicate-bonded, high-performance gunning mix
ANKERJET XW10-AT	Standard gunning	High	-85%	Silicate-bonded, high-performance gunning mix
ANKERJET XP15-AT	Standard gunning	Medium	-40%	Phosphate-bonded, high-performance gunning mix
ANKERJET XP10-AT	Standard gunning	High	-85%	Phosphate-bonded, high-performance gunning mix

Figure 5 gives an indication of the CO₂e savings a steel plant in Europe has achieved by changing from ANKERJET GW15-AT to one of the MgO-C circular material containing grades as the new standard. These calculations are based on the annual EAF gunning mix consumption of approximately 330 tonnes per year (EAF tapping weight approximately 150 tonnes). As illustrated in the diagram, the customer is saving 53 tonnes of CO₂e per year, which is an emission equivalent of a standard diesel car going around the world more than six times (assuming an average consumption of 8 litres per 100 km and emissions of 2.68 kgCO₂e/litre).

If the same steel plant switched to using one of the magnesia spinel containing gunning mixes, the CO₂e savings would increase to nearly 400 tonnes (Figure 6), which is an emission equivalent of a standard diesel car going around the world more than 45 times.

Figure 5.

Annual CO₂e savings achieved by using ANKERJET YW12-AT, which contains a low amount of MgO-C circular material.

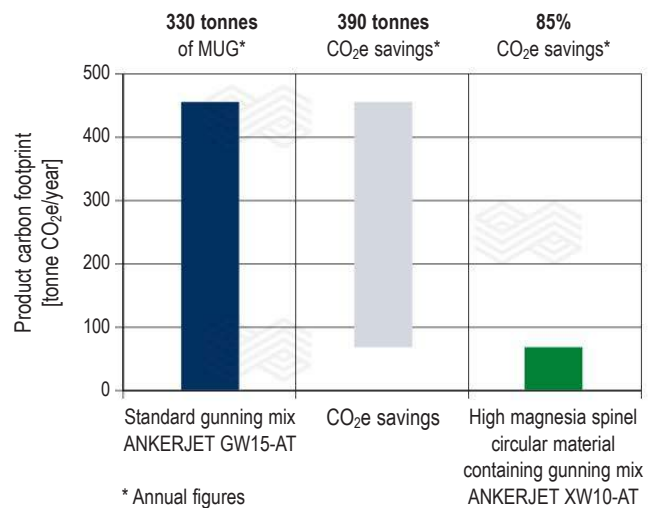


Conclusion and Outlook

Based on detailed R&D, RHI Magnesita has implemented completely new product lines for basic gunning mixes that are paving the way towards a more sustainable future. Through this new but well-established portfolio, customers are able to choose refractory products with lower PCFs and thereby minimise their scope 3 emissions. Due to the continuously increasing demand, RHI Magnesita is working on expanding these product lines to the production plant in Eskisehir (Turkey), thereby enabling further markets to be supplied with regional and sustainable products. To exploit the full potential of circular materials, additional investigations will be performed to determine the capabilities and limits of use, which will lead to an ever-growing sustainable product portfolio for basic gunning mixes as well as other refractory products.

Figure 6.

Theoretical annual CO₂e savings that could be achieved by using ANKERJET XW10-AT, which contains a high amount of magnesia spinel circular material.



References

- [1] Lammer, G., Jandl, C. and Zettl, K. Maintenance Matrices: Overview of Common Refractory Maintenance Methods for BOFs and EAFs. *Millennium Steel*. 2013, 61–65.
- [2] Mosser, J. and Siegl, W. High Lime Gunning Mixes for BOF and EAF. IREFCON 96: 2nd India International Refractory Congress, New Delhi, India, Feb. 8–9, 1996.
- [3] Petio, F. Top Quality Gunning Mixes for BOF, EAF and Ladles. Proceedings of UNITECR 97, New Orleans, USA, Nov. 4–8, 1997.
- [4] Siegl, W. High Quality Gunning Mixes for BOF and EAF. 9th Intercompany Conference, Japan, Nov. 23–28, 1995.

Authors

Julia Kirowitz, RHI Magnesita, Vienna, Austria.

Ronald Lanzenberger, RHI Magnesita, Leoben, Austria.

Bernd Petritz, RHI Magnesita, Leoben, Austria.

Laura Rechberger, RHI Magnesita, Leoben, Austria.

Uxia Dieguez, RHI Magnesita, Vienna, Austria.

Corresponding author: Julia Kirowitz, Julia.Kirowitz@rhimagnesita.com



Matheus Moraes, Alexander Leitner, Gustavo Nogueira, Barbara Zocratto, Stefan Heid and Jürgen Mühlhäußer

Technical Challenges for Refractory Recycling and Innovative Processing Solutions

RHI Magnesita is driving the refractory industry towards a carbon-neutral production footprint and in order to achieve this ultimate target, recycling is one of the most important strategic initiatives. Nevertheless, to drastically increase the recycling rate, adaptations to processing and product design are necessary. This article presents an overview of the current challenges to increase recycling utilisation, from sourcing to processing and use. Additionally, innovative solutions under development at RHI Magnesita are discussed, including sorting during or after dismantling, the removal or stabilisation of contaminants, as well as fragmentation methods to increase mineral circularity. These technology developments are providing customers from different industries with a low carbon footprint refractory product portfolio that offers high performance at competitive costs.

Introduction

RHI Magnesita has the objective to significantly reduce its carbon footprint, with intermediate targets clearly set towards this goal [1]. The use of recycling is an immediate approach to significantly decrease the CO₂ footprint of refractory products. Table I presents the carbon footprint of a representative lining concept for the cement industry (basic and nonbasic monolithics and fired bricks), exemplifying the raw material contribution to the overall CO₂ footprint.

Since the carbon footprint of recycling is substantially lower than the original raw material (depending on logistics and processing steps) [2], replacing a primary raw material

source by a circular mineral has the potential to save almost 60% of a mixed refractory lining carbon footprint and the value could be close to 90% for an unshaped material (no brick heat treatment necessity), such as a basic monolithic (see page 39). Additionally, the use of recycling can reduce the dependence on imported aggregates, simplify complex logistics, lower the amount of waste to be landfilled, and provide a competitive advantage by offering full circular solutions for customers [4,5]. Therefore, the benefits of recycling are clear and it's a latent opportunity with plenty of materials available on the market. However, only refractory companies with a clear strategy and dedicated investment in innovative technologies will be able to achieve significant recycling usage alongside appropriate performance, with RHI Magnesita leading the market towards a circular business model.

Table I.

Example of the carbon footprint per production step for a representative cement industry lining concept (basic and nonbasic monolithics and fired bricks) [3].

Processing Step	CO ₂ footprint [%]
Raw material	59.9
Processing (batch preparation and shaping)	2.0
Brick heat treatment	28.8
Finishing and packaging	2.3
Transportation	7.0

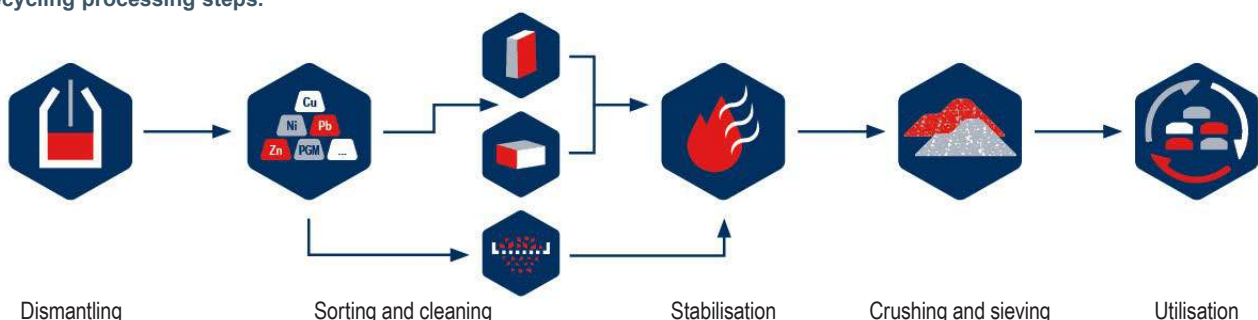
Challenges and Opportunities for Refractory Circularity

The maximum amount of recycling that can be returned to refractory compositions is highly dependent on material sorting as well as the process efficiency to remove contaminants, thereby reducing variability of the chemical and physical properties. Furthermore, the R&D capability regarding product and process design for refractories is also a major contributor.

The recycling process starts with the customer agreement and dismantling the lining, in addition to establishing the legal framework required to transport spent material to the processing plant. After these steps, the logistics and storage are key for the economic feasibility. After arriving at the processing plant,

Figure 1.

Recycling processing steps.



preprocessing (e.g., screening and metallic shell removal), sorting, stabilisation, crushing, and sieving are normally necessary before the materials can be reintroduced into the refractory production. Finally, determining applications for the leftover materials are necessary in order to keep the process both economical and truly sustainable. Figure 1 illustrates the recycling processing steps.

Sourcing and legal framework

The sourcing strategy of spent refractories is essential to ensure stable volumes and quality for the downstream processes. The agreements vary from simple spot purchasing to a full circular contract, linking the return of spent material to product supply. An important factor for sourcing quality is effective dismantling at the refractory user. The better the separation during an equipment dismantling, the higher the overall yield and stability achieved after processing. Additionally, licenses to transport and process waste materials are necessary for some refractory recycling, with special attention on dolomitic goods. Hence, the cost and timeframe to establish a recycling operation can vary according to source location and the material to be processed. Even though some regions, such as the European Union, try to foster circularity and a low carbon footprint economy, there is still conflicting legislation regarding waste handling and management for circular operations, which is a key topic to be addressed.

Sorting

After establishing a source of spent refractories, sorting the different products is essential to achieve the necessary chemistry range to reuse the materials in refractories or to direct them for further processing. This step is currently the most important challenge to be addressed since the operations are mostly carried out manually and dependent on workforce experience to identify the various classes. In the vast majority of cases, an operator is responsible for deciding which refractory product the recycling originally came from, relying on colour, fracture characteristics, sound upon impact, density, and lustre according to the light applied. Figure 2 illustrates a manual sorting operation.

Figure 2.
Manual sorting operation at RHI Magnesita in Brazil.



However, the main constraint of this process is the limited distinction possible with human senses (especially for carbon-containing materials), leading to suboptimal sorting of certain material types. Moreover, training a sorting expert requires extensive hands-on experience. Finally, the process productivity is low, leading to high operational expenditures, particularly in places with high labour costs. In order to avoid reducing the productivity even further, only the coarse fraction (normally above 80 mm) is sorted, making it necessary to find an application for the unsorted finer fraction. This is another major challenge regarding cost and landfill reduction, given that the more mixed the materials, the higher the variability in properties and the more difficult it is to find a use.

Stabilisation and beneficiation

The removal of contaminants such as iron and slag infiltration for materials coming from the steel industry and alkalis in infiltrated cement rotary kiln bricks, as well as the stabilisation of carbides that have formed in antioxidant-containing bricks are examples of essential steps required before spent materials can be returned to refractories. However, while the necessary processes are available in the market, they have to be upscaled according to the utilisation ramp up, posing a challenge for the design footprint, investment, and operational costs. Figure 3 illustrates a process for carbide stabilisation (i.e., weathering method), currently with a 3-month lead time and high storage area required.

Sizing and utilisation

After processing and appropriate quality control, the recycling material must be crushed, sieved, and prepared for reuse in refractory products. The design of high-performance product formulations optimised for the chemistry and physical properties of the available recycling is highly dependent on the R&D capability from a refractory company. RHI Magnesita relies on its five R&D centres around the globe and more than 140 masters and doctors among the 500 experts, to develop formulations and exchange knowledge on production processes to support its recycling strategy and targets.

Figure 3.
Carbide stabilisation using the weathering method.



RHI Magnesita's Innovation Roadmap

The development of recycling processing is part of RHI Magnesita's technology roadmap, reflecting the company's strong commitment to the topic. Currently, several novel processes and techniques are being developed to improve the business circularity.

Sourcing pool

The rapid increase of recycling utilisation by RHI Magnesita highlights the innovation capability of the company, but it also poses a challenge for sourcing to keep up with the demand. Therefore, the company has developed new circular business models with refractory consumers, benefiting the customer with a proper destination for the residues and ensuring reliable sources of spent refractories for RHI Magnesita, with both sharing the benefit of reverse logistics. Additionally, symbiosis with other industries and players is fundamental to further develop solutions. For example, recently RHI Magnesita announced the joint venture with Horn & Co. Group, creating MIRECO, a key recycling material supplier and processing technology hub, accelerating the value creation and environmental benefits from refractory recycling.

Automated sorting

The priority focus for recycling process R&D is on a fully automated identification and separation of materials and RHI Magnesita has been developing a prototype to be implemented in Austria that will completely change the status quo of spent refractory sorting [6]. Figure 4 shows the device design being constructed.

The prototype is just the first stage of a full sorting solution, comprising all size fractions (also addressing the fines) and difficult materials (carbon containing are not a constraint for the process). In this direction, RHI Magnesita is leading a consortium of 9 members from industry and academia, including 30 experts from 10 different nationalities. This project, called ReSoURCE, is funded by the European Union's Horizon Europe Framework Programme (HORIZON) under the Grant Agreement Number 101058310. Core developments comprise tailor-made multisensor solutions (e.g., laser-induced breakdown spectroscopy and hyperspectral imaging), artificial intelligence based analysis algorithms, and advanced material processing steps. Overall, these will set new standards for automated sorting of spent refractories.

Carbide stabilisation

Carbide stabilisation is essential for recycling markets where antioxidant utilisation in magnesia-carbon bricks is high (e.g., North America, South America, India, and China) because the aluminium added to reduce carbon oxidation is transformed into Al_4C_3 at temperatures ranging from 700 °C up to 1400 °C, according to equation 1.



While the in-situ formed Al_4C_3 is highly refractory, at ambient temperatures it hydrates to form $Al(OH)_3$ (leading to an approximately 110% volume increase) and methane (equation 2). Therefore, the Al_4C_3 in reclaimed material must be stabilised before being recycled in refractories or it will promote cracks and result in scrap production.

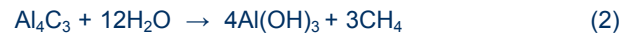


Figure 4.

Fully automated sorting prototype being implemented by RHI Magnesita.

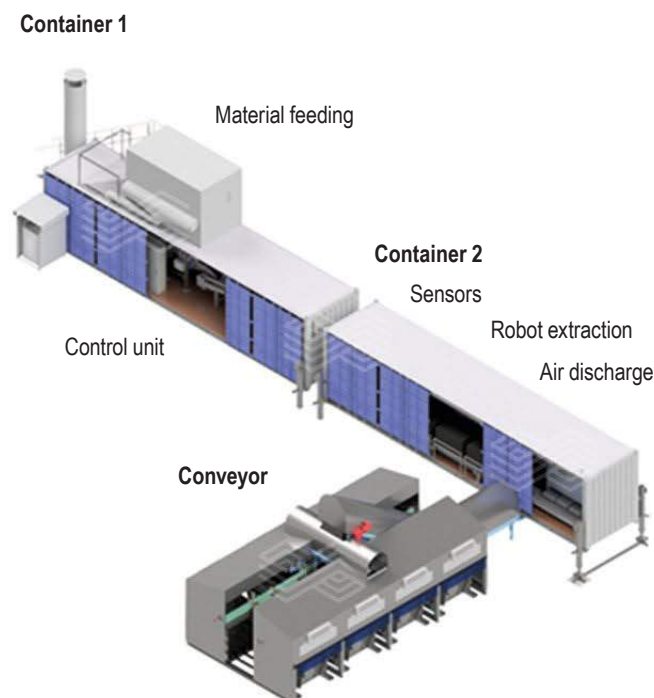
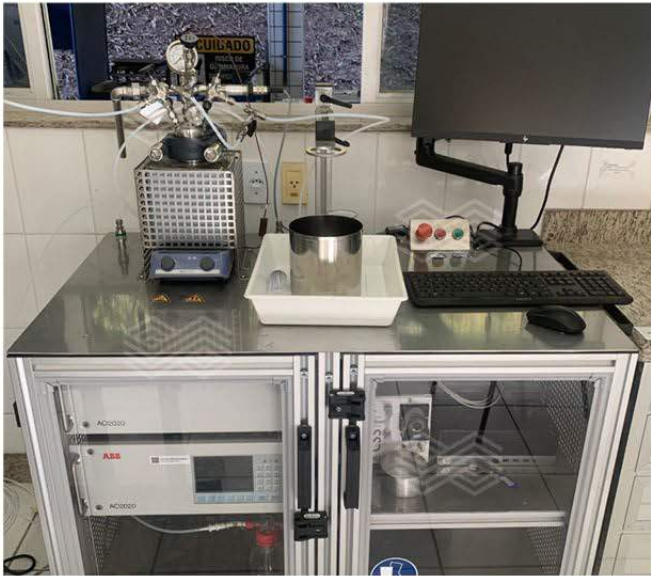


Figure 5.

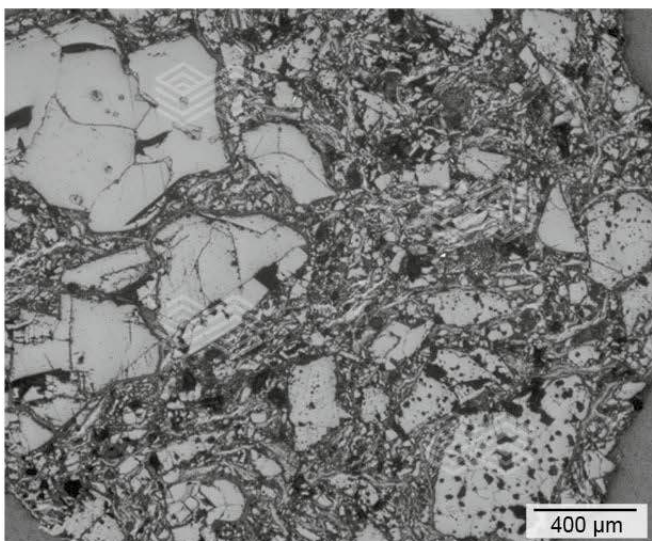
Aluminium carbide measurement device.

**Figure 6.**

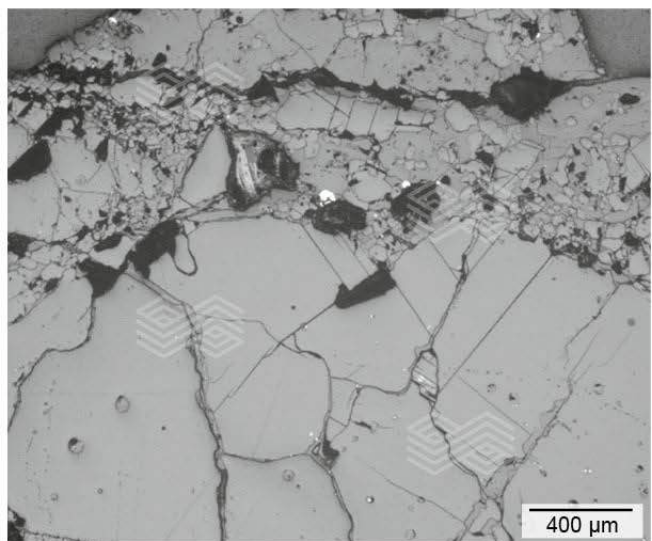
Novel carbide stabilisation device under implementation.

**Figure 7.**

Proof of concept for separation techniques. (a) high carbon containing particle and (b) fused magnesia particle.



(a)



(b)

Currently, this is mostly performed using a weathering process, which is achieved by spraying water over a brick pile and waiting for several months before recovering the material. In addition to the long processing time, process quality control is not possible using commercially available testing methods. Therefore, RHI Magnesita R&D worked on both fronts, developing a novel carbide measurement device (Figure 5) and an innovative stabilisation process (Figure 6) [7]. The carbide measurement can quantify the process efficiency, ensuring the final product quality delivered to customers is guaranteed [8].

Alternatives to the weathering process were developed by RHI Magnesita to reduce the processing time, operational costs, and footprint necessary for production ramp up. Moreover, these novel processes ensure the stabilisation efficacy since it is possible to have a real-time measurement of the carbide transformation. This new processing already has a prototype in the ramp-up stage at RHI Magnesita's recycling plant in Brazil, reducing the processing time from 3 months to approximately 12 hours.

Grain separation

A defined goal in RHI Magnesita's technology roadmap is the effective fragmentation of used bricks to enable recovery of the original raw materials, theoretically removing any constraints for achieving full circularity. Therefore, RHI Magnesita is dedicating time and research on the liberation and separation of the original raw materials from spent refractories. The R&D centres from different regions are working on proof of concepts and prototypes to test different technologies. Promising results, as illustrated in Figure 7, have already been observed, such as separating high carbon containing grains from fused magnesia aggregates in magnesia-carbon recycling.

Product carbon footprint

Another important innovation introduced by RHI Magnesita to the refractory market is reporting the carbon footprint of its products (see page 39). This transparency to customers is key to foster the selection of low carbon footprint products as well as to lead industry awareness and encourage partnerships with customers for circular business models. Figure 8 illustrates the section of a technical datasheet presenting the carbon footprint of a cement refractory brick.

Impact of Innovation, Strategy, and Business Models

Due to the clear strategy to ramp up recycling utilisation, targeting a lower carbon footprint intensity, RHI Magnesita has been able to constantly increase its recycling rate. In 2022, the company already reached the target set for 2025, replacing at least 10% of the virgin raw materials with circular minerals. Figure 9 shows the evolution of RHI Magnesita's recycling rate compared to the values published by the second largest refractory producer [1,9]. By reaching a recycling rate of 10.5%, RHI Magnesita avoided landfilling approximately 150000 tonnes of spent refractories and 300000 tonnes of CO₂ emissions.

Conclusions

RHI Magnesita has a strong commitment to sustainability, with defined targets and a recycling strategic initiative to reduce the carbon footprint of refractory products. However, developing significant recycling utilisation depends on overcoming various challenges including sourcing, logistics, legislation, processing, marketing, and product design.

Figure 9. Recycling rate evolution of RHI Magnesita compared to the second largest refractory producer [1,9].

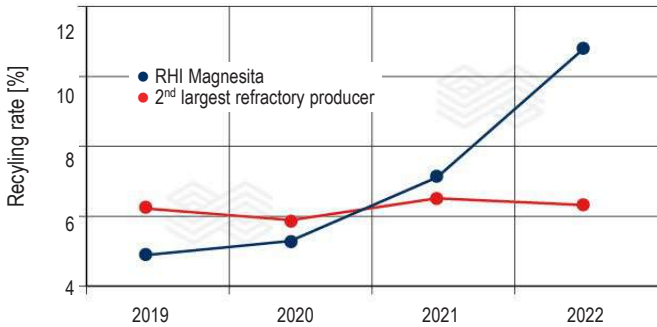


Figure 8. Technical data sheet detailing the product carbon footprint.

ANKRAL R1

General Information		
Classification	Magnesia-spinel product type MSp80 ISO 10081-2	
Main raw material components	High grade sintered magnesia, high purity sintered magnesia, MA-spinel	
Bonding type	Ceramic	
Type of brick	Fired	
Mortar to use	ANKERFIX NS60	
Environmental Indicators		
Product carbon footprint	2.211 [lt. CO ₂ e/t prod.]	ISO14067
The carbon footprint of the product (CFP) has been calculated following the principles of ISO14067		

Therefore, RHI Magnesita has been actively developing strategies and technologies to constantly, and significantly, increase the adoption of circular products.

For the recycling sourcing, partnerships are being established with customers to improve the quality of dismantling and material separation. Additionally, RHI Magnesita is working with recycling processors to expand the supplier pool and set up a joint venture with Horn & Co. Group, founding MIRECO as a key player in the European market.

Recycling sorting is a key technology to be explored and improved. ReSoURCE is a European Union funded consortium that is led by RHI Magnesita to address automated sorting techniques, targeting quality improvements and yield of separation. The main goal is to develop sensors specifically developed for the refractory recycling challenges, overcoming the limitations of off-the-shelf devices. Important advancements have also been achieved for contaminant stabilisation and quality control. For example, a new analytical method for aluminium carbide quantification was developed as well as novel process techniques for its stabilisation.

Longer-term developments are also included in the recycling technology roadmap, with techniques being explored to liberate and separate raw material aggregates from the matrix of recycled refractories. On the one hand this is a challenging approach, but on the other hand success in this area would remove several bottlenecks for recycling utilisation.

RHI Magnesita's strategy and focus on sustainability topics, taking advantage of the expertise of the R&D centres and process experts worldwide, is already bringing benefits and a record recycling rate of 10.5% was achieved in 2022. This value represents a landfilling reduction of around 150000 tonnes of used refractories and avoiding CO₂ equivalent emissions close to 300000 tonnes.

References

- [1] RHI Magnesita 2022 Sustainability Report. <https://ir.rhimagnesita.com/wp-content/uploads/2023/03/42705-rhi-sustainability-report-2022-web.pdf>
- [2] Moraes, M.N., Nogueira, G.G.R. and Silveira, F.T. Desafios Técnicos no Processamento de Reciclados. 42nd Alafar Conference Proceedings. Foz do Iguaçu, Brazil, November 7–12, 2022.
- [3] Strubel, S. *Developing a Model to Calculate the Carbon Footprint of Refractory Products*, Master's thesis, Leoben University, Austria, 2012.
- [4] Moraes, M.N., Nogueira, G.G.R., Lopez, M., Silveira, F.T. and Bonadia, P. Refractories Recycling—Challenges and Opportunities in a Path Towards CO₂ Footprint Reduction. 4th EMECR - International Conference on Energy and Material Efficiency and CO₂ Reduction in the Steel Industry Conference Proceedings. Sao Paulo, Brazil, June 7–9, 2022, 1–9.
- [5] Schutte, M. Refractory Recycling Earning Your Environmental Brownie Points. The Southern African Institute of Mining and Metallurgy Refractories 2010 Conference Proceedings. Johannesburg, South Africa, March 16–17, 2010, 75–86.
- [6] Leitner, A. Innovating Refractory Recycling – A Technology Review with Focus on ReSoURCE. Mineral Recycling Forum Proceedings. Dubrovnik, Croatia, March 28–30, 2023.
- [7] Heid, S., Leitner, A. and Königshofer, S. Innovative Aluminium Carbide Detection and Treatment Technologies to Increase Magnesia-Carbon Recycling. *Bulletin*. 2022, 11–16.
- [8] Niedermayer, S. and Ellersdorfer, M. Combination of Autoclave Treatment and NDIR Process Analytics for Quantification of Aluminum Carbide in Powder Samples. *Analytica*. 2022, 3, 106–199.
- [9] Vesuvius plc Sustainability Report 2022. https://www.vesuvius.com/content/dam/vesuvius/corporate/Sustainability/2023-update/Vesuvius_SR22_Interactive_FINAL.pdf

Authors

Matheus Naves Moraes, RHI Magnesita, Contagem, Brazil.

Alexander Leitner, RHI Magnesita, Leoben, Austria.

Gustavo Nogueira, RHI Magnesita, Contagem, Brazil.

Barbara Zocratto, RHI Magnesita, Rotterdam, Netherlands.

Stefan Heid, RHI Magnesita, Leoben, Austria.

Juergen Mühlhäußer, RHI Magnesita, Leoben, Austria.

Corresponding author: Matheus Naves Moraes, Matheus.Naves@rhimagnesita.com



Michael Joos-Bloch, Laura Rechberger, Christian Haider, Wagner Moulin-Silva, Johannes Wucher and Thomas Drnek

Product Carbon Footprint of Refractory Products

The refractory industry is part of the most CO₂-intensive value chains in the global economy and increasingly final customers are requesting the decarbonisation of these value chains (e.g., automobile production and construction industry). Therefore, final producers must report not only their direct CO₂ emissions but all CO₂ emissions inherent to their product. A product carbon footprint (PCF) provides greenhouse gas (GHG) information of a product from cradle-to-gate and is an important input to customer industries to declare their products' carbon footprint accurately. RHI Magnesita is the first refractory producer to implement a PCF on the technical data sheets of nearly all its products. To achieve this milestone, a quantification approach for the product-specific carbon footprint was defined and executed by a cross-functional team. The article aims to illustrate this approach, its implementation, as well as the limitations and way forward. Furthermore, a case study of a basic mix is presented to show the specific source and percentage of GHG emissions in a cradle-to-gate PCF.

Introduction

The climate crisis is affecting most parts of the world and global emissions are reaching record levels every year. At the same time, society as a whole and stakeholders are gaining an ever better understanding that urgent actions are imperative. The global cement and steel production—RHI Magnesita's key customer groups—cause approximately 14% of the global energy- and process-related emissions [1], types of emissions that are responsible for around 75% of global greenhouse gas (GHG) emissions [2]. This puts the steel and cement industry value chain under great pressure to be transparent and take meaningful actions to reduce their emissions.

Currently, GHG emissions from refractory materials contribute less than 1% of the total emissions in steel production according to an internal RHI Magnesita estimation. However, with the increasing drive towards green steel, this share will increase and put stronger focus and pressure to reduce the GHG intensity of refractories. RHI Magnesita has taken meaningful initial steps to reduce the GHG intensity of its products by becoming more circular and using secondary raw materials (i.e., 10% use of secondary raw materials in 2022). Additionally, in 2022 RHI Magnesita introduced product carbon footprint (PCF) information as a standard on its technical data sheets to increase climate transparency for its customers.

The PCF is a way to show the GHG emissions in direct relation to a product. A PCF is a life cycle environmental impact assessment focusing on the so-called "global warming potential" of a product expressed in tonnes of CO₂ equivalent (CO₂e) [3]. Typically, the PCFs are either cradle-to-gate or cradle-to-grave. Cradle-to-gate covers all GHG emissions from upstream sources and the direct manufacturing of a product. Commonly, this includes mining, raw material processing, transportation, and production of the product. Cradle-to-grave also considers transportation to the customer, emissions from product use, and emissions at the end of a product's life (e.g., from incineration or landfilling of the used product and transportation for disposal) [4].

In the refractory industry, RHI Magnesita is the first refractory producer providing PCFs systematically for most of its products as part of the standard product information on the technical data sheet. While the majority of refractory producers do not provide any product-specific GHG information, the first competitors have published PCF information as part of a complete environmental impact assessment but only on a selective basis for certain products. In the wider industry, front-runners have already created a comprehensive PCF portfolio (e.g., BASF in the chemical industry [5]).

Calculation Approach

Calculation of the PCF for RHI Magnesita products follows the principles of ISO 14067 (Greenhouse gases — Carbon footprint of products — Requirements and guidelines for quantification):

- Relative approach and functional or declared unit: To calculate the PCF of a product a reference unit is required. The declared unit for calculating the PCF of a refractory product is one metric tonne of refractory product.
- Relevance and completeness: The chosen approach to calculate the PCF must be appropriate to determine the relevant GHG emissions arising from the examined product and must be complete to cover significant emissions.
- Consistency and accuracy: The approach must be consistently applied for all products covered and results must be as accurate as possible.
- Transparency: Assumptions, data sources, as well as shortcomings and limitations must be transparently documented and disclosed.
- Life cycle perspective.

The defined life cycle is from cradle-to-gate. This means that all relevant emissions in the production of a refractory product and its precursors, as well as operating supplies must be considered. For refractory products from RHI Magnesita this entails its own raw material production including mining and sintering, as well as the actual

refractory production (Figure 1). Indirect emissions from precursors include purchased raw materials and resale goods as well as inbound and intra-company transport. Additionally, indirect emissions of fuels (e.g., from methane emissions at natural gas mining sites) and electricity consumed at RHI Magnesita’s operations are relevant emission sources. Downstream emissions such as transport from RHI Magnesita to the customer or GHG emissions from refractories at the customer are not considered as they are customer specific. From a customer perspective, the scope of the PCF covers upstream scope 3 emissions of refractory products excluding the transport from RHI Magnesita to the customer site. From a RHI Magnesita perspective, the PCF covers indirect upstream scope 3 emissions, indirect electricity emissions (scope 2), and direct emissions (scope 1).

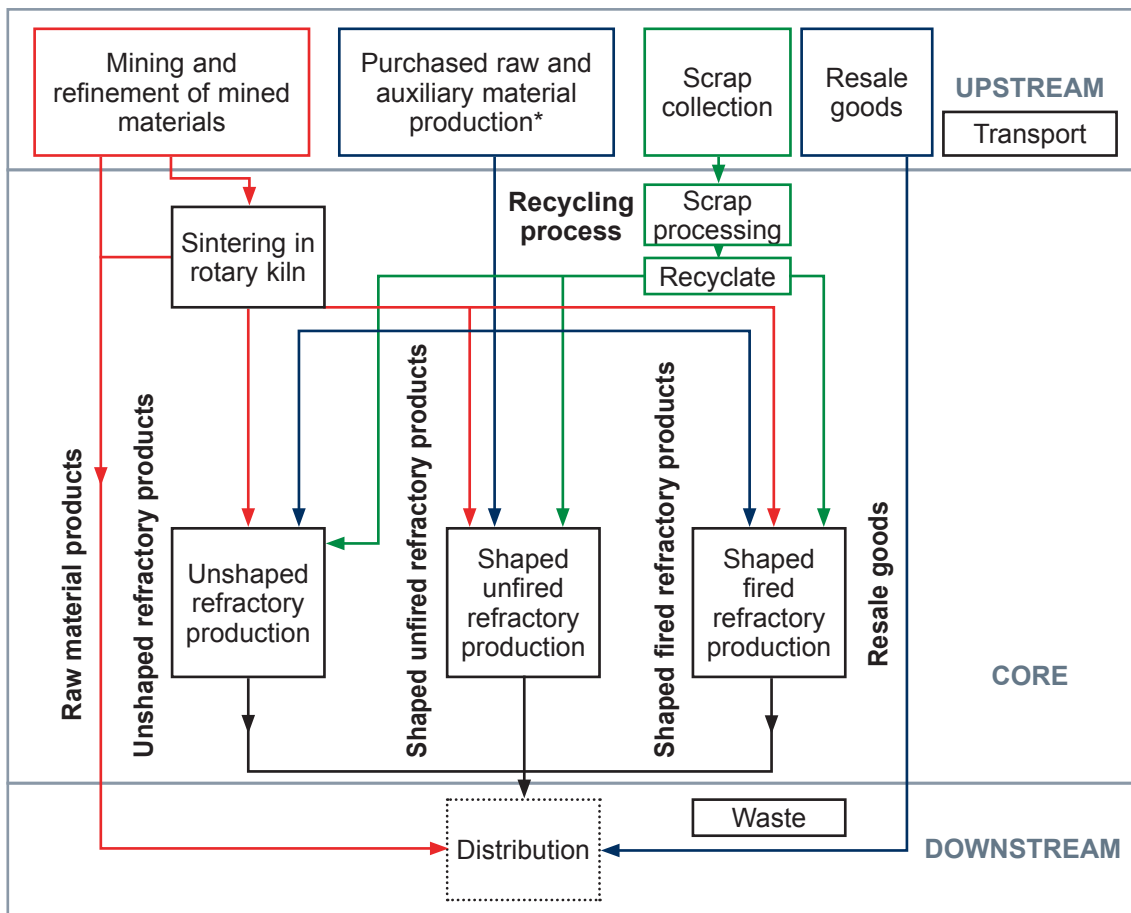
These scopes refer to a RHI Magnesita company perspective, if not stated differently. Scope 1 refers to direct emissions of an organisation (e.g., combustion of fuels), scope 2 refers to indirect emissions of an organisation directly associated with the provision of energy (e.g., emissions from a coal electricity power plant), and scope 3 refers to other indirect emissions upstream or downstream of an organisation (e.g., purchased raw materials and third-party transport).

The PCF is calculated and available for nearly all RHI Magnesita’s refractory products. Other products such as digital tools and services are outside the scope. For all products, product-specific direct emissions (scope 1), and product-specific indirect emissions are included (scope 2 and scope 3 from purchased raw materials). Additionally, indirect emissions in direct relation to the production process but where allocation is not possible on a product or plant level are added to each product-specific emission using an average value (i.e., overhead emissions). These overhead emissions include emissions from fuel-and-energy-related activities, upstream transportation and distribution, as well as waste generated in operations.

Specific raw material emissions depend on the actual raw material used and production processes. The carbon footprint of raw materials includes mining and production of the raw materials. In the case of carbonate raw materials, geogenic process emissions are also considered. The CO₂ footprint data of purchased raw materials is currently not available in a systematic way for each specific purchased raw material. To be able to reflect the GHG footprint of purchased raw materials, these were grouped in raw material categories. For purchased raw materials, one emission factor per raw material category (e.g., fused magnesia) is used to reflect the most plausible production

Figure 1.

Flow diagram illustrating the processes included in the product system to manufacture refractories, divided into upstream, core, and downstream processes.



* Including semi-products for own raw material production

- RHI Magnesita raw materials
- Purchased goods and raw materials
- Scrap
- Optional process

process (e.g., fuel used and electricity mix) based on the best available information. The sources include emission factors provided by suppliers, information from the literature or databases, estimations based on raw material production processes, and RHI Magnesita's internal expertise in raw material processing. As a fallback for raw materials where no plausible quantification approach could be identified, a generic emission factor of 1.8 tonne CO₂e per tonne of raw material is taken. This value was defined by expert judgement as a plausible average for refractory raw materials.

The calculated PCF of products consists of various elements with varying levels of granularity:

Raw materials

- Raw material category that is specific for purchased raw materials (e.g., fused magnesia).
- Plant-specific raw material category that is specific for raw materials produced by RHI Magnesita (e.g., dead burned magnesia mined and produced by RHI Magnesita's Breitenau plant).
- Specific quantities of each raw material in the recipe.

Processes to convert raw materials into a refractory product

- Plant-specific and product-group-specific (e.g., magnesia-carbon bricks from plant Veitsch). The exception is functional products where it is without plant-specific data.

Indirect emissions from transportation, energy generation, and waste disposal

- Average value across all products.

The value of a PCF for a finished refractory product is calculated according to the following formula:

(Recipe x GHG emission factors of the used raw material categories) + GHG emissions from the conversion processes per main product group and production plant + Average scope 3 overhead emissions

For resale refractory products, which are purchased from third-party refractory producers, a generic PCF is calculated. However, assumptions have to be taken regarding the product recipe, which results in increased uncertainty, as suppliers are currently not able to provide information on the carbon footprint of their refractory products.

Implementation of the Product Carbon Footprint on Technical Data Sheets

RHI Magnesita's technical data sheets are generated using product information in the SAP quality management system. Following the definition of CO₂ emission factors for raw material categories, a new data field in the SAP master data was created for the raw-material-specific emission factor. All raw materials were manually updated by a group of experts from R&D, Sales, and the Environment & Energy departments. In parallel, the Product Master Data team created and implemented a new SAP module to calculate the emissions of specific recipes based on master data emission factors. The calculation reflects the production of equivalent products at different plants considering plant- and main product-group-specific conversion-related CO₂ emissions by weighted average. Additionally, generic overhead emissions for transport, upstream energy emissions, and emissions from production waste are added.

Emissions from raw materials constitute by far the biggest part of the PCF for refractories (see the case study of a basic mix below). Therefore, special attention was given to the emission factors of raw materials. In a perfect world, supplier data would be used. However, while for some materials the supplier data are available, the majority of emission factors for third-party raw materials are either based on literature values or in-house calculations reflecting the raw material production process. In the case of internally sourced raw materials, plant-specific data is used. Around 50% of raw materials are internally sourced, mostly dead burned magnesia and doloma.

A special case are emission factors for secondary raw materials (recycling materials) and internal reclaim that is recycled as raw materials. For externally sourced secondary raw materials an emission factor of 0 tonne CO₂e/tonne is assumed as in most cases the secondary raw material processing involves very little energy and associated transport is addressed in the generic overhead emissions. Based on the insights gained from MIRECO, the RHI Magnesita and Horn & Co. Group minerals recovery joint venture, this emission factor will be adapted to actual values but will still be very low. The emission factor for internal reclaim is calculated on the basis of an economic allocation approach reflecting the economic value of internal reclaim relative to the virgin raw material value.

Uncertainty

Uncertainty of the PCF strongly correlates with the share of third-party raw materials in the recipe (Table I). Products with a high share of raw materials produced by RHI Magnesita have a low uncertainty—which comes from the generic overhead reflecting transport and indirect fuel-related emissions. In contrast, products with a high share of purchased raw materials have a significantly higher uncertainty due to uncertainties associated with the fuels used for production (e.g., coal or natural gas), process efficiencies, and the carbon intensity of any electricity used (particularly relevant for all fused products). Uncertainty is also high for resale goods, because not knowing the precise product composition increases uncertainty.

Data Maintenance

Having rolled out the PCF on technical data sheets, the data need to be maintained. This covers newly added raw materials, new refractory products, and maintenance of existing data. To reflect the latest emission data (e.g., conversion emissions on a plant main product group level) and improved data quality (e.g., supplier-sourced emission factors for third-party raw materials), CO₂e data is reviewed annually. Active supplier engagement to gain primary CO₂e data on third-party raw materials will contribute to the continuous improvement of the overall data quality and will reduce uncertainty.

Case Study—Basic Mix

To illustrate the varying sources of GHG emissions contributing to the PCF, a case study with a basic mix is presented. The product is a basic ramming mix produced in

Austria and used in the hearth of electric arc furnaces. Figure 2 shows the emissions considered in the calculation and their share in the PCF. Around 90% of the emissions result from the raw material production. The majority are internally produced (i.e., mining and sintering) and a minor part comes from third-party purchases (i.e., purchased raw materials). As the product is an unshaped mix, the raw materials do not require any additional firing or tempering. This is reflected in the barely visible production contribution. Upstream emissions and transport are generic overhead values reflected as a company average. The total PCF of the basic mix is 1.74 tonne CO₂e per tonne of product.

Table II illustrates the high impact of direct emissions from

Figure 2.

Source and percentage of GHG emissions in the basic mix PCF.

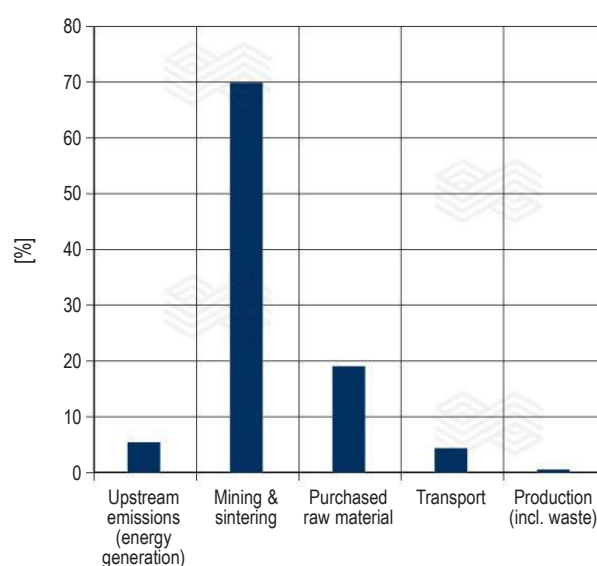


Table I.

Uncertainty assessment of data used to calculate PCFs (1 = low and 5 = high). A standard life cycle assessment uncertainty approach was used to generate the data [6].

Primary/secondary data	Data set	Flow reliability	Completeness	Temporal representativeness	Geographical representativeness	Technical representativeness	Average
Primary data	Recipe	1	1	2	1	1	1.2
Secondary data	Upstream transport emissions	3	1	2	5	3	2.8
Primary data	Raw material emission factor from own operations	2	1	1	1	1	1.2
Primary data	Conversion	2	1	1	1	1	1.2
Primary data	Production quantity (per site)	1	1	1	1	1	1.0
Secondary data	Energy scope 3	2	2	2	2	3	2.2
Secondary data	Waste	3	1	4	4	5	3.4
Secondary data	Emission factor for purchased raw material	3	2	2	2	3	2.4
Secondary data	Refractory resale goods	3	4	4	3	5	3.8

the process (i.e., nonfuel related) as the raw material is a carbonate ($MgCO_3$) and approximately 50% of the mined raw material decomposes to CO_2 . As all Austrian operations consume green electricity there are no electricity-related emissions.

In the case study, product uncertainty mainly comes from the generic overhead emissions (e.g., energy production and upstream transportation), which is not surprising as these are average values applied to all products (Table III).

Limitations

RHI Magnesita's implementation of PCF information on its technical data sheets is a step change in climate transparency that required significant effort from several departments in the company. At the same time, it is clear that this is a first step and more needs to follow to address the limitations of the current approach.

By far the biggest limitation is uncertainty in the data. The high share of indirect emissions in the PCF (on average around 50%), in conjunction with the limited availability of supplier-specific data, mark a major limitation with regard to

accuracy. This implies that current PCF values provide important indicative information but can only be used as a basis for purchasing decisions to a limited extent. However, the vertical integration of RHI Magnesita brings a unique value for the end-user in reducing the uncertainty of the calculated PCF for refractory materials.

A second source of uncertainty is the average data used for transportation and fuel generation emissions. The generic nature of these data adds relatively little uncertainty to GHG intensive products but for low carbon products, with a high share of secondary raw materials, it creates a very high overall uncertainty.

Thirdly, resale products where RHI Magnesita operates as a trader not as a producer, have the highest uncertainty because all reported emissions are indirect emissions and suppliers currently cannot provide PCF data. All these limitations, but in particular the very high uncertainty associated with resale products, prevent a third-party assurance of RHI Magnesita's PCF approach at the moment.

The Way Forward

Having highlighted the limitations of the current PCF on technical data sheets, the way forward is very clear: First and foremost, supplier engagement is key. Therefore, RHI Magnesita is reaching out to key suppliers to inform them about our initiative and their role in providing high-quality PCF information. This is happening in a highly dynamic setting where final customers are asking for climate transparency and low carbon products. So, the whole value chain in which RHI Magnesita operates is moving in the same direction towards increased transparency. This means that within a few years the uncertainty in relation to indirect emissions should significantly decrease.

At the same time, RHI Magnesita's ability to generate and process climate-related data is continuously evolving at a high pace. This will result in moving from generic transport emission data to plant-specific or even more granular transport emission data.

Table II.

Source and proportion of GHG emissions in the basic mix PCF highlighting the significant impact of geogenic process emissions (red: $\geq 5\%$, yellow: $< 5\%$ to $\geq 1\%$, and green: $< 1\%$).

Source	GHG emissions [%]
Upstream energy production	5.4
Purchased raw material	19.2
Scope 1 fuel (raw material)	24.5
Electricity	0.0
Scope 1 direct process emissions	45.8
Internal scrap	0.2
Upstream transportation	4.5
Fuel (basic mix production)	0.2
Waste	0.2

Table III.

Uncertainty assessment of the basic mix PCF data.

Source	PCF [tonne CO_2e]	GHG emissions [%]	Maximum deviation range [+/-]	Uncertainty origin
Upstream energy production	0.094	5.4%	22%	Emission factors
Purchased raw material	0.335	19.2%	31%	Unknown fuel usage and process
RHI Magnesita raw material	1.229	70.5%	3%	Recipes and emission factors
Conversion	0.004	0.2%	5%	Emission factors
Upstream transportation	0.078	4.5%	77%	Use of generic data
Waste	0.003	0.2%	21%	Generic calculation approach
Total	1.743	100%		
Weighted average			16%	

The biggest step ahead is establishing a unified approach to calculate PCFs across the entire refractory industry, thereby enabling an accurate comparison of PCF data from other refractory producers. However, this requires a major refractory industry alignment to define calculation and reporting approaches. So-called product category rules are industry-specific for PCF calculations and currently product category rules do not exist for refractories. PCFs calculated on industry-specific product category rules and external verification of provided data will be the basis for making GHG intensity a purchasing-relevant aspect for refractories.

Conclusion

As refractories are part of very GHG-intensive value chains and their production is GHG-intensive, transparency and meaningful actions to reduce refractory PCFs are vital. The PCF makes GHG emissions of a specific product transparent and RHI Magnesita is the first refractory producer to implement the PCF as standard information on its technical data sheets, considering its own and third-party raw materials, conversion, and other relevant indirect emissions. Current limitations with regard to uncertainty in certain areas are expected to significantly decrease in the near future making the information even more purchasing relevant.

References

- [1] International Energy Agency. The Challenge of Reaching Zero Emissions in Heavy Industry: <https://www.iea.org/articles/the-challenge-of-reaching-zero-emissions-in-heavy-industry>
- [2] Ritchie, H., Roser, M. and Rosado, P. CO₂ and Greenhouse Gas Emissions; <https://ourworldindata.org/co2-and-greenhouse-gas-emissions>
- [3] ISO 14067— Greenhouse Gases — Carbon Footprint of Products — Requirements and Guidelines for Quantification.
- [4] Cradle-to-Gate: What is it & How does it work in LCA? <https://ecochain.com/knowledge/cradle-to-gate-what-is-it-how-does-it-work-in-lca/>
- [5] BASF Product Carbon Footprint. <https://www.basf.com/global/en/who-we-are/sustainability/we-drive-sustainable-solutions/quantifying-sustainability/product-carbon-footprint.html>
- [6] <https://denkstatt.eu>

Authors

Michael Joos-Bloch, RHI Magnesita, Vienna, Austria.

Laura Rechberger, RHI Magnesita, Leoben, Austria.

Christian Haider, RHI Magnesita, Leoben, Austria.

Wagner Moulin-Silva, RHI Magnesita, Leoben, Austria.

Johannes Wucher, RHI Magnesita, Vienna, Austria.

Thomas Drnek, RHI Magnesita, Leoben, Austria.

Corresponding author: Michael Joos-Bloch, Michael.Joos@rhimagnesita.com



Florian Kek, Francisco Lopez, Marcus Kirschen, Paulo Souza and Patrick Stahl

Sustainable Slag Engineering in the Basic Oxygen Furnace Using Circular Metallurgical Additives and Modelling Tools

As recycling has a significant impact on decarbonising the refractory industry, RHI Magnesita is pursuing various initiatives to increase reusing refractory products. This includes establishing MIRECO, the key partner for a circular supply chain. In general, reclaimed refractory material comprises two categories: Pieces that are >80 mm and a fine fraction, which accounts for ~40%. Although in the last years efficient practices have been developed to process the larger material and incorporate it into new refractory products, currently it is uneconomical to sort the fines. Therefore, approaches to sustainably utilise this material, which has historically been landfilled, are integral for the recycling strategy. This paper describes one of the most important ways to valorise this fine material in the steelmaking industry, namely as circular metallurgical additives. Since the carbon footprint of these additives can be <10% of commonly used slag formers, using this material contributes to a steel plant's sustainability goals. To maximise the advantages of applying circular additives, RHI Magnesita can also provide metallurgical consulting and slag engineering tools. To illustrate these services, the article focuses on specific e-tech modelling tools available in the Customer Portal for basic oxygen furnace (BOF) slag optimisation, which are based on isothermal stability diagrams that combine MgO solubility at a specific basicity and temperature. A real case scenario is also provided to highlight the numerous benefits that can be achieved when circular metallurgical additives are applied in the BOF.

Introduction

The extraction and processing of refractory raw materials are both energy intensive and can cause geogenic emissions, resulting in savings of approximately 2 tonnes of CO₂ equivalent (CO₂e) emissions for every tonne of refractory material recycled [1]. Therefore in 2022, to support decarbonisation initiatives, RHI Magnesita's recycling activities were integrated with Horn & Co. Minerals Recovery, under the company name MIRECO [2]. While the current annual recycling stands at 160000 tonnes, this joint venture is pivotal for RHI Magnesita's sustainability strategy of increasing recycling utilisation, with a target of achieving 270000 tonnes per year by 2026. After use, spent material is dismantled and various approaches are in place to maximise the amount that can be utilised in new refractory products (see page 33). However, as a significant portion of the reclaimed material is finer than 80 mm (i.e., ~40%) and currently uneconomical to sort, it is being used for other applications, including circular metallurgical additives, rather than being landfilled with the associated costs and environmental impact.

This paper describes RHI Magnesita's ongoing initiatives to support the application of circular additives through sourcing strategies, metallurgical consulting, and slag engineering tools, with a focus on the basic oxygen furnace (BOF).

Metallurgical Additives

Metallurgical additives are integral in iron and steelmaking as the slag's chemical composition influences how it reacts with the liquid metal during refining. Slag components are divided into two groups: Basic oxides (e.g., CaO and MgO) and fluxing oxides (e.g., SiO₂, Al₂O₃, MnO, and FeO). These

compounds can be added to the slag intentionally, created through the oxidation of metallic elements in the scrap and hot metal (i.e., oxygen blowing), and/or derived from refractory lining wear. Slag engineering involves achieving the appropriate ratio of these two oxides groups required for a specific metallurgical process using additives. For example, dephosphorisation and desulphurisation reactions require CaO to be dissolved in the slag and while in the BOF CaO solubility is enhanced by FeO, in the ladle it is fluxed by SiO₂, Al₂O₃, and CaF₂. Additionally, a MgO saturated slag is necessary to prevent MgO-carbon refractory lining wear. This summary aims to illustrate the complexity of slag engineering, as well as highlight that the chemistry of metallurgical additives must be tailored to the specific process and optimised to control and/or reduce dissolution of the refractory lining.

Metallurgical additives are applied in numerous areas, from serving as MgO carriers for the sinter bed in blast furnaces to acting as fluxing agents in secondary metallurgy. They also function as slag formers in the BOF, electric arc furnace (EAF), and will be critical for future electric smelting furnace processes. Due to the diverse range of applications, more than 40 sustainable additives are currently available from MIRECO that can be customised to meet each customer's specifications and more than 45 steel plants in Europe are already using these green slag agents. In particular, integrated steel mills have a high demand for metallurgical additives as well as typically producing a substantial amount of spent refractory material. Therefore, MIRECO not only operates six European recycling plants for sorting and processing spent refractory material, but because these green additives are sensitive to freight costs, onsite steel plant solutions have also been established in Germany, with more in the planning stages.

Circular Metallurgical Additives and CO₂ Savings

The use of MIRECO’s circular metallurgical additives contributes to environmentally friendly steel production as the product carbon footprint (PCF) of these materials can be <10% of commonly used slag formers (Table I) and is detailed in the technical data sheet (see page 39). Additionally, these sustainable products are characterised by their cost competitiveness, as they do not require calcination and are not dependent on fuel price volatilities. In terms of chemistry, the MgO content protects a basic refractory lining from corrosion, while carbon is an energy source as well as a reducing and/or slag foaming agent. When compared to synthetic premelted slags, recycled alumina products have the advantage of containing accompanying oxides that lower the melting point, making them a competitive alternative for calcium aluminate slags or even a CaF₂ substitute.

As circular metallurgical additives are applied in significant quantities and with high frequency, the resulting carbon emission savings can be substantial. This is why an increasing number of steel plants are eager to adopt these sustainable additives. Nevertheless, there can be uncertainties associated with this approach including existing biases against using reclaimed materials, freight cost sensitivity, and the need for appropriate dissolution. However, laboratory and industry studies have demonstrated good solubility of circular additives in the EAF, even for MgO oversaturated slags [3].

In RHI Magnesita’s Customer Portal, refractory consumption and the associated scope 3 CO₂e emissions can be tracked in real time for individual steelmaking units and on a monthly basis (Figure 1). This digital service can also be customised to visualise the CO₂e savings that are achieved when

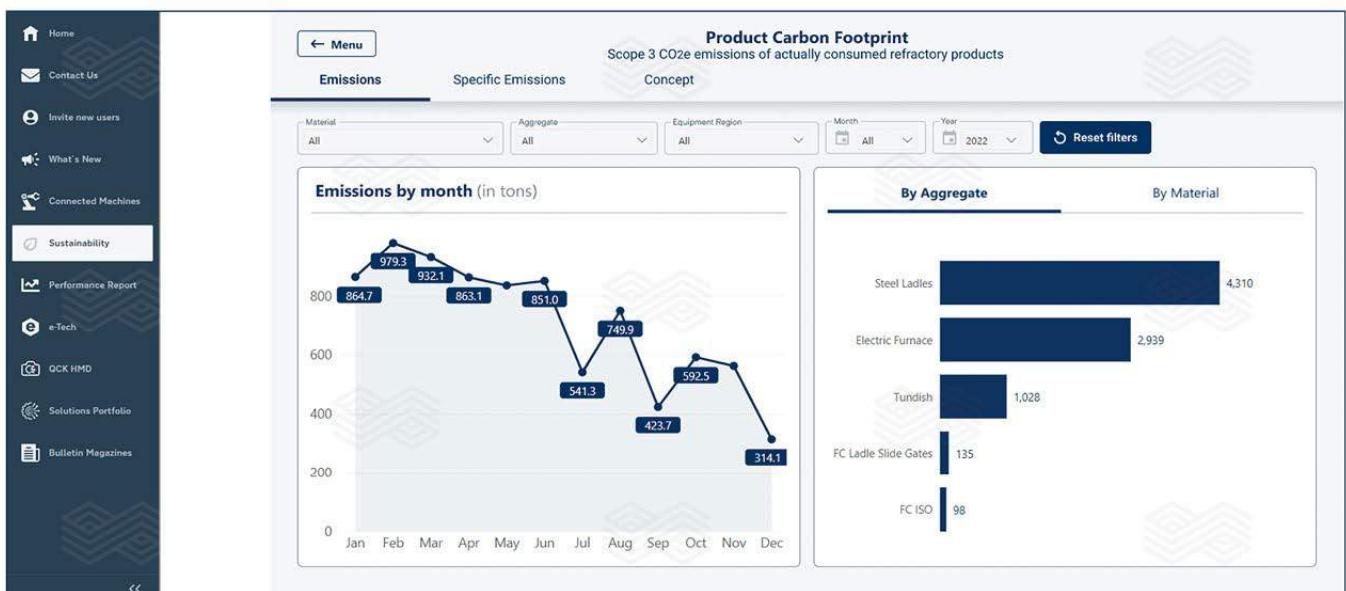
Table I.

Examples of MIRECO’s circular metallurgical additives, which can be adjusted to each customer’s specifications, and standard slag formers. Abbreviations include tonnes of CO₂ equivalent per tonne of metallurgical additive (t CO₂e/t). Figures for dolomite and lime are assumptions based on the best available technique reference documents.

	Product name	MgO [%]	CaO [%]	SiO ₂ [%]	Al ₂ O ₃ [%]	Fe ₂ O ₃ [%]	TiO ₂ [%]	C [%]	CaF ₂ [%]	t CO ₂ e/t
Basic oxides	MgO 55	55	20	5	10	5		8		0.05
	MgO 75	75	6	5	5	4		5		0.05
	MgO 80 A7	82	1.5	0.5	8	0.7				0.05
	Dolomite	35	63							1.84
	Lime	1	96							1.84
Fluxing oxides	TE 80	3	2	11	78	2.5	2	2		0.05
	TE 85	2.5		7.5	85	0.7	0.4	6		0.05
	TE 90	2.5	2.5	1.8	90	0.8	0.1			0.05
	Rehcal 10	6	15	9	55	2			10	0.05
	Rehcal 40-60	2.5	20	5	20	0.6	0.5		50	0.05

Figure 1.

The Customer Portal sustainability tracking enables scope 3 CO₂e emissions of consumed refractory products to be viewed by month and steelmaking unit.



circular metallurgical additives are being used, providing the customer with transparency regarding their decarbonisation potential. Another advantage of the Customer Portal is access to the slag modelling toolbox, known as e-tech [4,5]. e-tech streamlines and facilitates the use of circular additives by offering optimisation tools for CaO or MgO single saturation as well as dual saturation (Figure 2). In addition, there are tools for slag splashing and desulphurisation.

In summary, the diverse applications and sustainable impact on steelmaking processes makes offering circular metallurgical additives an extension beyond the typical refractory business, while complementing it. Not only is the chemistry tailored to a specific application, but customers can also be provided with a comprehensive consultancy service regarding their optimal application, including access to the e-tech slag modelling tools. This integration of circular metallurgical additives and slag engineering solutions propels RHI Magnesita further along the value chain and the aim is to serve as an interface between original equipment manufacturers (OEM) and steelmakers, to provide comprehensive process improvements and refractory life cycle management.

In the following sections the metallurgical consulting service is exemplified by describing the modelling tools available for BOF slag engineering and the benefits that can be achieved when circular metallurgical additives are used in the converter.

BOF Slag Modelling

During oxygen blowing, the addition of slag formers (e.g., lime, dolomite, dolomite, limestone, and circular metallurgical additives) to the BOF is primarily determined by the hot metal silicon content and other metallurgical considerations such as dephosphorisation, manganese levels, thermal balance, and the required tap composition. In addition, an appropriate MgO slag saturation is necessary to minimise refractory lining wear. At later stages in the BOF process, maintenance methods such as slag rocking and splashing are widely adopted to protect the lining from subsequent scrap charging and hot metal impact, as well as chemical and mechanical wear in the trunnion areas. The required slag viscosity and adhesion characteristics for these practices depend on temperature and the precipitated solid phases. When determining the amounts of additives necessary to achieve an appropriate slag chemistry for these requirements, one approach is to prioritise MgO saturation.

Several proposed models are available to calculate MgO saturation as a function of complex slag composition and temperature based on saturation experiments conducted with various metallurgical process slags [6–12], of which a number provide MgO saturation as a function of slag basicity [7,9,11]. Other approaches involve deriving saturation diagrams from published phase diagrams in the CaO-MgO-FeO-SiO₂-Al₂O₃ system [7] or utilising phase equilibrium software [13,14]. Table II provides an overview of published MgO slag saturation models for various metallurgical units.

Figure 2. e-tech slag modelling toolbox for different steelmaking applications [5].

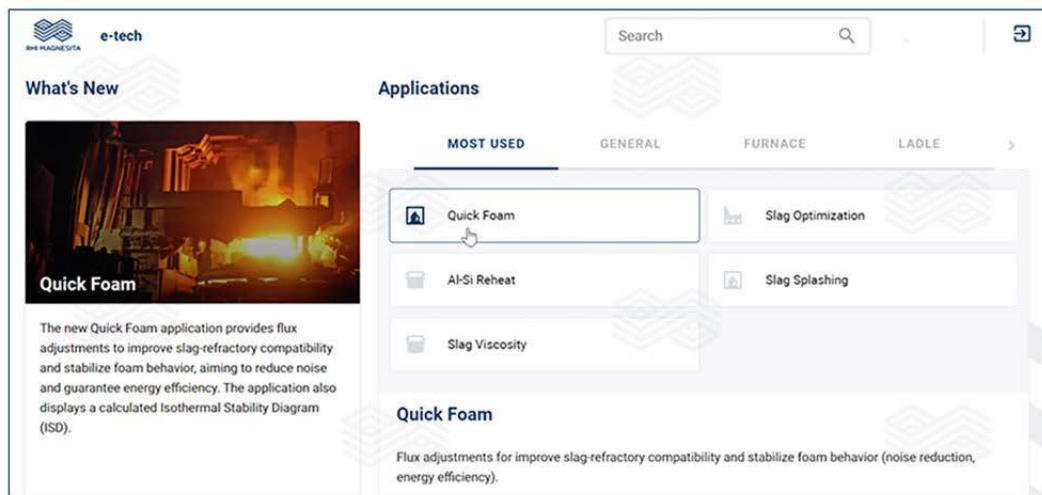


Table II. Published MgO saturation models for different steelmaking slags.

Author	Target function	Metallurgical unit	Variables
Schürmann and Kolm (1986) [8]	MgO saturation	BOF, EAF	CaO, SiO ₂ , FeO, Al ₂ O ₃ , MnO, temperature
Park and Lee (1996) [9]	MgO saturation	BOF, ladle	B3 basicity
Pretorius and Carlisle (1999) [7]	MgO (and C ₂ S) saturation	General	FeO, temperature, B3 basicity
Park (2001) [10]	MgO saturation	BOF	CaO, SiO ₂ , FeO, Fe ₂ O ₃
Tayeb, Assis, Sridhar and Fruehan (2015) [11]	MgO saturation	BOF, EAF	CaO, SiO ₂ , Al ₂ O ₃ , FeO

Isothermal stability diagrams (ISDs) combine MgO solubility at a specific basicity (e.g., B3) and temperature. They are derived from the CaO-MgO-SiO₂-FeO system [6,7] and have enjoyed widespread acceptance in the steelmaking community for several decades. Primarily used for optimising EAF and ladle slags, there are numerous case studies in the field that have substantiated the validity of these semi-empirical models. Furthermore, through FactSage simulations, involving complex slag compositions within the 6-component system CaO-MgO-FeO-SiO₂-Al₂O₃-MnO specifically tailored to real BOF slag compositions, the use of ISDs has been extended to calculating MgO saturation in BOF slags.

RHI Magnesita's e-tech software tool "Quick Foam" (also termed "Foamy Slag"), which is based on the previously described research [6,7], can be used to visualise the ISD as well as calculate the theoretical MgO saturation and other related figures for BOF slags.

Isothermal Stability Diagrams

The dependence of MgO solubility on slag basicity, temperature, and CaO-MgO-SiO₂-FeO phase relationships is used to construct the ISD [6]. Figure 3 shows the ISD of a customer's slag with a B3 of 2.6 and the stability regions of the various phases at 1660 °C. In addition to the liquid phase there are two stable solid mineralogical phases—MgO·FeO magnesiowüstite (MW) and dicalcium silicate (C₂S).

The e-tech Quick Foam application enables insights into BOF slag chemistry using the ISD. The software visualises the analysed MgO value (blue square), the calculated MgO value (green triangle), and the theoretical MgO saturation point (red dot) based on input data such as slag chemistry, additions, and temperature (see Figure 3). The calculated MgO point results from the amount and chemistry of slag formers applied.

The difference between the analysed and calculated MgO values (i.e., Δ MgO) shows the amount of MgO pickup in the slag from the refractory brick lining and gunning mix, which must be avoided. The difference between the analysed MgO value and theoretical MgO saturation point (i.e., MgO supersaturation) indicates the slag's affinity to dissolve MgO. The MgO supersaturation is positive or negative depending on whether the slag is over or undersaturated, respectively.

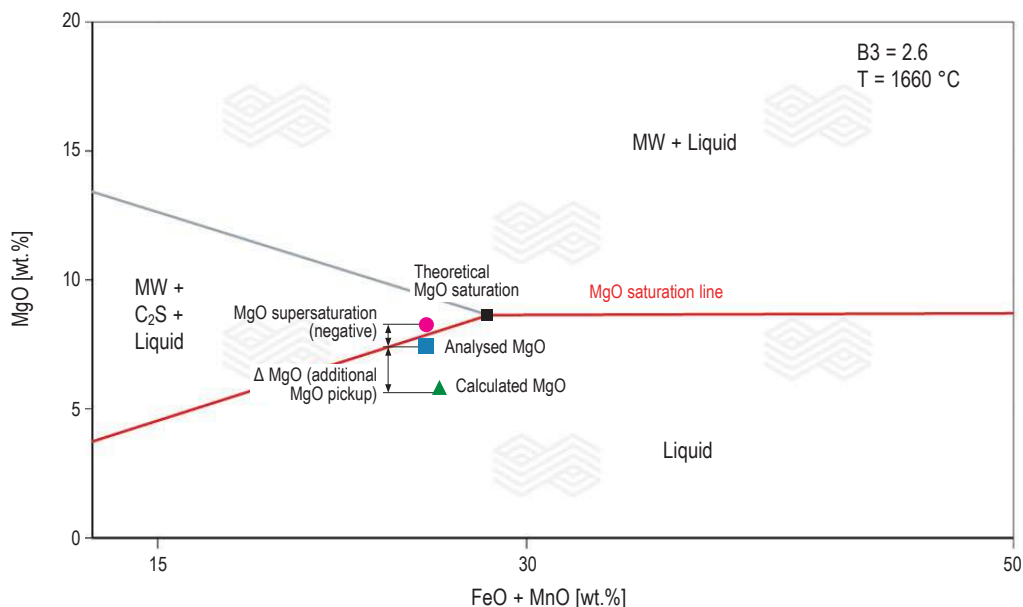
Based on the Quick Foam application, different trial scenarios for each customer's requirements can be set up and adjusted to close the gap between the analysed and calculated MgO values. This generates a slag with less affinity to dissolve MgO, thereby minimising MgO pickup from the lining and gunning mix.

BOF Slag Splashing

The most efficient approach for BOF maintenance involves adjusting the slag chemistry during the blowing process so the appropriate phases (i.e., MW and C₂S) precipitate when the BOF temperature decreases after tapping. However, there are several considerations during blowing that can make MgO saturation inappropriate at this stage. In such cases, the residual slag after tapping can be adjusted for proper maintenance using the e-tech "Slag Splashing" tool (Figure 4), which calculates the flux additions necessary for ideal slag adhesion and refractoriness. Initially, the slag's liquidus temperature at the end of blowing is determined from its chemical composition and temperature. Then the program outputs the weight of flux additions required to decrease the slag's liquidus temperature by 75 °C, thereby generating an appropriate slag viscosity for BOF maintenance as the solid phases precipitate when the temperature decreases.

Figure 3.

Example of an ISD generated with the Quick Foam application for a BOF slag with a B3 = 2.6 at 1660 °C.



Customer Application

To practically investigate the topic of BOF slag engineering using circular additives and slag modelling tools, a series of trials were conducted at a steel plant. These investigations involved the use of circular additives in both sieved and briquetted forms at various stages of the process. The trials observed the dissolution of MgO in a highly dynamic BOF slag, along with the FeO reduction capacity of carbon-containing additives. A total of 140 slag samples were collected during these trials that underwent analysis using X-ray fluorescence, X-ray diffraction, optical light microscopy, and selected samples were also examined using scanning electron microscopy with energy dispersive spectrometry. As was previously demonstrated in the study evaluating the solubility of different circular MgO materials in EAF slags [3], it was also shown that both the sieved and briquetted materials dissolved effectively in BOF slags. Furthermore, although there was an increased MgO carrier addition, the total cost of ownership (TCO) calculation revealed a six-digit annual saving in euros, which included the following advantages:

- Extension of the BOF refractory lining lifetime, resulting in lower specific refractory consumption.
- Reduced gunning mix consumption.
- Higher productivity as a consequence of the decreased gunning maintenance and reduced downtime for relining.
- Reduced lime input while retaining optimised dephosphorisation.
- Alloy savings.
- Landfilling spent refractory materials was eliminated.
- Decreased process CO₂ footprint.

Conclusion

Circular metallurgical additives deliver financial, environmental, and metallurgical benefits for steel producers, when appropriately processed and applied. Currently, MIRECO employs a large-scale circular raw material procurement and processing approach, resulting in three business cases that enable customers to take advantage of green additives (Figure 5). The first is direct sales, which targets providing customised additives for different process demands at a competitive price. With the “CERO Waste” opportunity, MIRECO offers recycling expertise such as how customers can optimally reuse their refractory fines for different metallurgical process demands and thereby reduce landfill costs as well as free up storage space. In the third option, the focus is on enhancing the steelmaking process with RHI Magnesita providing comprehensive metallurgical consulting for optimal circular additive application. For example, the slag modelling toolbox, e-tech, facilitates slag optimisation and maintenance adjustment with the Quick Foam and Slag Splashing applications performing calculations based on widely accepted and newly validated models for BOF slag engineering. Recently, a case study conducted at a BOF plant illustrated the practical applicability of circular additives in combination with slag modelling tools and resulted in financial benefits calculated from a TCO perspective.

Figure 4.
e-tech Slag Splashing tool interface [5].

Slag Splashing
The slag splash model calculates the addition of fluxes to adjust the slag to the ideal conditions of adhesion and refractoriness.

TUTORIAL | SAVED | + NEW

New Calculation 1 ×

Converter Slag Chemistry			
MgO	CaO	Fe Total	Al ₂ O ₃
10.49 %	47.76 %	19.1 %	0.28 %
SiO ₂	MnO	P ₂ O ₅	Total
11.14 %	3.58 %	2.1 %	99.92 %

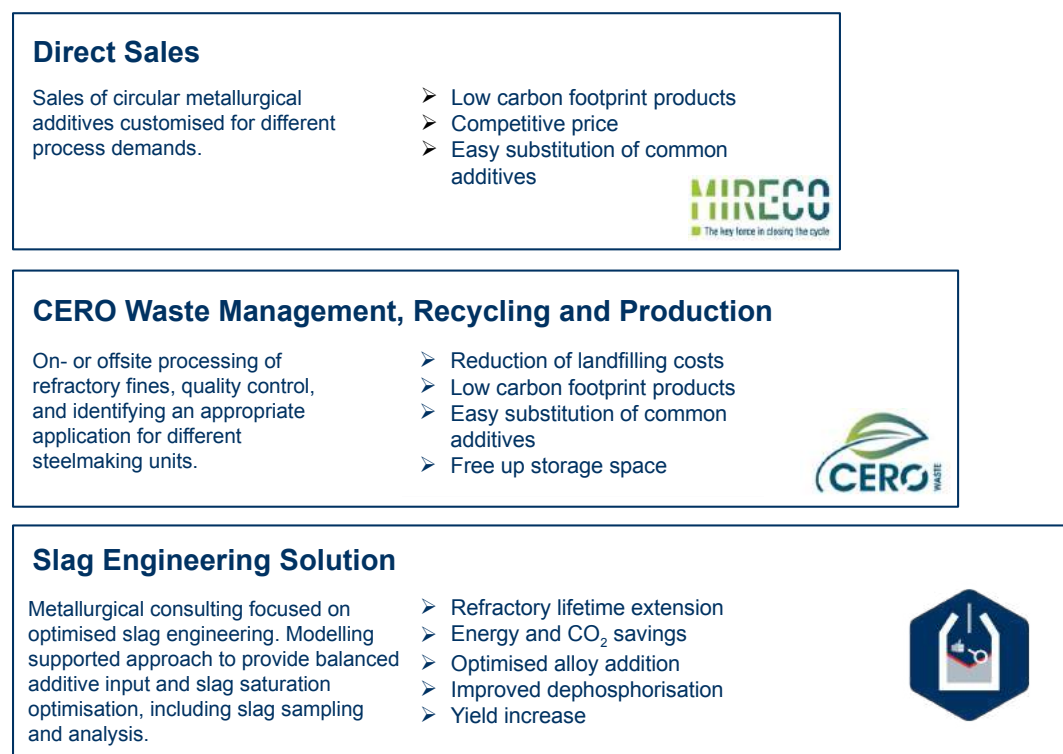
Slag Splashing Additives Proportion		
Dololime	100 %	🗑️
Material 1	0 %	🗑️
Lime	0 %	🗑️

Temperature: 1684 °C | Slag Weight: 21045 kg | Liquidus Temperature: - °C

+ ADD | EDIT ADDITIVES | DUPLICATE | CALCULATE

Figure 5.

Circular metallurgical additive business cases available for customers.



References

- [1] RHI Magnesita 2022 Sustainability Report. <https://ir.rhimagnesita.com/wp-content/uploads/2023/03/42705-rhi-sustainability-report-2022-web.pdf>
- [2] <https://www.mireco.com/>
- [3] Kek, F., Griessacher, T., Bauer, C., Zocratto, B., Krump, R. and Koubek, C. Refractory Waste to Slag Engineering Solution—Metallurgical Consulting Supports Steel Plant's Circular Economy Strategy. *Bulletin*. 2022, 21–28.
- [4] Souza, D., López, F., Moggee, H. and Lamare, C. A Toolbox of Slag Modelling and Metallurgy in Your Pocket. *Bulletin*. 2021, 72–77.
- [5] <https://etech.rhimagnesita.com/>
- [6] Pretorius, E.B. Introduction to Slag Fundamentals. Process Technology Group, LWB Refractories. <https://etech.rhimagnesita.com/>
- [7] Pretorius, E.B. and Carlisle, R.G. Foamy Slag Fundamental and Their Practical Application to Electric Furnace Steelmaking. *Iron and Steelmaker*. 1999, 26, 79–88.
- [8] Schürmann, E. and Kolm, I. Mathematische Beschreibung der MgO-Sättigung in Komplexen Stahlwerks-Schlacken beim Gleichgewicht mit Flüssigem Eisen. *Steel Research*. 1986, 57(1), 7–12.
- [9] Park, J.M. and Lee K.K. Reaction Equilibria Between Liquid Iron and CaO-Al₂O₃-MgO_{sat}-SiO₂-FeO-MnO-P₂O₅ Slag. 79th Steelmaking Conference, Pittsburgh, USA, March 24–27, 1996, 165–172.
- [10] Park, J.M. MgO Solubility in BOF Slag Equilibrated with Ambient Air. *Steel Research*. 2001. 72, 141–145.
- [11] Tayeb, M.A., Assis, A.N., Sridhar, S. and Fruehan, R.J. MgO Solubility in Steelmaking Slags. *Metallurgical and Materials Transactions B*. 2015. 46B, 1112–1114.
- [12] Jung, S.M., Rhee, C.H. and Min, D.J. Solubility of MgO in CaO-Based Slags. Procemin 2008: V International Mineral Processing Seminar, Santiago, Chile, October 22–24, 2008, 133–142.
- [13] Montecinos de Almeida, R.A., Vieira, D., Bielefeldt, W.V. and Faria Vilela, A.C. MgO Saturation Analysis of CaO-SiO₂-FeO-MgO-Al₂O₃ Slag System. *Materials Research*. 2018, 21(1), e20170041.
- [14] Khadhraoui, S., Hack, K., Jantzen, T. and Odenthal, H.-J. Study of the State of Industrial P₂O₅-Containing Slags Relevant to Steelmaking Processes Based on a New Thermodynamic Database Developed for CaO-FeOx-P₂O₅-SiO₂-MnO-MgO-Al₂O₃ Slags, Part I: Ternary and Lower Order Systems. *Steel Research International*. 2019, June, 1900085.

Authors

Florian Kek, RHI Magnesita, Vienna, Austria.
 Francisco Lopez, RHI Magnesita, Contagem, Brazil.
 Marcus Kirschen, RHI Magnesita, Mülheim-Kärlich, Germany.
 Paulo Souza, RHI Magnesita, Vienna, Austria.
 Patrick Stahl, MIRECO, Siegen, Germany.
Corresponding author: Florian Kek, Florian.Kek@rhimagnesita.com



Reinhard Ehrenguber, Verena Schmidt, Raphael Renggli and Maximilian Jani

INTERSTOP Automation, Robotics and Digitalisation Solutions for Flow Control Technology

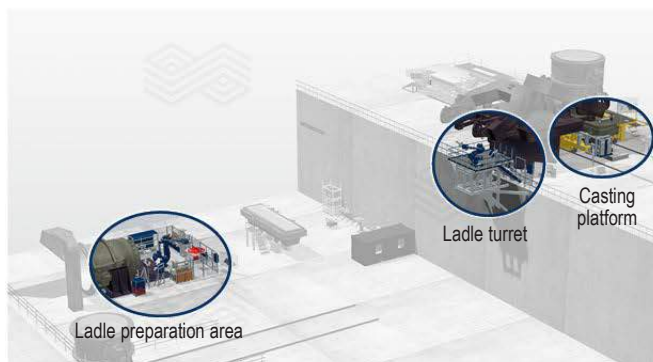
A major trend in continuous steel casting is the upgrade of flow control systems to meet new market demands. In addition to supporting clean steel production, ease of handling, and economic benefits, flow control systems must be designed to enable automatic and robotic operation. One reason for this is operator health and safety, while another is to ensure that critical process areas such as the ladle preparation area and continuous caster remain operational and become more attractive workplaces for the next generation of personnel. This article describes how INTERSTOP automation, robotics, and digitalisation solutions are setting standards in flow control and which products are now being introduced in the steel industry.

Introduction

The steel sector in general and the flow control area more specifically are undergoing a major change. In the past, a stable production process had by far the highest priority and the execution of manual activities in working areas critical for personnel due to hazardous conditions were subordinated to this. Systems were designed with handling ergonomics, clean steel support, ease of maintenance, and low operating costs in mind. However, the workers' interactions with the flow control systems and handling of the involved refractory parts play a crucial role for stability of the casting process on the continuous casting machine (CCM). Therefore, the following main tasks are being addressed by automation solutions (Figure 1):

- Inspection and maintenance of the ladle slide gate at the ladle preparation area.
- Connection of the casting cylinder and electrical plug for the slag detection system, as well as coupling shielding media like argon and/or cooling air from the ladle turret of the CCM to the ladle slide gate.
- Monotube exchange and mould powder feeding on the casting platform of a slab casting machine.

Figure 1. Areas for the INTERSTOP flow control automation solutions in the steel plant.



In recent years, the requirements for flow control systems have radically changed and technologies like robotic cells and digital tools are being adopted to perform these operations automatically. As a result, the workers' role is transformed from operator to supervisor of the robotic operation. The advantages of introducing robotic operation and digital tools in these areas are:

- Increased occupational safety as entering hazardous areas and manual handling of heavy loads are eliminated (complying with stricter safety laws).
- Precise and identical handling of the equipment and critical parts such as a heated monotube. This eliminates damage during handling or premature wear due to poor manual handling of electrical connectors for example.
- Improved decision-making leads to higher operational reliability and lower costs. The enabler for this is replacement of individual, experience-based decisions with fact-based, decision-support systems.
- Processes can be continuously improved by collecting and analysing data with algorithms. The introduction of robots into the operation and digitisation into decision-making also means that process knowledge remains available even when experienced employees retire. In addition, the digital system is able to learn by adapting its parameters to unforeseen events.
- The steel mill creates an attractive workplace where engineering skills are needed. In recent discussions with steel plant managers, it was always specifically emphasised that on the one hand it is difficult to fill the shifts due to the risk of injury and on the other hand there are hardly any young people interested in these jobs.

Therefore, INTERSTOP developed the core enablers to implement these technologies in the steel plants. These can be subdivided into:

- Automation-ready flow control systems.
- Position detection system.
- Health Check Platform.

Automation-Ready Flow Control Systems

In the past INTERSTOP systems were optimised for human operation. However, a robot works in a fundamentally different way to a human, for example it does not have two hands and can move much heavier loads with high precision. Therefore, one principle that was applied to the design of the automation-ready INTERSTOP systems is they must remain both ergonomically operable for humans and enable automated handling by robots. As a result, implementing robotic cells enables dual operation by humans and robots without interrupting operations. Furthermore, it allows quick manual intervention if the robotic cell has an operational interruption. The mechanical systems focused on were:

- INTERSTOP SX/AS ladle slide gates to enable robotic handling of the casting cylinder on the CCM, the so-called media coupler (MC), as well as robotic operation at the ladle preparation area.
- INTERSTOP MTC monotube changer ready for robotic monotube handling (MTH).

The following is a summary of these systems, which have previously been described in detail [1].

INTERSTOP SX/AS ladle slide gates

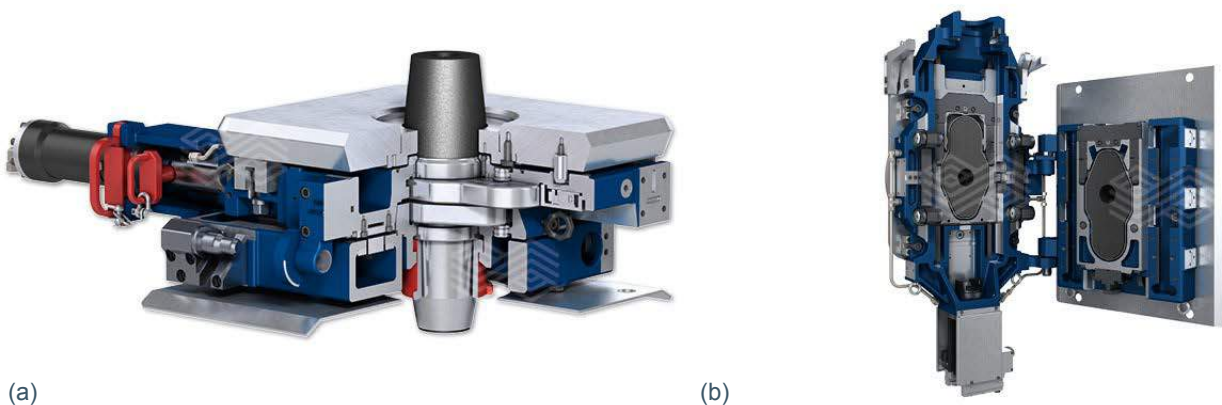
The SX ladle slide gate stands for:

- User-friendly design for fast, safe, and simple operation.
- Easy and quick handling at the preparation area.
- Low operational costs and high performance.
- Readiness for automation and robotic operation.

With the SX, several robotic operations can be performed on the CCM and at the ladle preparation area. However, to unlock the full automation potential the AS slide gate was developed that allows the robotic handling of all slide-gate-related refractory parts at the ladle preparation area (Figure 2).

Figure 2.

(a) standard SX ladle gate and (b) AS ladle gate to unlock the full automation potential at the ladle preparation area.

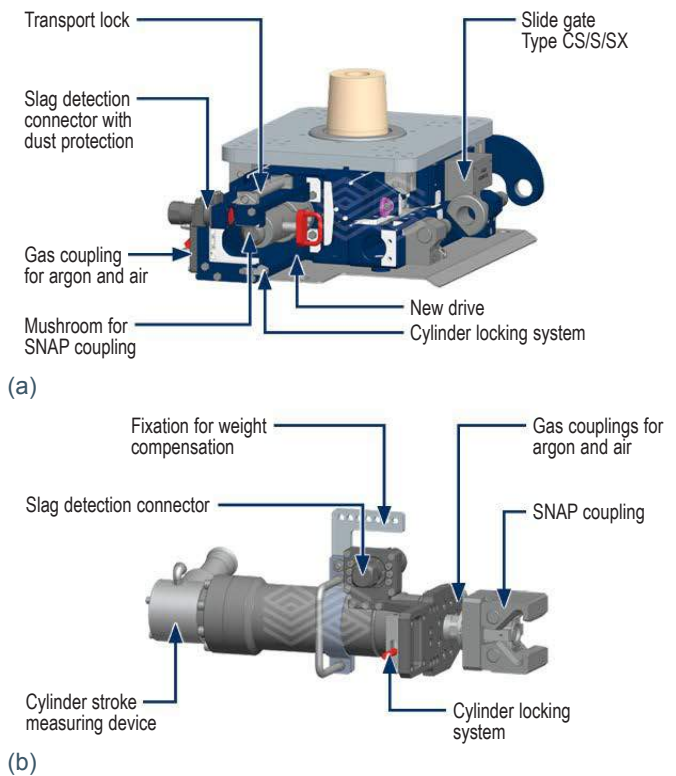


INTERSTOP media coupler

The MC ensures a quick and easy connection of the casting cylinder at the CCM to the slide gate, after the ladle is put into the loading position at the ladle turret. On the slide gate side, no parts need to be manipulated as the transport lock and cylinder locking system are activated “on the fly” by moving the cylinder in or out. This drive carries the slag connector plug as well as two pneumatic lines for cooling (e.g., compressed air) and/or sealing (e.g., argon) purposes (Figure 3a). On the cylinder side, the main features include the SNAP coupling, the cylinder locking system, slag connector plug, and the couplings for compressed air and/or argon (Figure 3b). Application of the automation-ready design on the MC has also greatly simplified manual handling, resulting in increased occupational safety and process reliability.

Figure 3.

(a) standard SX ladle gate with adapted drive for MC and (b) corresponding cylinder with integrated features for the MC operation.



INTERSTOP MTC monotube changer

The main benefits of the MTC monotube changer (Figure 4) are:

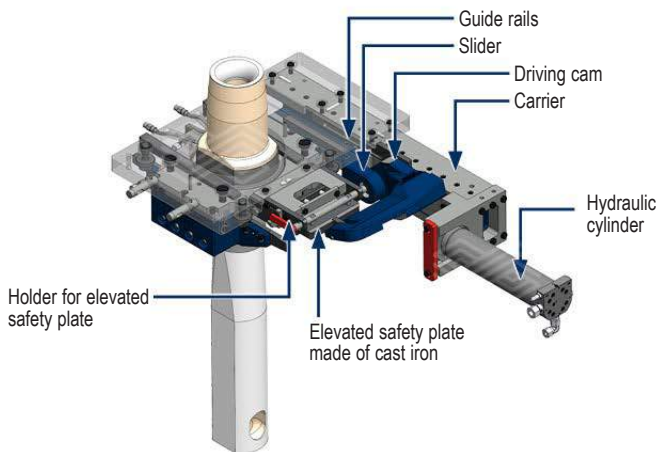
- No blind plate handling is necessary as the blind plate is integrated in the mechanics and automatically activated.
- No cylinder handling is necessary as the cylinder and drive is sideways.
- Reduced size and weight of the system.
- Readiness for automation and robotic operation.

Position Detection System

To enable a robotic operation and achieve permanent high availability, a reliable measuring system is essential. This system must ensure that the robot always receives precise coordinates of where to place the tools and the mechanical or refractory parts; the required accuracy is <1 mm for reliable continuous operation. The measuring system must also ensure that fluctuations occurring in the steel plant regarding distances between the measuring system, robot,

Figure 4.

MTC monotube changer system with the integrated safety plate and off-centre drive arrangement.



and slide gate system mounted to the ladle bottom are compensated. These fluctuations are caused, for example, by thermal expansion due to different temperatures. Furthermore, the measuring system must be immune to changes in the available light (e.g., day, night, spotlights, and sunlight through windows) as well as dust and steel splashes.

Up to now, various measuring systems have been used for flow control applications and most of them have one thing in common: The measurement reference is an externally mounted target. However, this method is susceptible to the influencing factors described earlier. The INTERSTOP in-house development overcomes these issues as no external target is required. Measurement by a stereoscopic camera delivers a point cloud that is matched with the 3D CAD model of the slide gate system (Figure 5). This technology is the basis for extremely high accuracies even under changing external conditions.

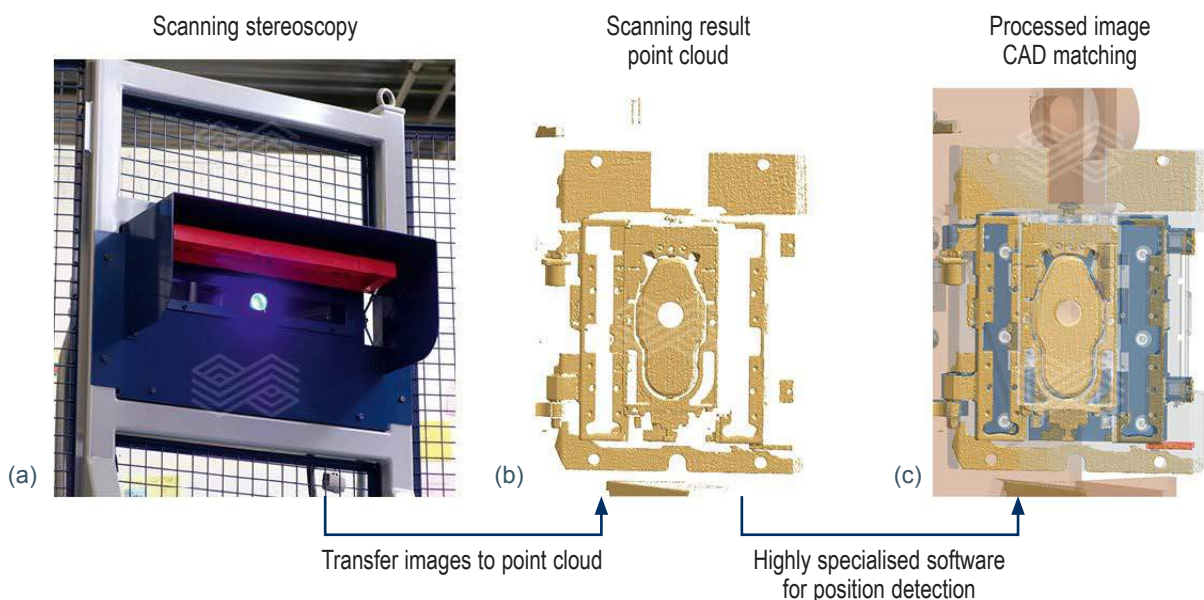
Health Check Platform

The Health Check Platform (HCP) is being developed to inform users about the condition of the mechanical and hydraulic systems as well as the refractory parts, especially at the ladle preparation area. Furthermore, it supports personnel in deciding which next steps to take, for example exchange of slide gate plates. The HCP considers data received from own measurements taken at the ladle preparation area and the CCM as well as from customer Level 1 and Level 2 data (Figure 6). The implementation of the HCP takes place in 2 phases:

- Phase 1: Learning and teaching phase where data sets including 3D scans of slide gate plates are collected and are the basis on which the algorithms are trained.
- Phase 2: Optimisation phase where the algorithms and machine learning are refined based on the phase 1 data sets and the ongoing received data.

Figure 5.

Position detecting system, consisting of the (a) stereo camera, (b) computing of a point cloud, and (c) matching with the CAD data.



The benefits of the HCP are:

- Replacing experienced-based individual decisions with machine-learning-based decision support.
- Preventing malfunctions.
- Precondition for the highest level of ladle preparation area automation (LPA) operation.

Based on the three core technologies described above, the following automatic and robotic solutions are currently being introduced to the market.

Ladle Preparation Area Automation

At the ladle preparation area, performance strongly depends on individual operator skills and experience. The heat load is high and operator safety is a constant issue. These circumstances have a direct influence on the reliability of the tasks performed [2].

Furthermore, the workers act in the tension between safety and cost considerations. One heat more on a slide gate plate saves costs, but a wrong judgement could lead to a substantial accident on the CCM during the next heat.

The INTERSTOP LPA provides robotic operation of the ladle preparation area and the core functions are (Figure 7):

- Cylinder handling and oxygen lancing.
- Handling of slide gate refractory parts.
- Inner nozzle surface cleaning.

The advantages of the LPA are:

- Safety—get operators away from liquid steel, heat, dust, and time pressure.
- Process stability—high reliability of tasks performed.
- Extension of refractory life.
- Data acquisition for predictive maintenance and lifetime prediction models.

Figure 6.

Overview of the HCP in phase 1 where 3D data is collected by a robot for a short learning phase to teach the algorithms.

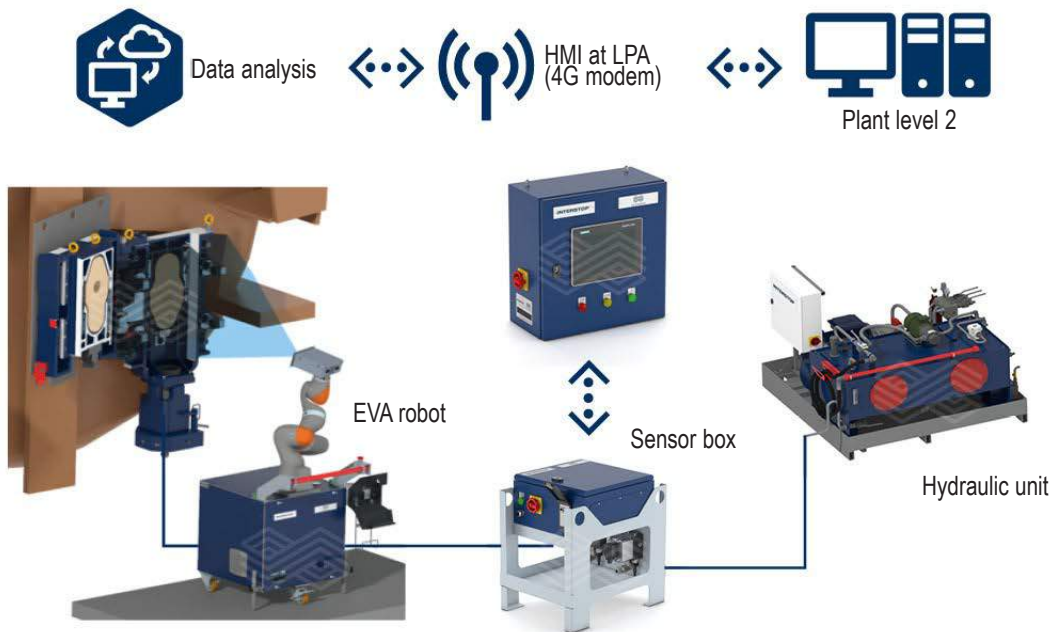
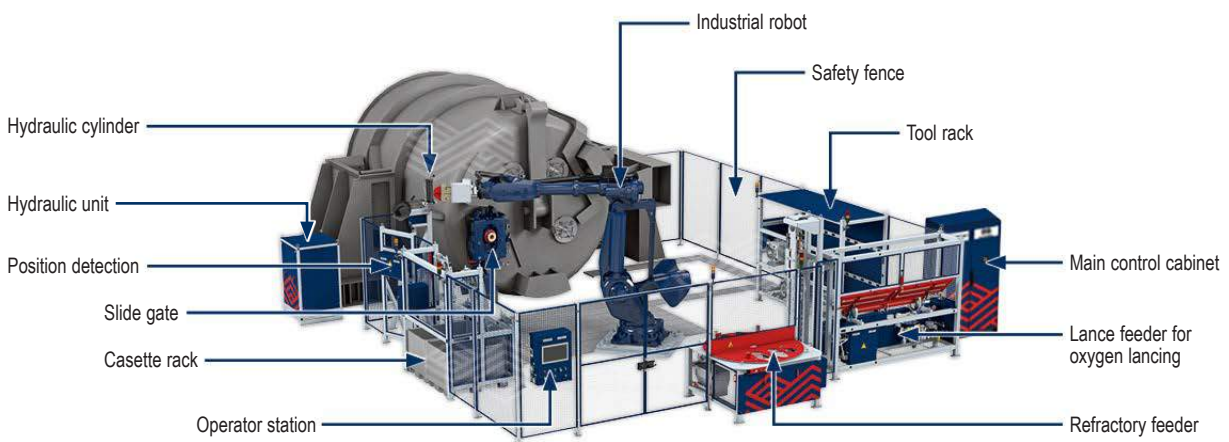


Figure 7.

Overview of the LPA robotic cell and main components.



Robotic Cylinder Handling and Integrated Media Coupling

Robotic cylinder handling (CYL) and integrated MC on the CCM is designed to keep the operator away from the danger zone under a full ladle. Since the hydraulic cylinder, process gases, and slag detection are coupled with one movement, the robotic operation of this system is significantly faster than conventional handling. Besides this, the manual operation is also improved, with one single movement in or out the cylinder is coupled and the media are connected.

The core functions of the CYL are (Figure 8):

- Robotic solution for fully automatic connection of the slide gate casting cylinder to INTERSTOP systems on the CCM.
- Coupling and uncoupling media like argon, cooling air, and electric connectors for slag detection systems.

The advantages of the CYL are:

- No-man operation on the ladle charging area—a robot fulfils the operator's tasks in the harsh environment.
- Enhanced health and safety standard.
- Increased efficiency and process control.

Robotic Monotube Handling and Mould Powder Feeding

Monotube changers are common on CCMs for slab casting. They enable extension of the sequence in case of monotube wear or the occurrence of clogging. The procedure of manual monotube exchange is an exhausting activity for the operators involved. A hot monotube of >20 kg must be handled with care to avoid damaging the ceramic and to avoid unnecessary disturbance of the mould level when inserting the monotube. After the monotube change, the used monotube must be taken out and moved to the waste container. Besides handling the monotube, operators must take care to feed the correct amount of mould powder into the mould. The core functions of the MTH are (Figure 9):

- Heating up the monotube.
- Automatic exchange of the monotube by grabbing the heated-up monotube from the heater and restoring the used monotube to the release station.
- Feeding the mould powder.

The advantages of the MTH are:

- Little space requirements and full front access to the mould with the unique INTERSTOP upside down mounted small robot on the backside of the tundish car.
- No-man operation on the CCM.
- Precise and uniform manipulation of the new and used monotube during exchange.
- Reliable and constant mould powder feeding without interruptions.

Figure 8.

Overview of (a) MC layout at the CCM and (b) main components of the MC.

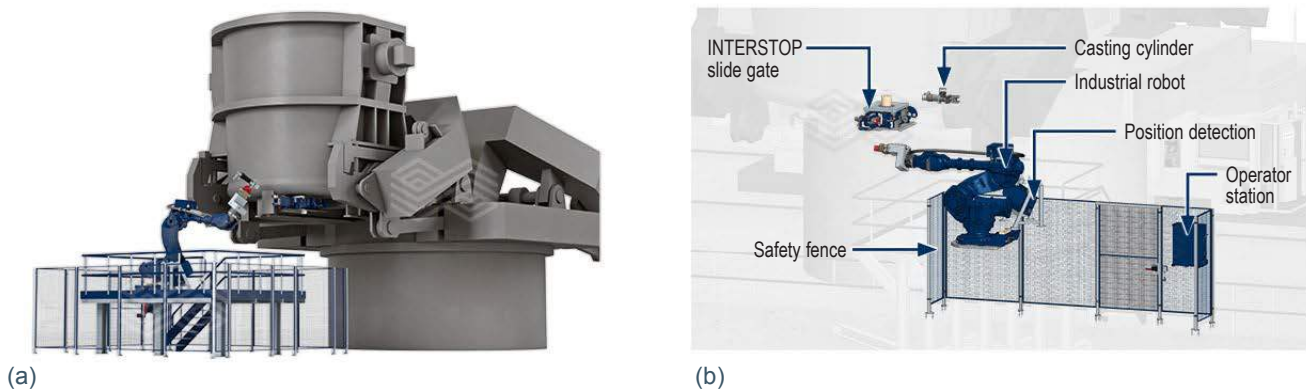
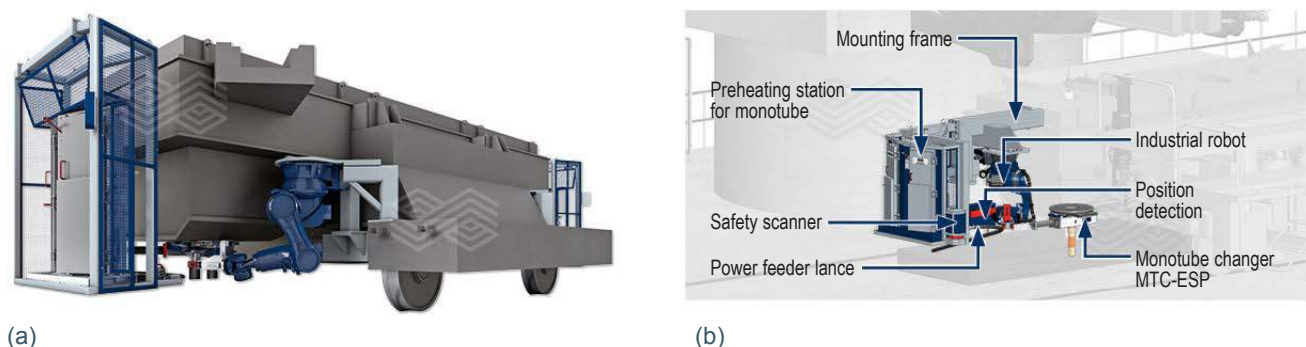


Figure 9.

Overview of (a) MTH robotic cell mounted upside down on the backside of the tundish car and (b) main components of the MTH.



Results/Conclusion

One very important design principle of INTERSTOP is the modularity of the different technologies. Several of the described systems or modules are already in operation at various customers. For example, a steel plant converted the whole ladle fleet to the automatable AS ladle gate, with the intention to now introduce the LPA. Other examples are references for robotic cylinder handling systems, which are operated in several steel plants.

The target of our developments and marketing in automation, robotics, and digitalisation is to provide steel plants with an automation solution for the operation of INTERSTOP flow control systems. For this purpose, we have built up a team of experts that can engineer customer-specific feasibility studies for the robot cells and install complete robot cells on this basis. Furthermore, at our company facilities in Switzerland, we have fully industrial 1:1 mock-ups running of the LPA, MC, and MTH to validate the long-term availability and to present to customers and original equipment manufacturers (OEMs).

In addition to marketing our automation, robotics, and digitalisation portfolio, we are pursuing an open strategy with customers and technology partners such as OEMs regarding the implementation of robotic cells. For example, on the basis of our automation-ready systems we support the option to jointly define the interfaces for the robotic operation with a partner like an OEM.

With the experience gained, the references established, the modularity of our technology, and the marketing strategies chosen, all requirements are fulfilled to provide customers with flow control systems that combine superior manual handling and automatic operation by robots.

References

- [1] Ehrenguber, R., Baumgartner, G., Steins, A. and Renggli, R. Latest INTERSTOP Ladle and Tundish Systems Ready for Robotic Handling. *Bulletin*. 2021, 48–52.
- [2] Steiner, R., Lammer, G., Spiel, C. and Jandl, C. Refractories 4.0. *BHM Berg- und Hüttenmännische Monatshefte*. 2017, 162, 11, 514–520.

Authors

Reinhard Ehrenguber, RHI Magnesita Switzerland AG, Hünenberg, Switzerland.
Verena Schmidt, RHI Magnesita Switzerland AG, Hünenberg, Switzerland.
Raphael Renggli, RHI Magnesita Switzerland AG, Hünenberg, Switzerland.
Maximilian Jani, RHI Magnesita Switzerland AG, Hünenberg, Switzerland.

Corresponding author: Reinhard Ehrenguber, Reinhard.Ehrenguber@rhimagnesita.com



João Pedro Santos, Julia Macedo, Haylander Ávila, Gilcimar Lima, Everton Arruda and Anderson Lazaroni

Innovative Refractory Wear Measurement Method for Steel Ladles Using 3D Laser Scanning

Determining the steel ladle refractory wear profile is a process used to ensure efficient and safe operation of the equipment throughout its campaign. Despite being an essential practice for steel ladle performance, the creation of this report is still done in an obsolete way, which includes exposure of the operator to hazardous conditions. This article describes the implementation of an innovative method that generates postmortem data using a portable 3D laser scanner. The solution creates and compares measurement models at two points in time: One before and another after the metallurgical process. This advancement can safely generate the residual lining thickness of the entire steel ladle, ensuring accurate and rapid refractory wear profiles at the end of campaigns.

Introduction

Refractory wear profile generation is an important practice used, among other things, to determine for a specific equipment how various regions of the lining are impacted by the metallurgical process. Since it is possible using this approach to monitor performance of the lining material in each specific situation and context, refractory suppliers are constantly developing innovative methods to carry out these measurements, with the focus on safety and efficiency.

This article presents a method that can be used in various scenarios and at different time points for steel ladle inspection using a portable, accurate, and safe 3D laser scanner. While the first 3D laser scanning technology was developed in the mid-twentieth century to recreate the surfaces of objects [1], it was only in the early 2000s that it started to be refined for the steel industry and is now a robust solution to rapidly generate refractory lining wear reports.

Wear Profile Measurement Technologies

Commonly, wear profile measurements are performed manually, with an operator inside the equipment using a tape measure to generate a report detailing residual measurements of the refractory lining at the end of a campaign. Although recently metallurgical companies have started using advanced technologies to perform hot equipment measurements during the campaign, manual measurement is still necessary to obtain actual values required to validate such tools. Therefore, to improve operational safety and decrease operator exposure to hostile environments, RHI Magnesita is now offering the metallurgical industry the ability to generate measurement reports at the end of an equipment campaign in a quick and accurate way using contactless cold scanning.

3D Laser Scanning

A common problem faced during the development of new methods for steel mills is the appropriate technology format, since each customer has a different plant layout, operating procedures, and challenges. In this regard, innovative solutions created to fulfil the diverse needs typically take two different directions: A specific and unique application or a more general, scalable technology. The path taken usually depends on how generic the issue is being solved and what benefits must be reached during the implementation.

In line with these considerations, it was determined that a quick and efficient solution to safely generate an accurate refractory wear profile in a generic way while not limiting the specific needs of each client was 3D laser scanning, a technology that can take measurements of various pieces of equipment and generate useful, dynamic, and crucial information for the plants.

The scan can be controlled remotely and due to its portability the operator can put the scanner in more than one position around the ladle to capture the lining perfectly. The method is used before the campaign starts, during the campaign when needed (e.g., during slag line renewal), and at the end of the process. Following the measurements, software generates a comparison between the reference and the worn refractory in a highly accurate report, containing valuable information such as the remaining thickness, wear index, potential according to a critical limit, and the equipment internal volume, with and without considering a free board [2].

Steel Ladle Scanning and Point Cloud Generation

The steel ladle is key for transferring liquid metal from the basic oxygen furnace to the continuous casting machine. Due to its crucial importance and the need for continuous operation, measuring the refractory lining thickness is a constant challenge during and after its campaign, but also essential to maximise plant safety and efficiency [3]. Although hot measurement is a very interesting tool for this application, since it is possible to follow the development of the equipment throughout the campaign and monitor its wear, it requires high investment costs to apply such technologies.

Aiming to achieve better results, greater accuracy, measurement agility, and above all, to protect the operator from risks related to manual measurements, the 3D laser scan provides a solution for our customers. To ensure success of this approach, several developmental processes were carried out including:

- Validation of the programming code and results generated.
- Validation of the generated point clouds.
- Comparison of values generated by the scan and actual measurements in the steel plant area.
- Software development and report automation.

In the first process step, the equipment, for example a ladle with a newly installed wear lining, is scanned before any metallurgical operations are carried out to establish reference data for comparison at the end of the campaign (Figure 1a). The 3D laser scanner is positioned around and inside the ladle to generate point clouds that include reference points for aligning the images (e.g., steel ladle trunnions), as well as the refractory lining surface. After the ladle has been measured with the intact refractory components, it is released for operation. The scanning process is then typically repeated at the end of the campaign to get the final postmortem results (Figure 1b).

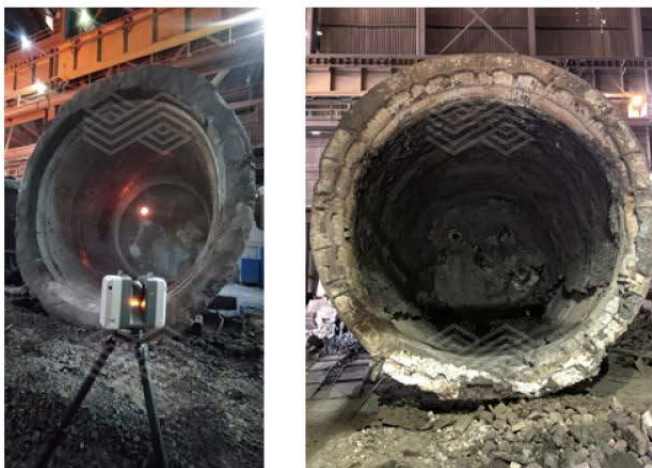
Point Cloud Preparation

Once a ladle has been scanned in multiple positions, the following steps are required to generate a point cloud that can be used for subsequent comparative analyses:

- Combine multiple point clouds of the same ladle into a single point cloud.
- Optimise the point cloud using image alignment.
- Remove points of the image unrelated to the ladle.
- Separate the steel shell from the refractory lining, while retaining the trunnions and other reference points.
- Export the refractory lining point cloud in a defined file format.

Figure 1.

Steel ladle 3D laser scanning on site. Refractory lining (a) prior to use and (b) at the campaign end.



(a)

(b)

Point Cloud Comparison

Currently, two approaches can be used to compare point clouds and generate lining wear data: A guided mode in a software requiring specific know-how and powerful computing capacity, and a RHI Magnesita Web-based solution.

When using the software to compare point clouds from different time points of an equipment campaign, it is possible to achieve two main analyses: The wear measurements depicted as a coloured image (Figure 2) and a report detailing the actual values as well as the limiting values, wear rates, and potential heats (Figure 3). In this respect, the results not only visualise the ladle lining wear but also provide essential information in a user-friendly way.

Figure 2.

3D laser scan image showing the wear colour scale that indicates lining wear and slag/steel adhesions in comparison to the ladle profile at the beginning of the campaign.

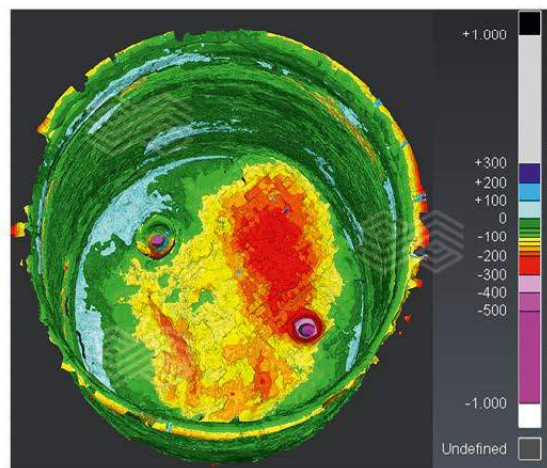


Figure 3.

Detailed wear profile report.

WEAR PROFILE - STEEL LADLE									
Client		Companhia Siderúrgica Nacional							
Ladle	30	Campaign	109	Heats	92	End Date			
New Ladle - Full Capacity		236 t		End Of Campaign Ladle - Full Capacity		247 t			
New Ladle - Capacity with 44 cm of free edge		204 t		End Of Campaign Ladle - Capacity with 44 cm of free edge		211 t			
Regions	Sign	Angle	Depth	Limit (mm)	Residual (mm)	Location of the Residual	Wear Rate (mm/heat)	Potential (heats)	
Slag Line SW	✓	1° a 90°	2.91m a 3.93m	50	56	88.08° a 3.59m	1.876	95	
Slag Line NW	✗	90° a 180°	2.91m a 3.93m	50	34	154.02° a 3.64m	2.122	84	
Slag Line NE	✗	180° a 270°	2.91m a 3.93m	50	62	241.09° a 3.64m	1.811	99	
Slag Line SE	✓	270° a 0°	2.91m a 3.93m	50	64	274.09° a 3.59m	1.789	100	
M. L. SW 10 and 11	✓	1° a 90°	2.443m a 2.9m	30	83	35.02° a 2.53m	0.960	147	
M. L. NW 10 and 11	✓	90° a 180°	2.443m a 2.9m	30	86	123.00° a 2.51m	0.922	153	
M. L. NE 10 and 11	✗	180° a 270°	2.443m a 2.9m	30	117	249.05° a 2.58m	0.585	241	
M. L. SE 10 and 11	✓	270° a 0°	2.443m a 2.9m	30	93	301.04° a 2.60m	0.843	167	
M. L. SW	✓	1° a 90°	1.095m a 2.443m	30	82	76.00° a 1.82m	0.967	146	
M. L. NW	✗	90° a 180°	1.095m a 2.443m	30	-219	170.03° a 1.27m	4.034	30	
M. L. NE	✗	180° a 270°	1.095m a 2.443m	30	-50	180.00° a 1.59m	2.192	56	
M. L. SE	✓	270° a 0°	1.095m a 2.443m	30	90	315.01° a 2.29m	0.884	159	
M. L. SW 2 and 3	✓	1° a 90°	0.64m a 1.095m	30	79	20.09° a 0.66m	1.005	140	
M. L. NW 2 and 3	✗	90° a 180°	0.64m a 1.095m	30	-273	173.03° a 0.88m	4.615	26	
M. L. NE 2 and 3	✗	180° a 270°	0.64m a 1.095m	30	60	213.01° a 0.92m	0.998	122	
M. L. SE 2 and 3	✓	270° a 0°	0.64m a 1.095m	30	87	320.03° a 0.91m	0.910	155	
1st Row SW	✗	1° a 90°	0.356m a 0.62m	100	95	20.08° a 0.40m	1.454	89	
1st Row NW	✓	90° a 180°	0.356m a 0.62m	100	173	102.06° a 0.41m	0.611	211	
1st Row NE	✗	180° a 270°	0.356m a 0.62m	100	158	243.05° a 0.56m	0.768	168	
1st Row SE	✓	270° a 0°	0.356m a 0.62m	100	165	358.01° a 0.53m	0.699	185	
General Bottom	✓	0° a 0°	0.00m a 0.344m	100	192	36.01° a 0.19m	1.639	148	
Channel Bottom	✓	0° a 0°	0.00m a 0.382m	100	214	42.03° a 0.21m	1.811	155	
Impact Bottom	✗	0° a 0°	0.00m a 0.306m	100	71	320.08° a 0.06m	2.546	81	

Legend:
M. L. = Metal Line; SW = South-West; NW = North-West; NE = North East; SE = South East.

Observations

Before the wear profile analysis tool is brought into routine use at a particular steel plant, it is necessary to determine the system accuracy and make any necessary adjustments regarding possible sources of errors. This is achieved by installing new refractory linings in numbered steel shells, performing a 3D laser scan before use, and then measuring the lining wear at the campaign end using both the 3D laser scanner and manually at specific positions. It is essential that the same ladle is used for a comparison between the beginning and end of the campaign because the deformations specific to each steel shell must be taken into consideration.

Following data collection, deviations between the scanned and manual measurements for specific positions are calculated (Table I) and if necessary operational adjustments are performed (e.g., ensuring reference points are clean) to achieve an average error of <2% with a standard deviation <1.7%. These errors are often related to some particularities of the assembly (e.g., application of backfill with a greater or lesser thickness) or deformation of the steel shell that has happened during the campaign. Following verification that the setup is appropriate, the system is put into standard operation with the knowledge that the data can be trusted and used to support the decision-making process [4].

Web Interface

In parallel with the development of this new measurement method, a fully interactive and automated platform was also created to streamline and facilitate easy generation of the refractory wear profile.

The platform features a portal where the point clouds can be uploaded individually according to the type of lining and the lining campaign. This information is then used to create a database of all the campaigns analysed.

Once the images are uploaded, a comparison is automatically performed using parameters previously programmed for the alignment and within just a few minutes all the data related to the wear profile of the analysed equipment is available. Furthermore, it is also possible to visualise and analyse an image of the ladle lining after the upload, because the platform generates an interactive 3D image that can be rotated (Figure 4).

Figure 4.

Interactive 3D ladle image with the wear colour scale indicating the residual lining thickness.

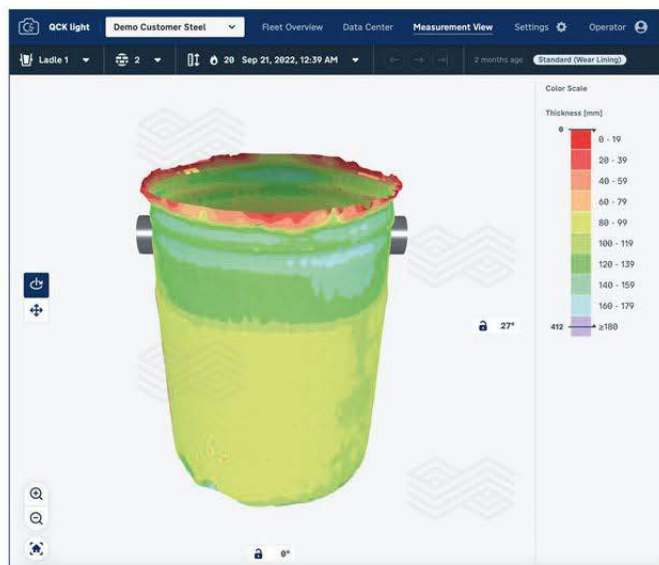


Table I.

Comparison of manual and 3D laser scan wear measurements for specific lining positions within a ladle, including the absolute deviations between the two measurement methods.

Position	Manual	Scan	Deviation	Deviation	Absolute deviation	Absolute deviation
	[mm]	[mm]	[mm]	[%]	[mm]	[%]
1	155	155	0	0	0	0
2	135	133	-2	-2	2	2
3	100	97	-3	-3	3	3
4	90	89	-1	-1	1	1
5	105	110	5	5	5	5
6	110	112	2	2	2	2
7	115	117	2	2	2	2
8	115	119	4	3	4	3
9	105	105	0	0	0	0
10	120	119	-1	-1	1	1
11	95	94	-1	-1	1	1
12	95	96	1	1	1	1
13	60	63	3	5	3	5
14	75	72	-3	-4	3	4

Results/Conclusion

The main goal of the laser scanning technology is to achieve operational safety and ergonomics. By eliminating the need to remove the refractory material from the ladle to perform measurements, it is no longer necessary for personnel to stay inside the equipment for long periods in unsafe conditions. In terms of ergonomics, the operator can remain outside the ladle while monitoring progress of the scan, a process that typically takes around 5 minutes. In contrast, before using the measurement tool, exorbitant amounts of time were required for manual measurement. Steel ladles take about 48 hours to cool, then it is necessary to wait for demolition of part of the lining before finally allowing the operator to measure the ladle, totalling approximately 3 days to complete the measurement.

From a technical standpoint, it is possible to achieve many benefits by monitoring the ladle lining and understanding the entire wear profile. For example, it is possible to determine the process's influence on each region of the ladle. In terms of refractories, the technology enables areas that are more susceptible to wear to be identified, which provides the opportunity to address possible root causes with more certainty. Finally, the collected data can be used to develop models that predict refractory wear, which enables greater forward planning in the steel plant.

References

- [1] Edl, M., Mizerák, M. and Trojan, J. 3D Laser Scanners: History and Applications. *Acta Simulatio - International Scientific Journal about Simulation*. 2018, 4, 1–5.
- [2] Macedo, J.F., Ribeiro, A.S., Nonaka, F., Guimarães, B.F., Morais, V.L. and de Ávila, H.C. How 3D Laser Scan is Adding Value and Performance to Refractory Lining Inside Steel Industry. Presented at AISTech 2022 Technology Conference, Pittsburgh, USA, May 16–18, 2022.
- [3] Vert, T. *Refractory Material Selection for Steelmaking*; John Wiley & Sons: New Jersey, 2016.
- [4] Lamm, R. Laser Measurement System for the Refractory Lining of Hot Torpedo Ladles. Presented at AISTech 2012 Technology Conference, Atlanta, USA, May 7–10, 2012.

Authors

João Pedro Santos, RHI Magnesita, Rio de Janeiro, Brazil.

Julia Macedo, RHI Magnesita, Vienna, Austria.

Haylander Ávila, RHI Magnesita, Rio de Janeiro, Brazil.

Gilcimar Lima, RHI Magnesita, Rio de Janeiro, Brazil.

Everton Arruda, RHI Magnesita, Rio de Janeiro, Brazil.

Anderson Lazaroni, RHI Magnesita, Rio de Janeiro, Brazil.

Corresponding author: João Pedro Santos, Joao.Santos2@rhimagnesita.com



Jacob Kerr, Pedro Henrique Couto Almeida, David Wappel, Rodrigo Nazareth Borges, Matheus Naves Moraes and Felipe de Jesus Olvera

Innovative Spray Tundish Mix for Energy Savings and CO₂ Footprint Reduction

As modern steel plants and manufacturing processes evolve, additional demands are placed on refractory installation and performance. Many traditional tundish working lining materials require long drying and preheating curves, which can inhibit equipment availability and production output. These heating requirements also result in high energy usage and CO₂ generation for the plant. To support the industry’s productivity and environmental goals, the FAST TO CAST tundish spray product line was formulated. Developed as a cross-regional R&D collaboration, FAST TO CAST products can be sprayed onto the tundish permanent lining and taken directly to final heating, shortening or bypassing the traditional drying step. The resultant lining maintains its physical integrity and refractory performance, while offering reduced fuel requirements and a lower carbon footprint.

Introduction

Over the years, methods for effectively lining the tundish in continuous casting steelmaking operations have progressed to optimise efficiency, increase equipment availability, minimise cost, and reduce energy usage. The tundish is the last piece of processing equipment that encounters molten steel and while historically treated as a simple containment vessel, has evolved to become a key metallurgical vessel for maximising cast steel quality and yield [1].

Modern tundish wear linings generally fall into one of three categories: Dry-setting (or dry vibratable) mixes, cold-setting (or self-hardening) mixes, and slurry gunning (or sprayable) mixes. Each product category has inherent advantages and disadvantages over the others, both in terms of installation and performance (Table I). Advantages of slurry gunning mixes include their ability to be applied quickly, their lower density, lower specific consumption, higher insulation value, and their flexibility of use. Disadvantages include long dry-out times due to high amounts of water that are needed for proper installation. With this type of product, a working lining thickness can be applied in a variable manner, which can allow for thicker layers to be installed in high-wear areas such as the slag line.

It has also been found that sprayable compositions lead to considerably lower levels of carbon pickup in steel when compared to dry mixes [2,3]. Due to these advantages, this mix type quickly gained in popularity throughout the world after its introduction to the market in the 1980s and it remains one of the most dominant technologies to this day [3,4]. As a result of this popularity throughout the industry, special focus has been given to improving the efficiency of utilising this technology, while also reducing the energy consumption and resulting carbon footprint.

Design Requirements

To achieve the objectives of improving efficiency, equipment availability, and fuel consumption of slurry gunning refractory mixes, several considerations had to be addressed. For standard slurry gunning products that are prevalent in today’s marketplace, there is an inherent demand for careful dry-out and preheating practices to maintain the physical integrity of the refractory and promote the best possible performance. Typical slurry gunning mixes incorporate water additions around 20–30 wt.% to achieve the proper application consistency and behaviour. For this water to be removed effectively, dry-out heating curves can reach

Table I. Comparison of current tundish wear lining technologies. Abbreviations include not applicable (N/A).

	Dry setting	Cold setting	Slurry gunning
Equipment needed	Steel form/mandrel/ template, burner	Cold-setting machine, steel form/mandrel/template	Spray machine, burner
Liquid addition	N/A	Water or liquid binder	Water
Thickness flexibility	N/A	N/A	++
Heating requirement	Curing	N/A	Drying
Heating time	+	N/A	++
Energy requirement	+	-	++
Material density	High	High	Low
Insulating properties	+	+	++
Material consumption	High	High	Low
Casting sequence length	++	++	+

4–6 hours or more, depending on several variables such as specific material choice, lining thickness, and burner configurations. This controlled drying step is critical to reduce the likelihood of cracking, blistering, and spalling in the refractory working lining. By reducing or eliminating the drying requirement, the overall application process time can be reduced, while necessary energy inputs can be lowered as well. Other main aspects of the mix, such as equipment compatibility, application methodology, and overall refractory performance are expected to remain constant while the changes to drying requirements are made.

Methodology

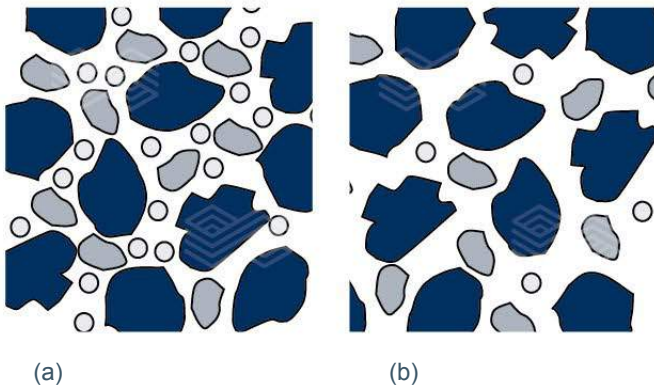
Compared to the traditional products, the new FAST TO CAST series relies on both a modified binder package and grain size distribution to achieve the desired application advantages. By creating open channels of porosity within the refractory structure, water release can occur more freely (Figure 1). Modifications to the binder package enable

uninhibited moisture escape, while maintaining mechanical integrity of the mix in both the as-applied and dried conditions. The combination of binder and grain size distribution also allows for proper compaction, sintering, insulation, and performance of the mix.

Small-scale laboratory tests of the FAST TO CAST concept in both North and South America aimed to push the limits of this technology when exposed to aggressive heating. In addition to standard testing of the chemistry, water demand, and flowability, panels of slurry containing 20–30% water were subjected to direct flame exposure. In the North American study, the wet slurry was allowed to air set for 15 minutes, followed by application of a passing propane torch (flame temperature ~1980 °C) for 4 minutes. In the South American testing, a similar approach was taken where a panel was sprayed onto a vertical wall and subjected to direct, localised flame contact. In both cases, the material dried sufficiently within minutes and without signs of cracking, blistering, or spalling (Figure 2).

Figure 1.

Changes in particle size distribution can create (a) a denser, packed structure that is more likely to entrap free moisture or (b) an open structure through which moisture is more quickly and easily removed.



Field Trial Results—North America

Following the favourable laboratory studies, larger-scale field trials were commissioned. In North America, a series of four consecutive field trials were conducted at various customer sites, working to validate the FAST TO CAST materials over a wide range of conditions and to prove that repeatable results could be maintained.

The first trial in North America was conducted over a series of five individual tundish linings. Each lining was applied to a thickness of 50 mm and required an application time of 30 minutes per lining. All equipment parameters including water and air settings were kept consistent with the settings used for standard slurry gunning material. For this trial, thermocouples were installed on the surface of the permanent lining to determine the point at which complete dry-out of the wear lining was achieved.

Figure 2.

Measuring the FAST TO CAST (a) resistance to a propane torch in North America and (b) localised flame application to a vertical panel in South America. In both tests, cracking, blistering, and spalling were not experienced, and the refractory maintained proper strength characteristics.



(a)



(b)

Figure 3 shows a comparison of drying curves used for the FAST TO CAST materials compared to the standard mix. For the FAST TO CAST, complete drying could be achieved in 2 hours with the burner going from room temperature directly to 550 °C, compared to a profile of more than 6 hours used for the standard mix. Thermocouple data shown in Figure 4 illustrates that all of the installed thermocouples reached a minimum of 100 °C within this time period, indicating that complete drying had been reached. When an aggressive heating curve such as the one used for FAST TO CAST is applied to a standard mix, significant cracking, spalling, and blistering can occur, as shown in Figure 5.

Further trials with the FAST TO CAST materials in North America tested variables such as spray lining thickness (ranging from 40–100 mm thick), permanent lining temperature (ambient and warm), and cast sequence length (6–18 heats). In these trials, the following were achieved:

- No slumping of the slurry on the tundish wall.
- No cracking, blistering, or spalling.
- Drying time reduced by up to 70%.
- Energy demand and CO₂ emissions from drying were reduced by up to 50%.
- Specific refractory consumption was reduced by an average of 20%.
- Lower shell temperatures were reached due to reduced thermal conductivity.
- Equipment turnaround time and availability was improved.
- No change in water demand, refractory performance, or desking behaviour.

Figure 3.

Comparison of the drying curves for FAST TO CAST and a standard slurry gunning mix.

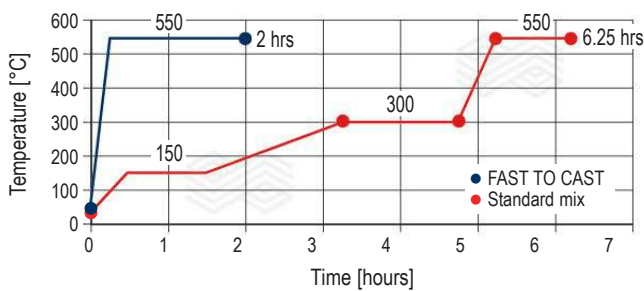


Figure 4.

Thermocouple (a) positions and (b) readings from one of the trial tundish linings. All of the thermocouples (T) reached temperatures above 100 °C within 2 hours, indicating that complete drying was achieved.

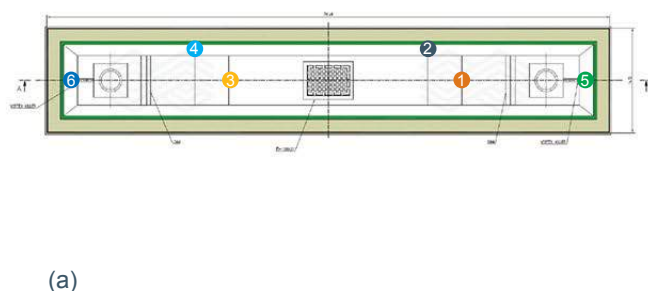
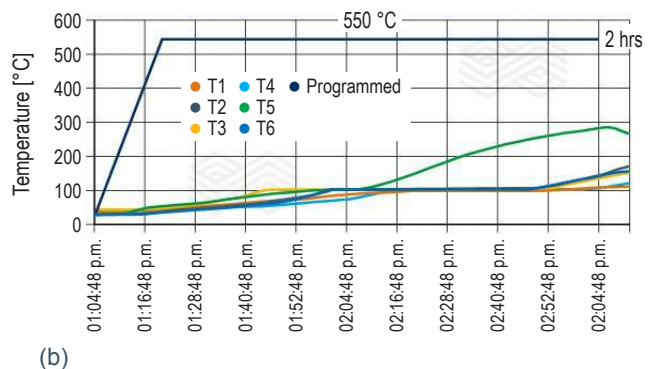
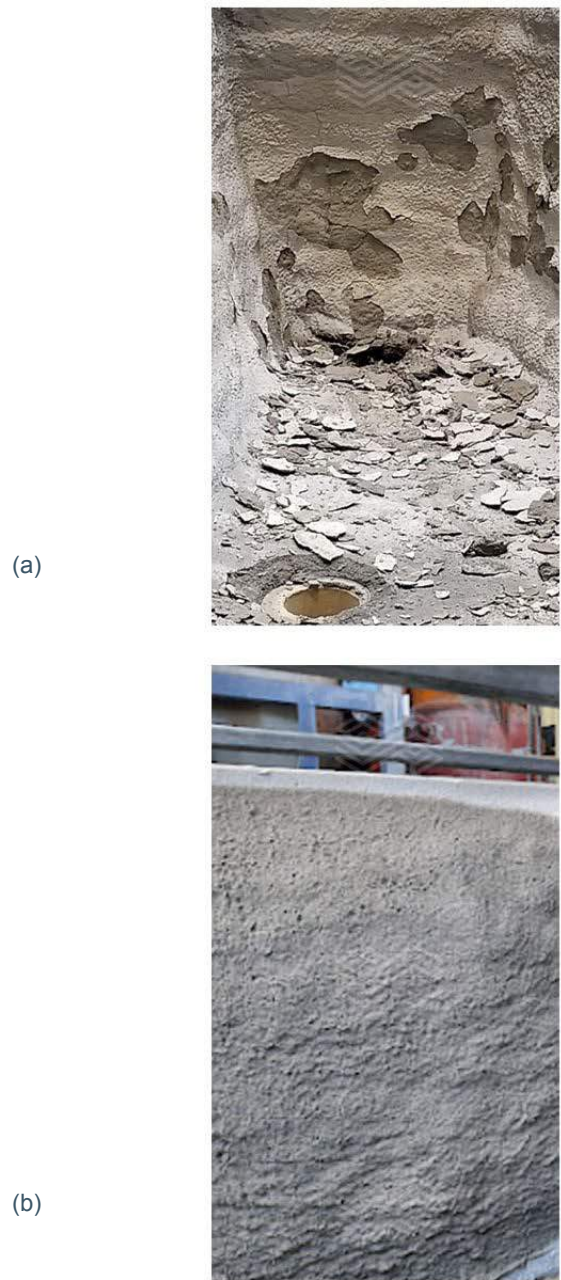


Figure 5.

(a) standard slurry gunning mixes have the potential to crack, blister, and spall when subjected to aggressive heating conditions. (b) the FAST TO CAST formulation can absorb the stress of aggressive heating conditions without experiencing physical damage.



Trial Results—South America

In parallel to the trials in North America, trials in South America were also performed, but with a different objective. Instead of reducing the drying out time, the aim in this study was to take the tundish from the preparation area directly to the preheater, eliminating the dry-out process completely.

The first field trials have shown promising results. For example, a 50 mm lining thickness was applied and all equipment parameters including water settings were kept consistent with the settings used for standard slurry gunning material. The tundish bypassed the drying stage and was sent directly to the preheating station, then to the caster. Figure 6 shows pictures of the tundish after application, preheating, casting, and deskulling. No abnormal results were observed in these steps, such as cracks and spalling in the working lining or blackening of the permanent lining.

As shown in Figure 7, the temperature in all thermocouples was over 100 °C after 100 minutes of preheating, indicating that complete drying had been reached in the working lining within this time frame.

Figure 7.

Thermocouple (a) positions and (b) readings during the trial with direct preheating. All of the thermocouples (T) reached temperatures above 100 °C within 100 minutes.

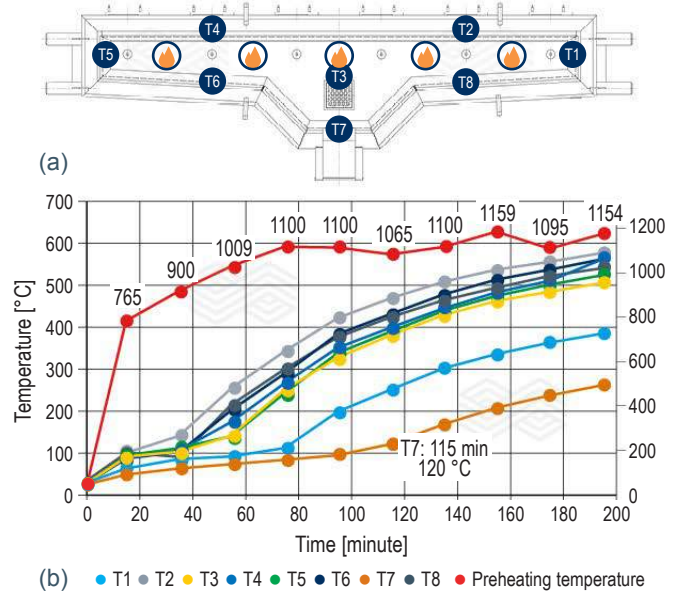


Figure 6.

Tundish after (a) application of the working lining, (b) preheating, (c) casting, and (d) deskulling.

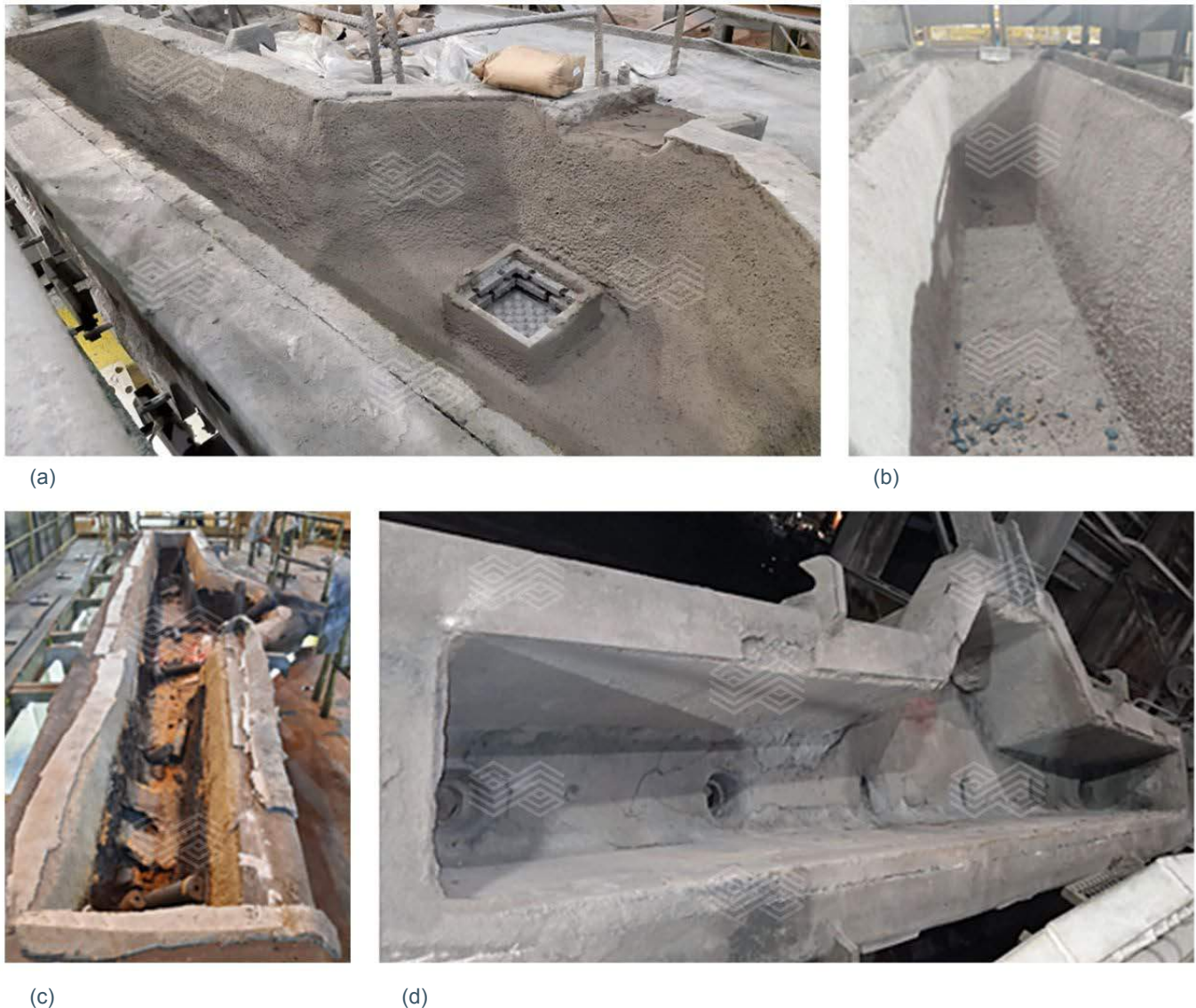


Table II.

Available FAST TO CAST grades and typical chemical compositions.

Brand Name	MgO [%]	Al ₂ O ₃ [%]	SiO ₂ [%]	CaO [%]	Fe ₂ O ₃ [%]
ANKERTUN FTC11-BR	87.2	1.2	7.4	0.8	2.1
ANKERTUN FTC21-BR	74.8	1.4	19.5	0.7	2.3
ANKERTUN FTC10-MX	88.7	0.5	7.6	1.7	1.3
ANKERTUN FTC21-MX	79.8	0.5	13.9	1.7	2.1
ANKERTUN FTC24-MX	70.8	0.5	23.6	1.2	3.7

Current FAST TO CAST Product Portfolio

Following the successful field trials, the FAST TO CAST product portfolio detailed in Table II is now available.

Conclusion

As demand for efficiency in steelmaking operations continues to increase, the importance of equipment turnaround and availability is at an all-time high. For continuous casting, this means reliably having tundish vessels that perform well and are available quickly. Trials of FAST TO CAST grades in North and South America have produced results showing that the necessary drying time can be reduced by 70% or even eliminated completely, while energy requirements and CO₂ emissions from drying are also reduced accordingly. Additionally, the low density of these materials can decrease specific refractory consumption by an average of 20%, while also lowering heat transfer to the tundish shell. Furthermore, trial results showed that other important properties such as sprayability, refractoriness, and deskulung are unchanged as a result of the improved drying behaviour.

References

- [1] Tassot, P. and Turrel, C. Actual Trends for the Tundish Refractory Lining. *Refractories Worldforum*. 2011, 3, 93–98.
- [2] Krausz, I., Tassot, P. and Turrel, C. Element Pick-Up in Liquid Steel from Tundish Lining Refractories. Presented at the 11th Unified International Technical Conference of Refractories (UNITECR), Salvador, Brazil, Oct. 13–16, 2009.
- [3] Correa, A., Resende, R., Borges, R., Bellandi, N., Brito, M. and Abrao, E. Why is Spray Mix Still a Dominant Technology for Tundish Coating Application? Presented at the 15th Unified International Technical Conference of Refractories (UNITECR), Santiago, Chile, Sept. 27–30, 2017.
- [4] Helmus, D., Bross, R., Fechner, R., Ratto, J. and Ratto, J. Tundish Wear Lining: Taylor Made Dry Vibratable Material Concepts and Lining Installation Technologies. *2nd Refractory Material Seminar*, IAS. 2013.

Authors

Jacob Kerr, RHI Magnesita, York, USA.
 Pedro Henrique Couto Almeida, RHI Magnesita, Contagem, Brazil.
 David Wappel, RHI Magnesita, Leoben, Austria.
 Rodrigo Nazareth Borges, RHI Magnesita, Contagem, Brazil.
 Matheus Naves Moraes, RHI Magnesita, Contagem, Brazil.
 Felipe de Jesus Olvera, RHI Magnesita, Ramos Arizpe, Mexico.
Corresponding author: Jacob Kerr, Jacob.Kerr@rhimagnesita.com



Alexandre Resende, Rubens Freire, Gernot Lukesch, Gernot Hackl and Daniel Meurer

Avoiding Asymmetric Flows Caused by Off-Centre Pouring into the Tundish: A Novel Impact Pot Design

Off-centre and angled pouring of molten steel into the tundish by a misaligned ladle shroud can result in several problems caused by the asymmetric flow, such as short-circuiting flows, inhomogeneous temperature distribution, and a higher tendency of vortex formation with consequent slag entrainment. Although many different impact pot designs are available in the industry, to date none have effectively addressed the issue of asymmetric flows caused by off-centre pouring. This paper presents the development of a novel impact pot design that can perform well even under such adverse conditions, as shown by mathematical and physical modelling studies.

Introduction

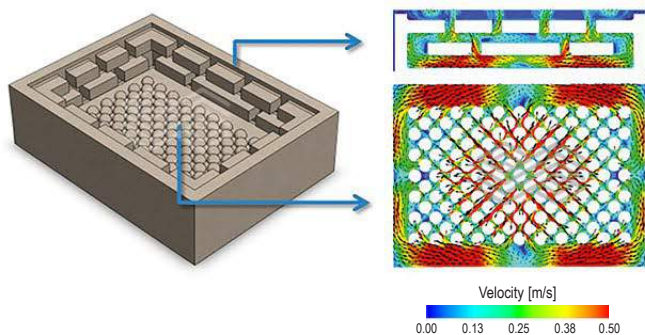
The tundish is an important vessel in the continuous casting process, connecting the incoming steel flow from the ladle to the moulds. In the past, the role of the tundish was limited to distributing molten steel to the moulds, enabling continuity of the casting process even between ladle changes. As the requirements for quality became more severe, flow optimisation in the tundish was afforded more consideration, as steelmakers worked to make this vessel a place of further molten steel refining. The impact pot has several important functions in a continuous casting tundish, including:

- Dissipating the kinetic energy of the entry jet from the ladle.
- Protecting the refractory lining from excessive wear.
- Promoting inclusion flotation.
- Increasing the vessel's mixing efficiency and minimising dead zones.

The effectiveness of a given impact pot in complying with these requirements depends largely on its geometric features. Figure 1 shows the effect of the impact pot inner geometry on the internal flow pattern of the steel. The internal features of the impact pot design influence the flow velocities, dissipating the kinetic energy of the entry jet [1].

Figure 1.

Effect of the impact pot internal geometry on steel flow [1].



The effects of different flow control devices have been thoroughly studied by many researchers [1–5]. What all these studies have in common is they show that the influence of the impact pot design on the tundish flow pattern is very significant. Various techniques, such as physical modelling and numerical simulation, have been adopted to assess the effectiveness of alternative impact pot geometries in improving the tundish flow pattern.

One operating condition of concern is when the incoming jet from the ladle is not centred in the impact pot. Most impact pots are designed under the assumption of a perfectly centred jet, which is often not true in the real casting process. As a result, many impact pots underperform when subject to off-centre jet conditions, as the resulting tundish flow becomes asymmetric, presenting issues such as:

- Short-circuiting flows.
- Inhomogeneous temperature distribution.
- Higher tendency of vortex formation with consequent slag entrainment.

Although there is a high number of publications about new impact pot designs, none has yet effectively addressed the issue of asymmetric flows caused by off-centre pouring. This paper presents the development of a novel impact pot design that can perform well even under such adverse conditions, as shown by mathematical and physical modelling studies. The modelling methods will be further detailed in the next section.

Mathematical Modelling Procedure

Computational fluid dynamics (CFD) modelling solves the Navier-Stokes equations for continuity and momentum (equations 1 and 2):

$$\frac{\partial \rho}{\partial t} + \frac{\partial}{\partial x_j} (\rho U_j) = 0 \quad (1)$$

$$\begin{aligned} \frac{\partial \rho U_i}{\partial t} + \frac{\partial}{\partial x_j} (\rho U_i U_j) \\ = - \frac{\partial P}{\partial x_i} + \frac{\partial}{\partial x_j} \left[\mu_{eff} \left(\frac{\partial U_i}{\partial x_j} + \frac{\partial U_j}{\partial x_i} \right) \right] + S_M \end{aligned} \quad (2)$$

Where ρ is the fluid's density, t is the time, x_j is the coordinate in the j -direction, U_j is the velocity component in the j -direction, P is the pressure field, S_M is the sum of the body forces, and μ_{eff} is the effective viscosity accounting for turbulence given by equation 3:

$$\mu_{eff} = \mu + C_\mu \rho \frac{k^2}{\varepsilon} \quad (3)$$

Where μ is the fluid's molecular viscosity, C_μ is a constant, k is the turbulent kinetic energy, and ε is the dissipation rate of turbulence [1].

Equations 4 and 5 represent the transport equations for turbulent kinetic energy and dissipation rate of turbulence:

$$\begin{aligned} \frac{\partial \rho k}{\partial t} + \frac{\partial}{\partial x_j} (\rho U_j k) \\ = \frac{\partial}{\partial x_j} \left[\left(\mu + \frac{\mu_t}{\sigma_k} \right) \frac{\partial k}{\partial x_j} \right] + P_k - \rho \varepsilon \end{aligned} \quad (4)$$

$$\begin{aligned} \frac{\partial \rho \varepsilon}{\partial t} + \frac{\partial}{\partial x_j} (\rho U_j \varepsilon) \\ = \frac{\partial}{\partial x_j} \left[\left(\mu + \frac{\mu_t}{\sigma_\varepsilon} \right) \frac{\partial \varepsilon}{\partial x_j} \right] + \frac{\varepsilon}{k} (C_{\varepsilon 1} P_k - C_{\varepsilon 2} \rho \varepsilon) \end{aligned} \quad (5)$$

Once the flow field has been calculated, a residence time distribution (RTD) analysis is performed to characterise the flow according to the definitions of plug volume, dead volume, and mix volume [6]. To conduct the RTD study, a numerical simulation of tracer transport in the calculated flow field is performed. The transport equation for the tracer is given in equation 6:

$$\begin{aligned} \frac{\partial (\rho \varphi)}{\partial t} + \nabla \cdot (\rho \mathbf{U} \varphi) \\ = \nabla \cdot \left(\left(\rho D_\varphi + \frac{\mu_t}{Sc_t} \right) \nabla \varphi \right) + S_\varphi \end{aligned} \quad (6)$$

Where φ is the tracer concentration, Sc_t is the turbulent Schmidt number, S_φ is a source term for the concentration, μ_t is the eddy viscosity, and D_φ is the kinematic diffusivity of the tracer [1].

Physical Modelling Procedure

The practical experiments were carried out using a model representing a twin strand slab casting tundish without any additional flow modifiers except an impact pot. The water model was operated on a scale of 1:3, fulfilling Froude similarity. According to the literature [7], this approach is most likely to simulate flow phenomena of the corresponding full-scale system accurately. The Froude number, which is the ratio between inertial and gravitational forces, is defined by equation 7:

$$Fr = \frac{u^2}{g.l} \quad (7)$$

Where u is the flow velocity, g is the gravitational acceleration, and l is the characteristic length of the system [1]. Table I provides information on the operating conditions considered in the model and values of the real application.

Table I.

Operating conditions in the water model and the real application.

	Water model	Real application
Throughput	2.5 m ³ /hour	4.5 tonne/min/ strand
Bath level	380 mm	1150 mm
Ladle shroud immersion	70 mm	210 mm

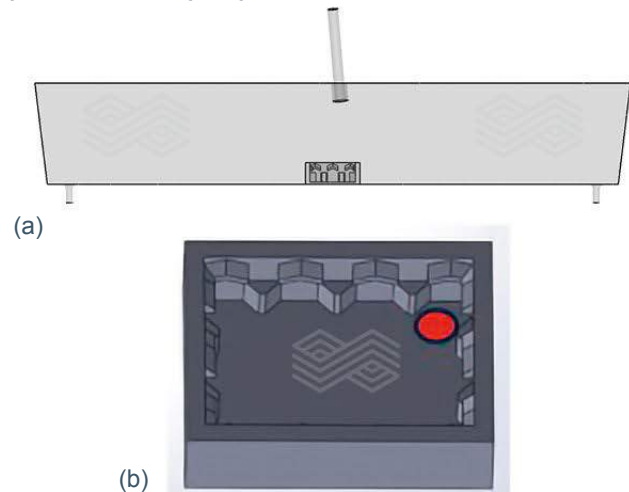
To characterise the flow performance of the given tundish setup, the stimulus response technique, in which the concentration of an injected tracer fluid (e.g., dye) is recorded at the outlets, was applied. Analysis of the measured curve provides key information on the flow characteristics in the tundish such as the minimum residence time and other parameters. Besides the dye concentration measurements, a video was recorded synchronously to get an impression of the general flow characteristics [1].

Representation of the Flow Under Asymmetric Conditions

The first step in the development of a solution to avoid asymmetric flows into the tundish was to understand in detail how the flow develops in the impact zone when an off-centre jet situation occurs. A two-strand slab tundish was chosen as a reference for this study. Figure 2 shows the tundish geometry and positioning of the off-centre jet in the impact pot.

Figure 2.

(a) schematic of the tundish setup and (b) off-centre jet position in the impact pot.



After the incoming jet enters the impact pot, it circulates inside the box and then flows upward towards the slag layer. This process dissipates some of the kinetic energy of the jet, reducing the average velocities of the flow downstream and is one of the reasons impact pots are widely used in the industry.

Figure 3 shows the velocity contours on the bottom surface of the impact pot and Figure 4 depicts the contours of the upward flow velocities as a cross section of the impact pot's top surface, with both figures comparing centred (Figures 3a and 4a) and off-centre jet conditions (Figures 3b and 4b).

The results illustrate that for the centred jet case, the flow is distributed evenly across the cross section, which would result in a symmetric flow into the tundish, as the flow is distributed equally in all directions. However, for the off-centre case, the upward flow is strongly concentrated on the opposite side of the incoming jet, as that is the path of least resistance. Such behaviour would very likely result in

Figure 3.
Velocity contours on the bottom surface of the impact pot for (a) centred and (b) off-centre jet conditions with the impingement point at the bottom left.

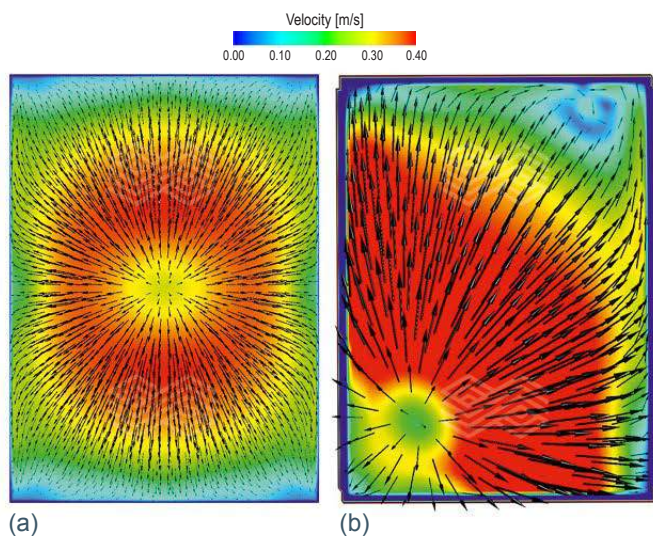
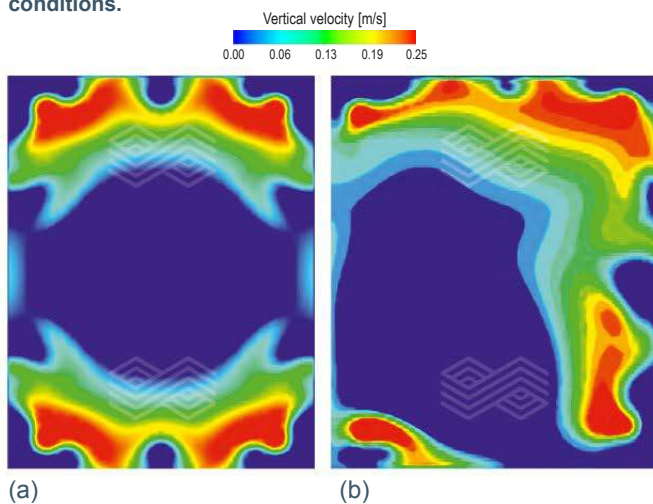


Figure 4.
Cross section of the upward flow distribution on the top surface of the impact pot for (a) centred and (b) off-centre jet conditions.



an asymmetric tundish flow, as there is a clear preferred flow direction. Figure 5 shows contours of the flow on the top surface of the molten steel bath, downstream of the contours shown in Figures 3 and 4, comparing the centred and off-centre conditions. An asymmetric tundish flow can be clearly observed for the off-centre case, in all directions (Figure 5b). Figure 6 shows dye dispersion pictures taken from the front of the tundish at the same flow time in the experiment (i.e., 10 seconds) for both configurations in the water modelling study. The asymmetry of the flow field in the off-centre jet configuration can also be clearly seen, with the incoming jet off-centre to the left side and the downstream flow asymmetric towards the strand on the right side.

If it occurs in a real caster, an asymmetric tundish flow is likely to cause several issues, including accelerated and uneven refractory wear in the region of the preferred flow path, temperature and steel chemical composition differences between strands, shorter residence times, nonmetallic inclusions flowing into the moulds, and a higher tendency of vortex formation due to the rotational flow. Such a scenario created the strong motivation to develop an alternative impact pot solution that would be able to handle off-centre jet conditions, which unfortunately are common in real casters.

Figure 5.
Contours of the flow on the top surface of the molten steel bath for (a) centred and (b) off-centre jet conditions.

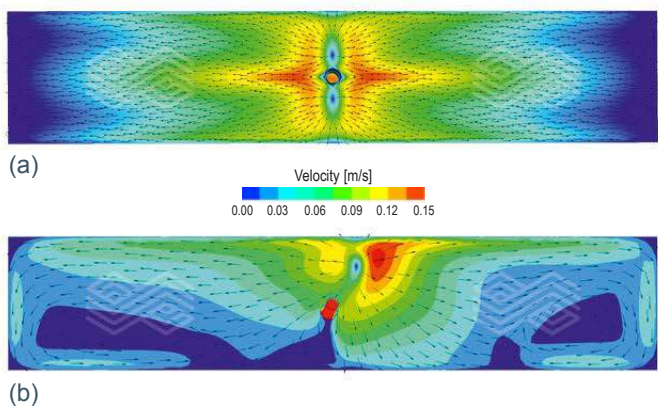
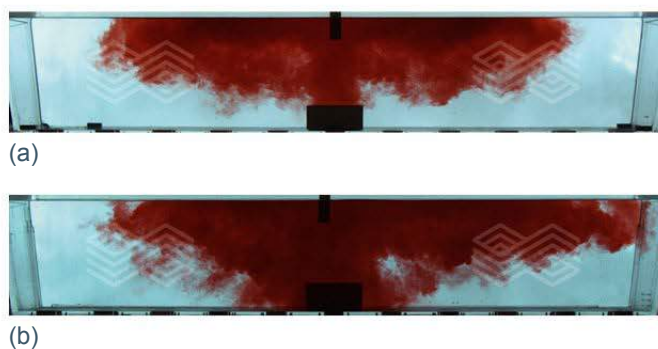


Figure 6.
Snapshot of the dye dispersion in a water modelling experiment at $t = 10$ seconds for (a) centred and (b) off-centre jet conditions.



Development of a New Impact Pot

An impact pot designed to work well even under off-centre jet conditions must, on a fundamental level, equalise the upward flow distribution at its top opening cross section. The upward flow out of the impact box is typically skewed towards the path of least resistance, which is the opposite side of the incoming jet. Only by having an even flow distribution out of the impact pot can a symmetric tundish flow be obtained.

An effective solution for off-centre jet conditions has been obtained with an impact pot design comprising a plurality of vertical barriers arranged below several horizontal barriers. The vertical barriers' working principle consists of breaking the asymmetrical horizontal velocity components of the liquid metal flow and promoting ascending flow throughout the entire horizontal cross section of the impact pot. This effect minimises the concentrated upward flow at the opposite side of the entry jet. However, the vertical barriers alone are not enough to homogenise the flow since different vertical channels (between adjacent vertical barriers) can have

different flow velocities. Therefore, to achieve proper flow homogenisation, horizontal barriers are positioned at some distance above the vertical channels. As a result, the liquid metal flowing upwardly through the vertical channels collides with horizontal barriers and homogenises the flow. Such homogenisation occurs due to the mixing generated as the flows from adjacent vertical channels are forced against each other. Another beneficial effect is dissipation of the flow's kinetic energy caused by the longer path the fluid needs to take to go around the horizontal barriers after colliding with them. The combination of both vertical and horizontal barriers provides a homogeneous flow out of the impact pot and into the tundish, even under the unfavourable conditions of a misaligned ladle shroud.

This effect is shown in Figure 7, where the velocity contours on the bottom surface and at the top opening of the impact pot are displayed. The prior art design shows velocity vectors following the path alongside the impact pot walls, which causes most of the fluid to flow upward in a concentrated stream located at the opposite side of the box relative to the impingement point. The vertical barriers disrupt such motion, causing fractions of the flow to be entrapped in the vertical channels formed by adjacent vertical barriers. Such an effect, in combination with the flow kinetic energy dissipation caused by collision of the upward flow with the horizontal barriers located above the vertical channels, avoids the concentrated flow behaviour, as the fluid is forced upward along the entire perimeter of the impact box. Comparing the distribution of the upward flow along the top surface of the impact pot, the new development provides a significantly more even flow distribution, minimising concentrated flow spots and reducing dead zones. Consequently, asymmetry of the tundish flow is also significantly reduced, as it can be seen in Figure 8.

Figure 7.

Effect of vertical and horizontal barriers in disrupting the asymmetric flow caused by off-centre jet conditions. Velocity contours on the bottom surface of the impact pot for the (a) prior art and (b) new development. Cross section of the upward flow distribution on the top surface of the impact pot for the (c) prior art and (d) new development.

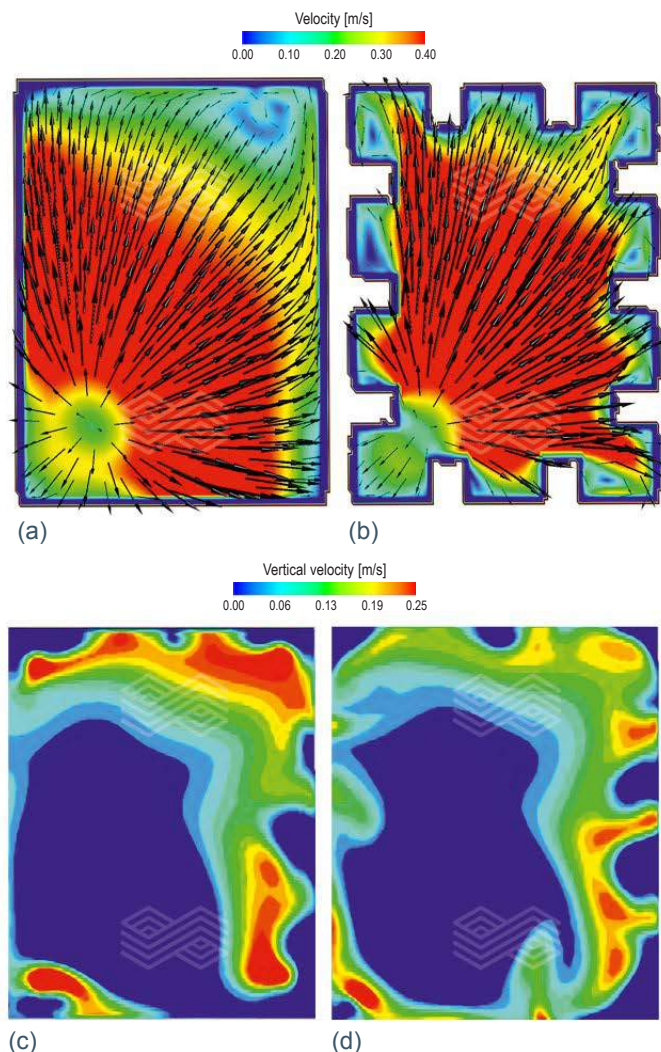
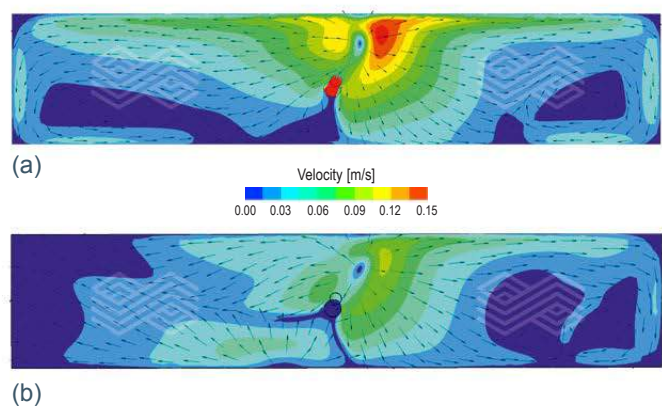


Figure 8.

Contours of the flow on the top surface of the molten steel bath for off-centre jet conditions comparing (a) the design with exclusively horizontal barriers and (b) the new development.



Another comparison between the new development and designs with exclusively horizontal barriers or exclusively vertical barriers can be seen in Figure 9, where a lateral view is depicted, and the incoming jet impinges off-centre to the right. When there are only horizontal deflectors, the concentrated jet on the left side is clearly visible and an angled and strong upward flow from right to left occurs (Figure 9a). For the configuration with exclusively vertical barriers, even though it avoids the concentrated or angled upward jets, it shows the disadvantages of lacking mechanisms to dissipate kinetic energy, as this is typically achieved by collisions of the upward flow with horizontal barriers. Thus, stronger upward velocities are seen in this case (Figure 9b). The absence of horizontal barriers also

makes it not possible to homogenise the flow between adjacent vertical channels, as achieved by the new development, which is a crucial aspect of avoiding asymmetric flows into the tundish.

Figure 10 shows a comparison of the three different designs performed using water modelling experiments. The design with horizontal barriers (Figure 10a) displays a strong bias towards the right strand already at $t = 10$ seconds, whereas the design with exclusively vertical barriers has a bias towards the left strand at $t = 20$ seconds (Figure 10b). The best results in terms of mitigating asymmetric flow were obtained for the new development, with no bias towards any of the strands (Figure 10c).

Figure 9.

Lateral view of the tundish to compare impact pot designs with (a) horizontal barriers, (b) vertical barriers, and (c) the new development. The incoming jet impinges off-centre to the right.

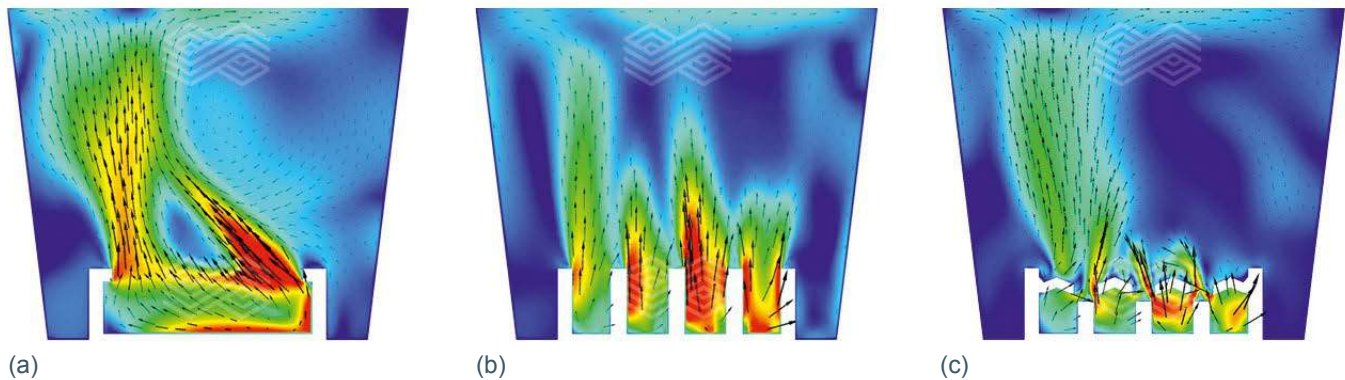


Figure 10.

Dye dispersion snapshots of water modelling experiments to compare impact pot designs with (a) horizontal barriers, (b) vertical barriers, and (c) the new development at $t = 10$ seconds and $t = 20$ seconds.

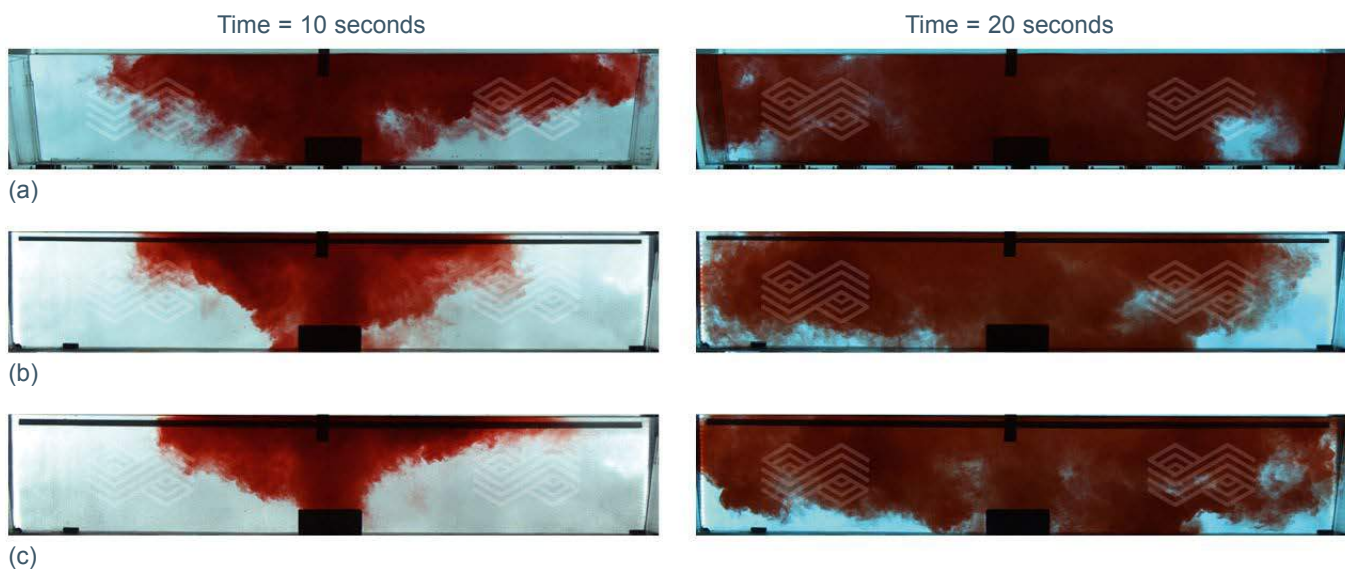
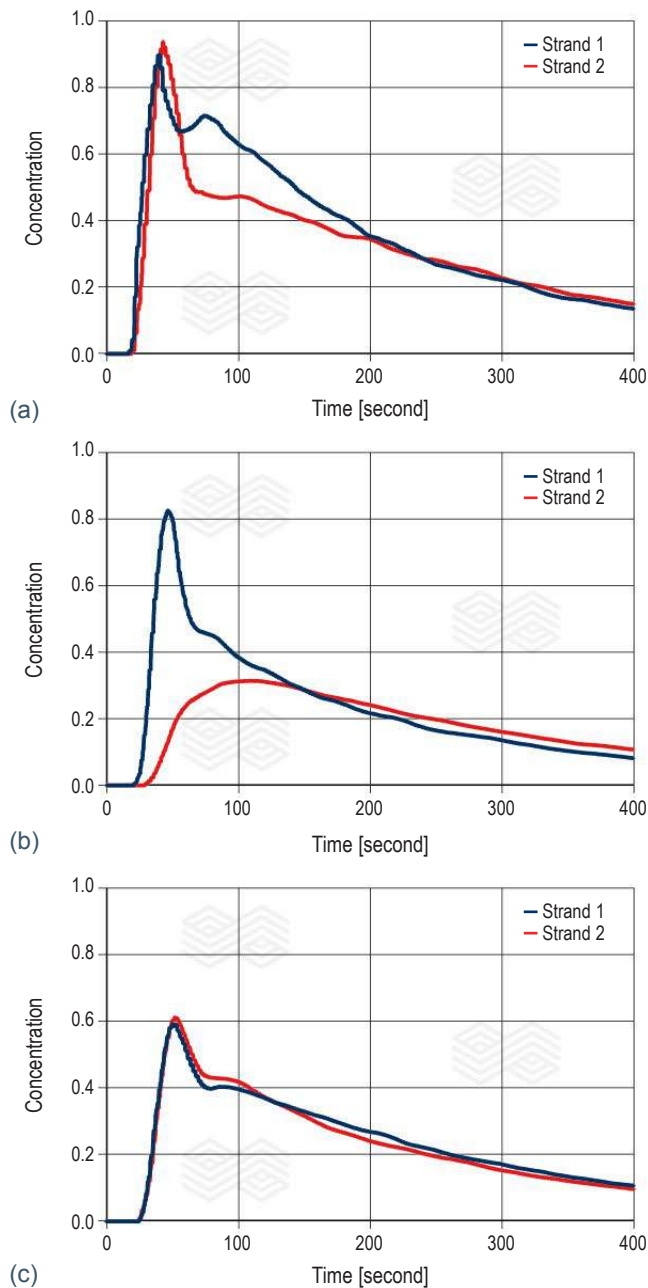


Figure 11 shows the RTD curves obtained for the three compared configurations. The designs with exclusively horizontal barriers or exclusively vertical barriers show visible differences between the curves for each of the strands, which is a quantification of asymmetry in the tundish flow. In contrast, the new development shows an almost perfect match between the curves for each strand, even though the incoming jet was asymmetric. These results confirm the effectiveness of this design as a solution for avoiding asymmetric flows into the tundish.

Figure 11.

RTD curves comparing designs with (a) horizontal barriers, (b) vertical barriers, and (c) the new development.

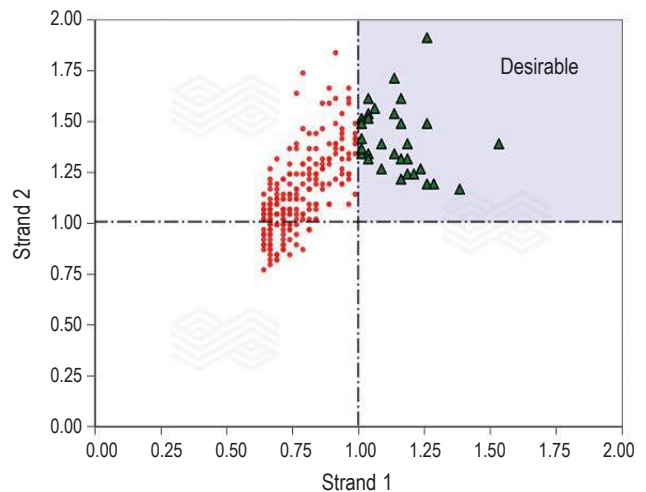


Parametric Studies

Once the effectiveness of the solution developed for avoiding asymmetric flows into the tundish had been validated through water modelling experiments, the next step was to understand which design variables were most influential on the desired outcome. Such a study was performed through a design of experiments (DOE) in which each sample was the CFD result for a different design. About 250 different designs were simulated and the corresponding minimum residence times for each sample were plotted in a chart (Figure 12). For each strand, the minimum residence times were normalised according to the average minimum residence time obtained among all the samples. If the chart is divided in four quadrants, with the axes located at the normalised average value for all samples, the results shown in the top-right quadrant will be the samples with an above average minimum residence time for both strands. From a practical perspective, this is the most desirable outcome, as higher minimum residence times are associated with several benefits for the process and ideally should be obtained for both strands. Analysing the plot, it can be concluded that, from all the samples simulated, only a fraction of those are desirable designs. Therefore, by studying the design dimensions of the desirable designs compared to the full design range evaluated, some insights about the influence of each design parameter can be obtained.

Figure 12.

Plot of the normalised minimum residence times obtained for each strand of each design.



For example, this method can be applied to evaluate the influence of the height of the vertical barrier, as shown in Figure 13. Even though an equal number of designs were simulated for each range of this design parameter, it was only above a certain threshold value that the designs were in the desirable quadrant. This means that not only the height of the vertical barrier is an important design parameter, but also that it should not be too low, otherwise its effect on the flow will not be noticed and the design will fail to work as it should. Such information is very relevant to design effective impact pots for several different steel plants that might each require a tailor-made solution. The same method can be applied to other design parameters of interest, such as protrusion length of the vertical and horizontal barriers, angles of the barriers, and distance between the barriers.

Figure 13.

Desirable range of the vertical barrier height. (a) number of simulated designs for each vertical barrier height range, (b) number of good designs and vertical barrier height range, and (c) diagram indicating barrier height measurement (red arrow).

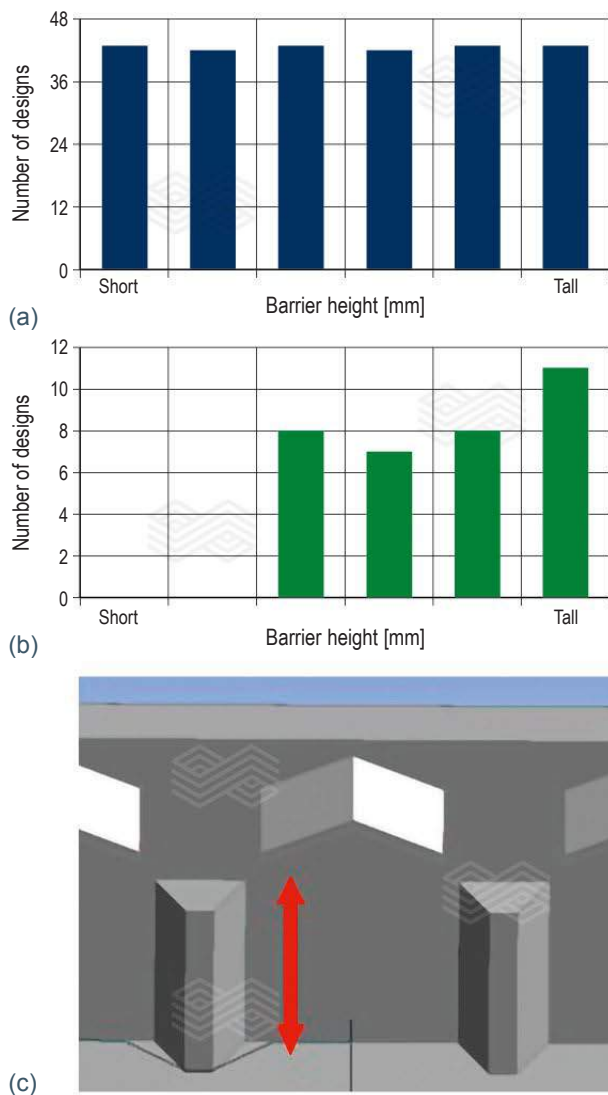


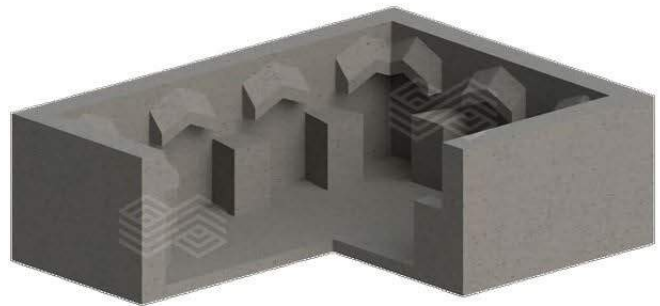
Figure 14 shows a representation of a specific design that performed very well in the simulations and experiments described in this paper, following the concept of the novel development. The next steps planned are to perform plant trials with this new development and measure the improvements obtained in the caster, particularly when off-centre or angled jet conditions are present.

Conclusions

The combination of CFD simulations and appropriate DOE methods can provide a deep understanding of how to design an effective impact pot for any desired purpose. The premise of this paper was to develop a novel design to solve the issue of asymmetric flows caused by off-centre pouring into

Figure 14.

Novel impact pot design that performs even under off-centre jet conditions.



the tundish. The effectiveness of the new solution was confirmed by water modelling experiments, in which it was compared to prior art designs, in particular to designs following the concept of having exclusively horizontal barriers or exclusively vertical barriers. The results from dye dispersion experiments and RTD analysis demonstrated that the novel design was the only effective solution for avoiding asymmetric flows into the tundish, subject to an off-centre pouring condition. This innovative solution illustrates the potential of modelling and simulation tools to develop new technologies for the refractory and steelmaking industry.

References

- [1] Resende, A., Lukesch, G., Hackl, G. and Meurer, D. Tundish Impact Pot Optimization Through Mathematical and Physical Modeling. Proceedings of the 10th European Conference on Continuous Casting, Bari, Italy, October 20–22, 2021.
- [2] Hackl, G., Tang, Y., Lukesch, G., Meurer, D., Shivaram, P. and Resende, A. Impact Zone Solutions for an Improved Flow Performance in the Tundish. Proceedings of AISTech, Pittsburgh, USA, May 6–9, 2019, 2851–2858.
- [3] Chattopadhyay, K., Isac, M. and Guthrie, R. Effect of Flow Modifiers on Liquid Metal Cleanliness in Four-Strand Delta Shaped Billet Caster Tundish. *Ironmaking and Steelmaking*. 2012, 39, 454–462.
- [4] Fan, C.M., Shie, R.J. and Hwang, W.S. Studies by Mathematical and Physical Modelling of Fluid Flow and Inclusion Removal Phenomena in Slab Tundish for Casting Stainless Steel Using Various Flow Control Device Designs. *Ironmaking and Steelmaking*. 2003, 30, 341–347.
- [5] Espino-Zárate, A., Morales, R., Nájera-Bastida, A., Macías-Hernández, M.J. and Sandoval-Ramos, A. Fluid Flow and Mechanisms of Momentum Transfer in a Six-Strand Tundish. *Metallurgical and Materials Transactions B*. 2010, 41B, 962–975.
- [6] Sahai, Y. and Emi, T. Melt Flow Characterization in Continuous Casting Tundishes. *ISIJ International*. 1996, 36, 6, 667–672.
- [7] Mazumdar, D. and Guthrie, R. The Physical and Mathematical Modelling of Continuous Casting Tundish Systems. *ISIJ International*. 1999, 39, 524–547.

Reprint permission

Reprinted with permission from the AISTech 2023

Authors

Alexandre Resende, RHI Magnesita, Contagem, Brazil.

Rubens Freire, RHI Magnesita, Vienna, Austria.

Gernot Lukesch, RHI Magnesita, Leoben, Austria.

Gernot Hackl, RHI Magnesita, Leoben, Austria.

Daniel Meurer, RHI Magnesita, Leoben, Austria.

Corresponding author: Alexandre Resende, Alexandre.Resende@rhimagnesita.com



Philip Schantl and Christian Majcenovic

Reaction Textures in $\text{Al}_2\text{O}_3\text{-SiO}_2$ Bricks Induced by Gaseous SO_x Attack: New Insights From Mineralogy and Thermodynamic Modelling

In the sulphate process, $\text{Al}_2\text{O}_3\text{-SiO}_2$ refractory bricks are used to line rotary kilns. During calcination of hydrated TiO_2 , these bricks are subjected to highly aggressive and corrosive SO_x gas attack at operating temperatures between 850–950 °C. A systematic mineralogical study on mineral reaction textures and compositional zoning from the hot face towards the cold end of a representative used fireclay brick in combination with thermochemical modelling and the application of the Dietzel's field strength enabled the thermochemical modifications of the brick microtexture and the acting wear mechanisms to be reconstructed. Gaseous SO_x supply resulted in a strong alteration of the mullite dominated brick matrix up to a depth of ~28 mm from the immediate hot face through mullite decomposition and aluminium sulphate plus quartz forming reactions. Based on thermochemical calculations these reactions appear between 760 and 440 °C. In a second step, the newly formed aluminium sulphate decomposed and transformed to flaky corundum by SO_x gas releasing reactions. This could only be observed at the very hot face of the brick, up to a depth of ~10 mm, where minimum temperatures of 720–780 °C were reached. These temperature estimations were obtained by the combined application of thermochemical phase equilibrium and reaction delta G^0 calculations. This two-step corrosion texture development led to a significant weakening of the brick bonding structure and enabled consequent discontinuous material loss at the refractory hot face by abrasive wear during the feed material transport through the rotary kiln. As a result of the postmortem study, a special silica-sol impregnation is recommended to improve the resistance of the brick matrix against volatile SO_x attack.

Introduction

The usage of concentrated sulphuric acid during the production of highly pure TiO_2 pigment challenges refractory producers because products lining the rotary kiln used to calcine hydrated TiO_2 must withstand highly aggressive and corrosive SO_x gas. To resist such a gas attack, SiO_2 -rich fireclay bricks are preferentially used to line these kilns, as silicon is known to have a high resistance against sulphur attack. This is deduced from the Dietzel's field strength which indicates that both silicon and sulphur have a high field strength of 1.56 \AA^{-2} and 2.60 \AA^{-2} , respectively [1], and thus have a low affinity for each other to form a new binary oxidic compound. However, aluminium within these fireclay bricks is much lower in the Dietzel's field strength (0.84 \AA^{-2}) than silicon and has a high potential to interact with acidic SO_x gas to form new phases that can destruct and weaken the microtexture of the bricks' hot face. As a result, the refractory product is vulnerable to mechanical wear and mass loss by abrasion.

In this study, new insights into the microtextural and microchemical modification and the consequent wear phenomena of a fireclay brick that was used in a TiO_2 rotary kiln are presented. These findings are based on detailed microscopic observations of mineral reaction textures, the measured compositional zoning from the hot face towards the cold end of the investigated brick, and thermochemical phase equilibrium modelling. In addition, a solution that improves the bricks' resistance against volatile SO_x gas attack to avoid microtextural modifications is provided.

Sulphate Process

Due to its whiteness, high refractive index, and resulting light-scattering ability, TiO_2 is commonly used for whitening papers, paints, rubbers, plastics, and other materials. Since the early twentieth century, this pigment can be produced commercially by the sulphate process [2–5]; a batch process where finely ground ilmenite or high- TiO_2 slag is digested in concentrated sulphuric acid. After initial heating, a strong exothermic reaction (+220 °C) starts between the titanium-bearing raw material and the acid. This leads to the formation of a porous solid cake which is then dissolved in diluted acid and water to yield a titanyl sulphate + iron sulphate solution according to the equation:



By adding scrap iron, any ferric iron present is reduced to the ferrous state to avoid any precipitation of embrowning ferric iron during the following process steps and to facilitate washing of the titanium-bearing material, as ferric iron is less absorbing than ferrous iron. This reduction step is not necessary when high- TiO_2 slag is used as feed material since low amounts of iron in the slag are already in a reduced state. To remove any unreacted solids after the reduction of ferrous iron, the solution is clarified by filtration and settling. Ferrous sulphate heptahydrate, which crystallises from the iron sulphate, is then filtered out from the solution.

After iron removal, the solution is concentrated and titanium sulphate is hydrolysed (at 95–110 °C) to hydrated TiO₂ according to the equation:



In a final step, the hydrated TiO₂ is calcined in a rotary kiln to precipitate rutile or anatase. This calcination needs temperatures in the range of 850–950 °C. A representative image of the interior of a fireclay brick lined rotary kiln is presented in Figure 1.

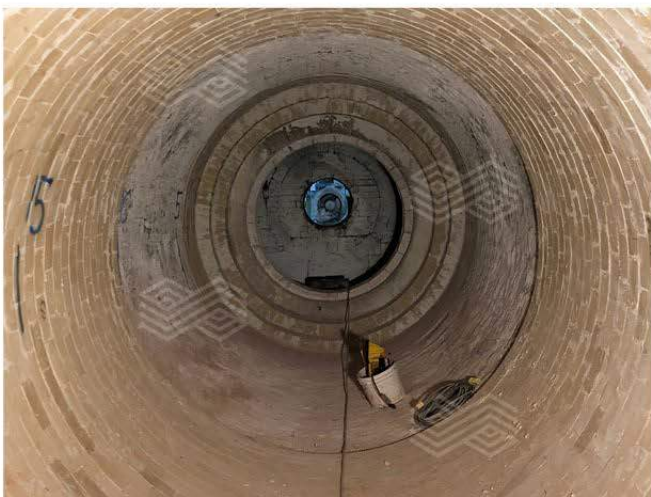
Methods

After furnace shut down, a worn clay-bonded fireclay brick was taken from the rotary kiln for a postmortem study at RHI Magnesita's Technology Center Leoben (Austria). The investigation aim was to provide information about the condition of the refractory, the wear mechanism, and possible optimisation potential. Firstly, a visual inspection was conducted on the worn brick and its cross-section. Succeeding detailed mineralogical investigations and quantitative mineral analyses were carried out on two polished sections prepared from the hot face area using a reflected light microscope and a JEOL JSM-6460 scanning electron microscope (SEM) equipped with an Oxford X-Max 100 energy dispersive system (EDS) and an Oxford wavelength dispersive system. Additional high-resolution, back-scattered electron (BSE) images were obtained from a JEOL JSM-7900F field emission gun SEM. Measurement conditions of the SEM were a 20 kV acceleration voltage, 2 nA beam current, and ~1 µm beam diameter. Natural and synthetic mineral standards were used for element calibration.

In order to evaluate the chemical modification and penetration of corrosive species into the brick matrix from the hot face towards the cold end, an ~38 mm long "semi-quantitative" compositional profile was obtained by measuring twenty-five 1.5 x 1.5 mm EDS matrix area analyses within the two prepared polished sections.

Figure 1.

Representative photograph of the interior area of a fireclay brick lined rotary kiln used for the calcination of hydrated TiO₂ to precipitate rutile or anatase.



Postmortem Study

On visual inspection (Figure 2), the investigated clay-bonded fireclay brick showed a crumbly hot face area up to a depth of ~4 cm. The surface was rough and irregular which pointed to discontinuous mass loss.

Three zones labelled with A, B, and C had developed from the hot face towards the cold end of the worn brick. These zones differed in their colouration and textural appearance. While zone A and B were friable, zone C appeared widely dense and compact.

Microscopy and Mineral Chemistry

Zone A

Based on the mineralogical compositions, zone A could be subdivided into zone A1 and A2. In zone A1, comprising the very first 5 mm from the immediate hot face, fireclay coarse grains showed patchy, granular rim areas (Figure 3a) which were strongly enriched in SiO₂ and depleted in Al₂O₃ (Figures 3c and 3d). The inner parts of these fireclay grains appeared widely unaltered and consisted of the original assemblage mullite and glassy phase. The former mullite dominated matrix was entirely modified. It appeared porous and was defined by abundant newly formed tiny corundum plates, up to 4 µm in size (Figure 3b). SiO₂ disappeared completely within the matrix (Figure 3d).

In zone A2, from a depth of ~5 mm to ~10 mm, it was similar to zone A1 but showed the additional occurrence of rare aluminium sulphate within the corundum dominated matrix (Figures 3e and 3f). Typically, this aluminium sulphate showed decomposition features on its crystal boundaries and was partly replaced by tabular corundum crystals on its edges.

Figure 2.

Photograph of the worn clay-bonded fireclay brick showing a rough hot face and three distinct zones (A, B, and C). Polished sections for microscopy were taken from the black box (M). The compositional EDS profile line from zone A towards zone C is indicated as a grey arrow labelled P.

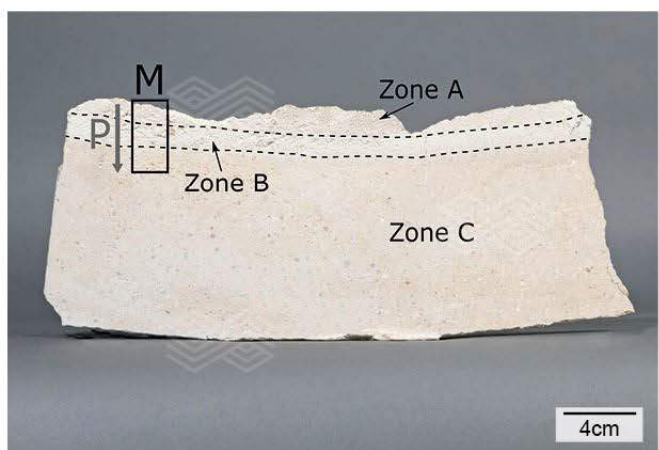
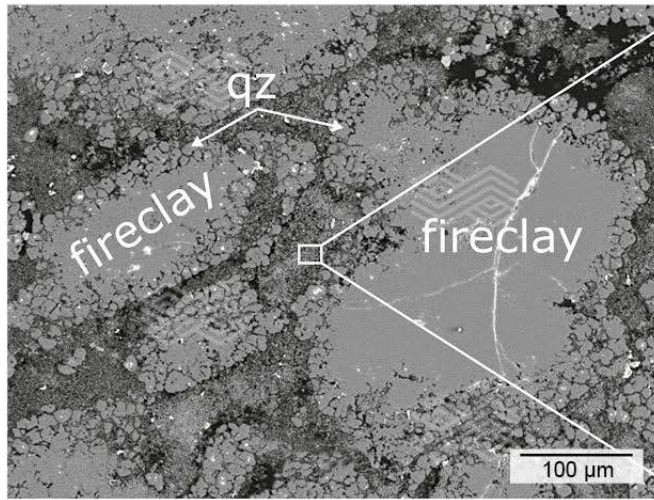
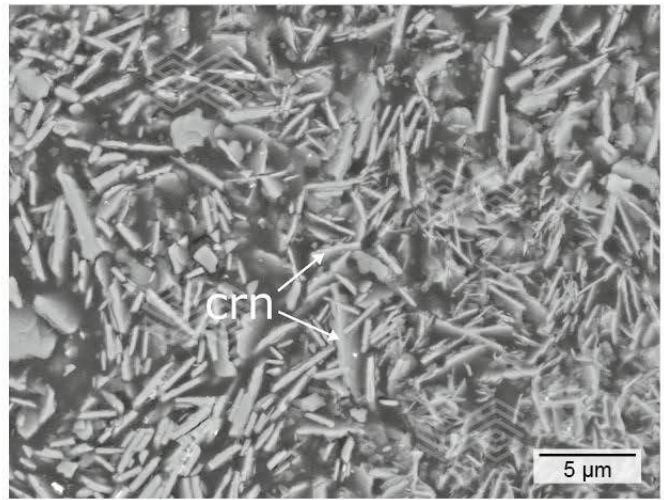


Figure 3.

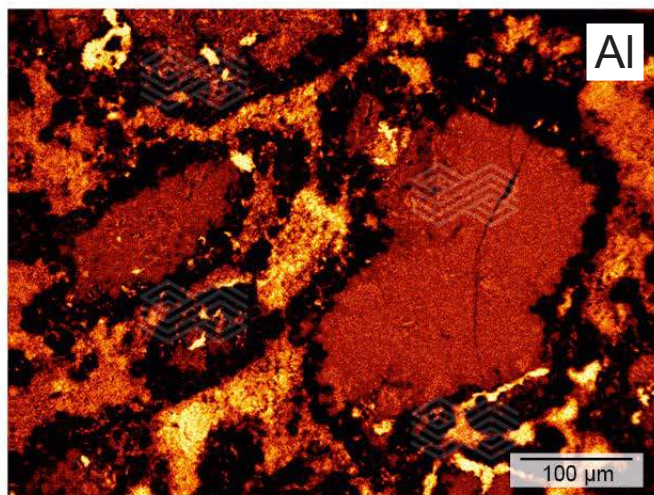
BSE images and X-ray element distribution mappings of zone A. (a) fireclay coarse grains with a patchy, granular rim area consisting of quartz (qz). (b) the matrix appears porous and is composed of tiny tabular corundum (crn) crystals. (c, d) X-ray element distribution mappings of Al and Si indicate that the rim area of the fireclay coarse grains is strongly depleted and enriched in Al and Si, respectively. (e) aluminium sulphate occurs rarely within the brick matrix in a thin layer in zone A, near to zone B. (f) the matrix within this thin layer in zone A is mainly composed of tiny tabular corundum (crn) crystals.



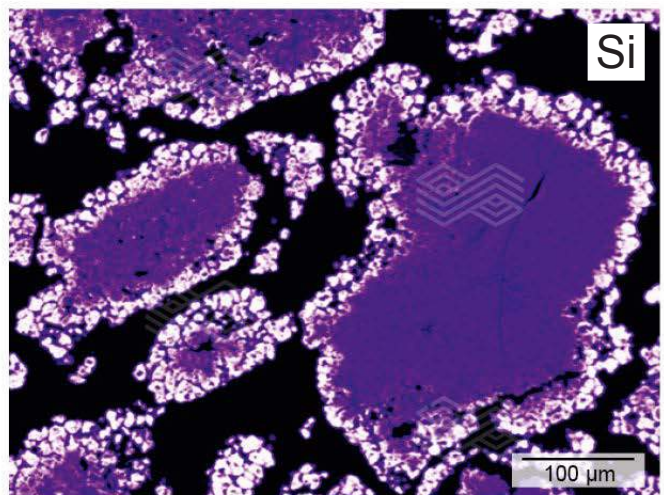
(a)



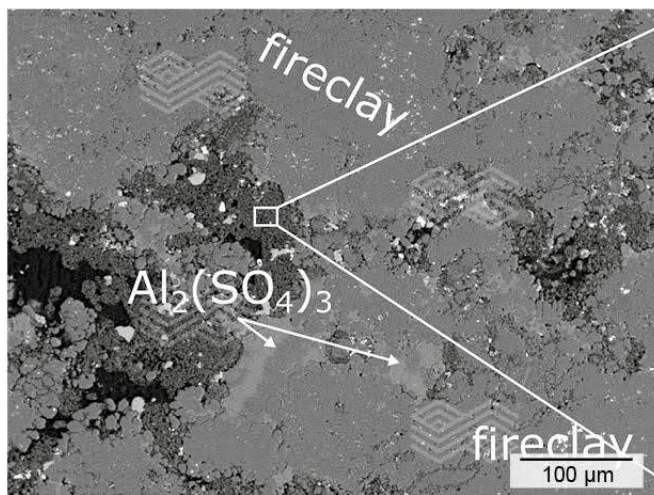
(b)



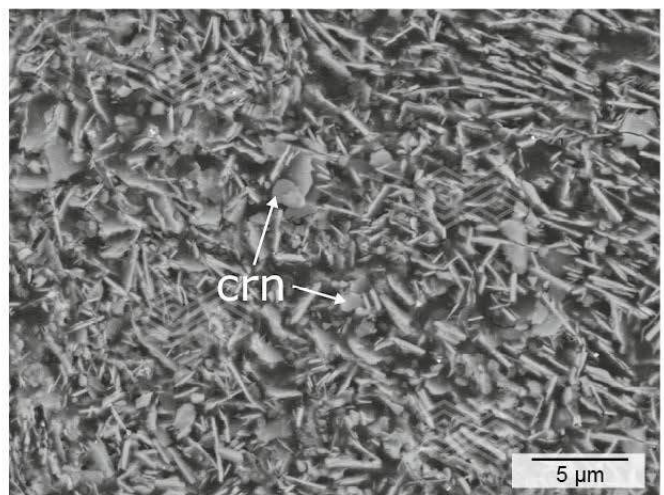
(c)



(d)



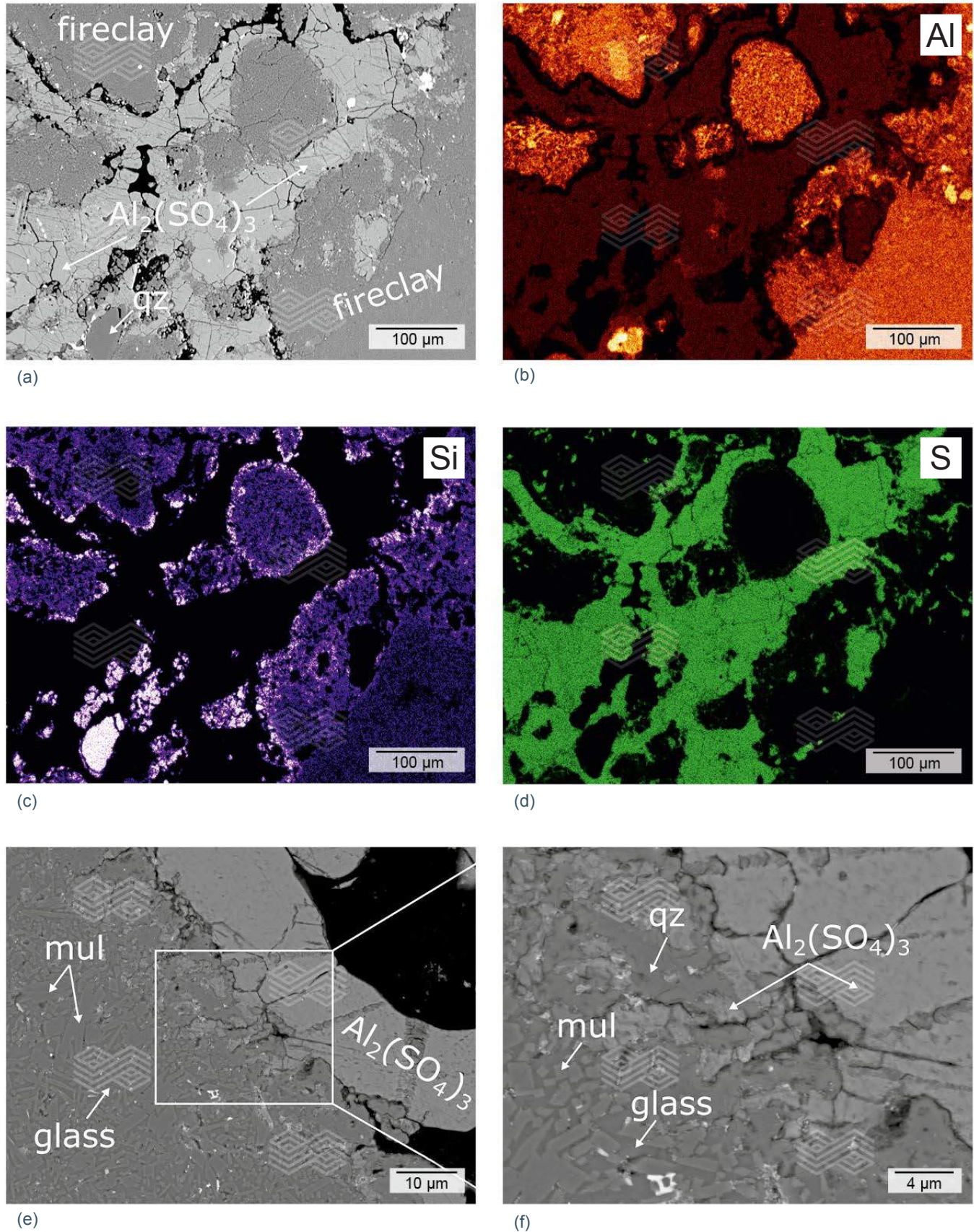
(e)



(f)

Figure 4.

BSE images and X-ray element distribution mappings of zone B. (a) fireclay coarse grains show an altered rim area and are surrounded by pores. The matrix is totally modified and consists of newly formed aluminium sulphate and minor quartz (qz). No primary mullite (mul) can be found within this matrix. (b–d) X-ray element distribution mappings of Al, Si, and S show that the rim of the fireclay coarse grains is strongly depleted in Al and enriched in Si. The matrix consists of high S and moderate Al concentrations. No primary Si can be found within this matrix. (e, f) primary mullite (mul) crystals at the edges of fireclay coarse grains are decomposed to form aluminium sulphate and quartz (qz).



Zone B

Fireclay coarse grains in zone B showed similar textural and chemical features as in zone A. The rim areas were modified and had high SiO₂ and low Al₂O₃ concentrations (Figure 4). The central part was unaffected by chemical and textural modifications and consisted of primary mullite and glassy phase. These fireclay grains were embedded within a strongly altered matrix that mainly consisted of newly formed aluminium sulphate and minor quartz (Figure 4a). Typically, the aluminium sulphate was highly pure and contained low Fe₂O₃ (0.74–1.19 wt.%), MgO (0.34–0.57 wt.%), and Na₂O (<0.52 wt.%) concentrations (Table I). Based on mineral formula calculations, these phases could be identified as millosevichites.

Aluminium sulphate was found locally with high K₂O concentrations in the range of 15.98–16.20 wt.% (see Table I) and was determined to be yavapaiite. High-resolution BSE images of the interface area between fireclay grains and aluminium sulphate revealed that primary mullite crystals of fireclay grains had decomposed into aluminium sulphate and quartz (Figures 4e and 4f).

Zone C

No textural or chemical alterations could be found in zone C of the studied brick. Fireclay coarse grains consisted of primary mullite and glassy phase. They occurred within an unaltered fine-grained matrix composed of small mullite crystals and interstitial glassy phase.

Semi-Quantitative Compositional Profile

The compositional matrix profile from the immediate hot face up to ~38 mm depth (Figures 2 and 5) showed a strong correlation between changes of the Al₂O₃, SiO₂, and SO₃ contents, which fitted with the mineralogical observations.

The very first ~5 mm of zone A1 were characterised by high Al₂O₃ (30–40 wt.%), low SiO₂ (<10 wt.%), and even lower SO₃ (<4 wt.%) concentrations. In zone A2, from a depth of ~5 to ~10 mm, Al₂O₃ started to decrease, while SiO₂ and SO₃ showed a slight increase. At ~10 mm from the immediate hot face, SO₃ showed a sharp and pronounced increase and marked the onset of zone B. The following 18 mm of the profile were highly enriched in SO₃ with varying contents between 30 and 45 wt.%. SiO₂ and Al₂O₃ was generally low in this zone and showed a strong fluctuation at <20 wt.%. At ~28 mm depth, zone B had a sharp and pronounced depletion of SO₃ and a coincident increase of Al₂O₃ and SiO₂. The following zone C showed a SO₃ concentration close to 0 wt.% and constant Al₂O₃ and SiO₂ concentrations at ~36 and ~49 wt.%, respectively. This indicated a chemically unaltered fireclay matrix.

Figure 5.

Compositional matrix profile from the immediate hot face of the investigated worn fireclay brick up to a depth of ~38 mm. A strong correlation between changes of the Al₂O₃, SiO₂, and SO₃ contents can be observed.

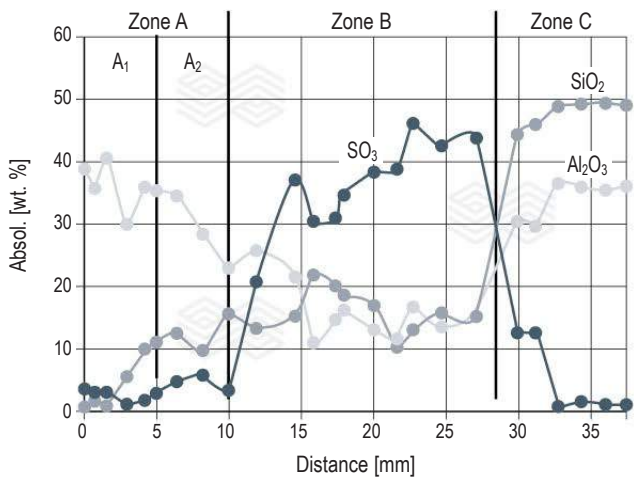


Table I.

Representative composition of aluminium sulphates within the matrix of zone B. Abbreviations include below detection (b.d.).

[wt.%]	Millosevichite						Yavapaiite			
SO ₃	70.06	68.74	69.78	69.39	69.19	68.12	61.98	61.87	62.14	60.94
Al ₂ O ₃	28.82	29.52	29.37	29.13	28.76	29.29	19.58	19.36	20.37	19.10
Fe ₂ O ₃	1.10	0.84	0.74	0.77	1.19	1.07	1.14	1.40	1.40	0.89
MgO	0.57	0.34	0.36	b.d.	0.70	0.44				
Na ₂ O	0.44	b.d.	b.d.	0.33	0.52	0.29	0.84	0.85	0.90	1.14
K ₂ O							16.20	16.00	15.98	16.02
Total	100.99	99.44	100.25	99.62	100.36	99.21	99.74	99.48	100.79	98.09
	Atoms per 12 O						Atoms per 8 O			
S	2.987	2.970	2.983	2.991	2.974	2.959	1.994	1.996	1.979	1.996
Al	1.907	2.003	1.983	1.972	1.942	1.998	0.989	0.981	1.019	0.983
Fe ³⁺	0.047	0.036	0.032	0.033	0.051	0.047	0.037	0.045	0.045	0.029
Mg	0.048	0.029	0.031		0.060	0.038	0.070	0.071	0.074	0.096
Na	0.048			0.037	0.058	0.033				
K							0.886	0.877	0.865	0.892
Σ Cations	5.037	5.038	5.029	5.033	5.085	5.075	3.976	3.970	3.982	3.996

Phase Equilibrium Modelling

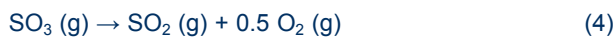
In order to gain additional information about the gas attack and corrosive reactions in zone A and B of the studied worn brick, thermochemical phase equilibrium diagrams based on the observed mineral textures and newly formed phases were constructed. The Gibbs free energy minimisation software FactSage [6,7] was used, employing the thermodynamic datasets FactPS, FToxide, and FTmisc.

Reconstruction of Gas Species Attacking the Refractory

The high abundance of aluminium sulphate in zone B implies a supply of SO_x gas and its interaction with the refractory material. It is therefore reasonable to assume that remnants of liquid H_2SO_4 from either the dissolution procedure (equation 1) or the hydrolysis step (equation 2) were dragged into the rotary kiln where it evaporated to gaseous SO_x species at operating temperatures of 850–950 °C. To estimate the relative quantities of acting SO_x gas species in this temperature range, the phase stabilities of 1 mole H_2SO_4 from 0–1000 °C were modelled. The computed diagram is shown in Figure 6 and indicates that liquid H_2SO_4 changes to gaseous species at about 310 °C. From ~310 to ~500 °C the gaseous H_2SO_4 shows a pronounced dissociation according to the equation:

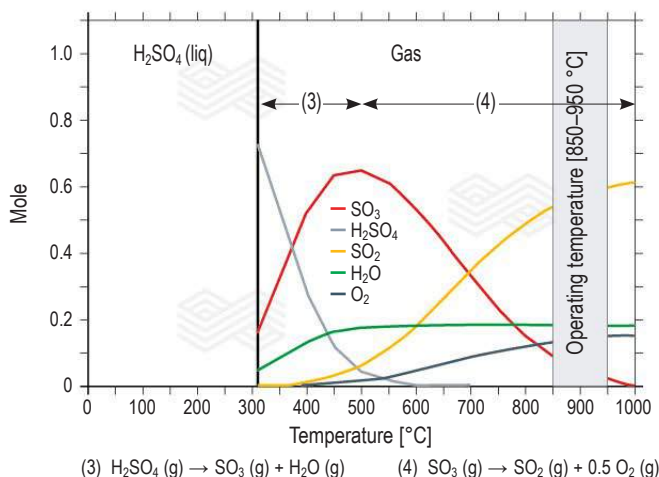


This leads to a pronounced decrease of H_2SO_4 (g) and a significant increase of SO_3 (g) species, while H_2O (g) increases moderately. At ~500 °C the dissociation reaction changes and SO_3 (g) starts to decompose generating SO_2 (g) and O_2 (g) as follows:



Based on the computed stabilities of sulphur-bearing species (see Figure 6), relatively high SO_2 (g) and low SO_3 (g) concentrations that interact with the refractory material at operating temperatures of 850–950 °C during the calcination of hydrated TiO_2 can be assumed. In addition, the presence of H_2O (g) and O_2 (g) is given.

Figure 6. Phase stabilities of 1 mole H_2SO_4 from 0–1000 °C, computed by FactSage.



Temperature Estimation of Acting Corrosive Reactions in Zone A

Although the matrix of zone A was defined by a pervasive mineralogical and microtextural alteration, microscopic observations (see Figure 3) in combination with a semi-quantitative chemical profile (see Figure 5) indicated the formation of abundant small corundum plates at the expense of previously stable aluminium sulphate via SO_x (g) releasing reactions. Assuming a pure aluminium sulphate end member (millosevichites, see Table I), the following temperature driven equations can be formulated as responsible for the mineralogical observations in zone A:



To obtain meaningful temperature estimates for these reactions, the phase stabilities of 1 mole $\text{Al}_2(\text{SO}_4)_3$ over the temperature range of 300–1000 °C were performed. The resulting diagram is shown in Figure 7a. Accordingly, aluminium sulphate appears up to temperatures of 722 °C. Corundum, which was observed as a stable phase in zone A, occurs at temperatures higher than 722 °C in the presence of gaseous SO_3 , SO_2 , and O_2 . The amounts of SO_2 and O_2 show an increase from 722 °C to 1000 °C, which correlates with a SO_3 decrease. This is due to the progressive SO_3 dissociation with increasing temperature. Additional temperature restrictions were achieved by calculating delta G^0 for equations 5 and 6 from 300–1000 °C (Figure 7b). It can be seen that delta G^0 of both reactions decreases with increasing temperature. This confirms the raising tendency of corundum formation due to aluminium sulphate decomposition with increasing temperatures. It also shows that delta G^0 reaches 0 Joule at 780 °C. Thus, a minimum of 780 °C can be assumed for the corundum formation in zone A according to equations 5 and 6. This is about 60 °C higher than the minimum temperatures obtained from the phase stability diagram in Figure 7a, as only the pure end member reactions were considered.

Temperature Estimation of Acting Corrosive Reactions in Zone B

Based on the observed microtextures, mullite within the brick matrix and fireclay rims decomposed to form aluminium sulphate and quartz in the presence of SO_x gas (Figures 4a, 4e, and 4f). Assuming pure end members, two equations can be postulated to explain these textures:



Using the stoichiometry of these reactions (e.g., 1 mole $\text{Al}_6\text{Si}_2\text{O}_{13}$ and 9 mole SO_3), the phase stabilities from 300–1000 °C were computed to estimate the temperature dependent stability of mullite in the presence of SO_x gas (Figure 7c). It shows that mullite is stable at temperatures higher than 760 °C and decomposes from 760–440 °C to form aluminium sulphate and quartz.

At temperatures lower than 440 °C only aluminium sulphate and quartz appear. Based on these calculations, the formation of the observed phase assemblage aluminium sulphate + quartz at the expense of mullite can only be formed in the temperature range of 760–440 °C. This was also confirmed by the delta G^0 calculations for equations 7 and 8 over the temperature range of 300–1000 °C (Figure 7d). There, it shows that delta G^0 of both reactions decreases with decreasing temperatures, which implies that mullite decomposition in the presence of SO_x is intensified with decreasing temperatures. As delta G^0 of both reactions reaches 0 Joule at 760 °C, it is estimated that equations 7 and 8 occur at temperatures lower than 760 °C.

Aluminium Sulphate Formation Explained by the Application of Dietzel's Field Strength

The tendency of new compounds to form from a refractory and externally supplied chemical species depends on the difference in their basicity/acidity, which was first described by Adolf Dietzel in 1948. In order to quantify the basicity/acidity of a single species, he defined the so-called Dietzel's field strength (Fs). It is expressed through the equation:

$$F_s = Zc/a^2 \quad (9)$$

Where Zc is the valence of the cation and a is the distance in Å between the cation and the bonded oxygen.

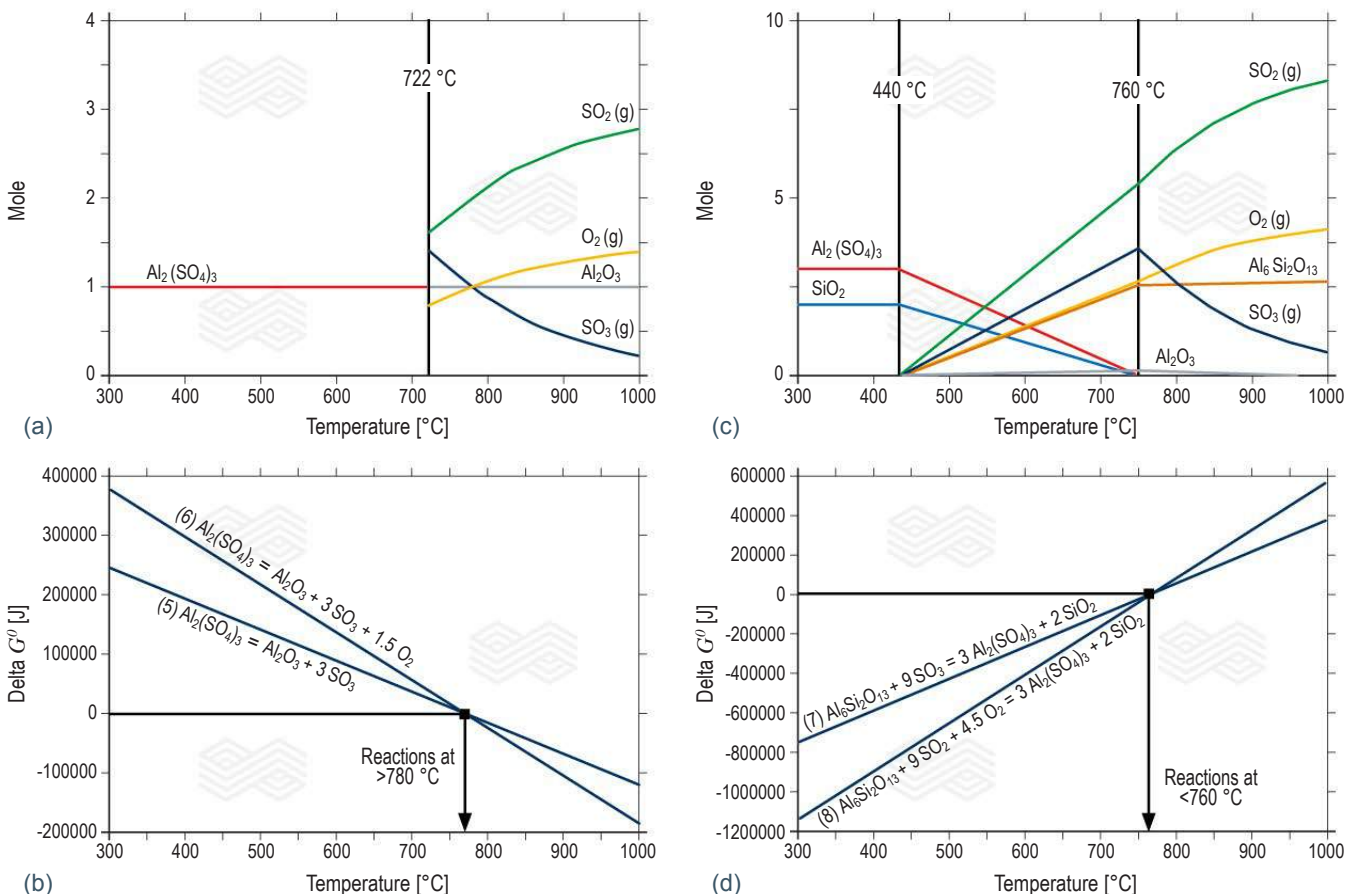
This approach is based on the bonding strength due to the Coulomb force (attraction/repulsion) between cations and anions in a liquid glass [8]. Accordingly, elements with a high F_s are defined as acidic and elements with a low F_s are defined as basic species.

The field strength difference (ΔF_s) between two species gives indications about their tendency to form a binary oxidic compound. In this respect, a minimum ΔF_s of 0.3 \AA^{-2} is needed to form a new compound and the higher the difference between two species, the higher the tendency of new compound formation. If the F_s of two species is similar and ΔF_s is lower than 0.3 \AA^{-2} , no compound formation will occur [8].

In the present study, the refractory compound mullite was found to strongly interact with externally supplied SO_x gas species to form the new binary oxidic compound aluminium sulphate and remnant quartz (Figure 4a). This interaction can be considered in terms of the respective cation's Dietzel's field strength (F_s), where the F_s of $\text{Al}^{3+} = 0.84 \text{ \AA}^{-2}$, $\text{Si}^{4+} = 1.56 \text{ \AA}^{-2}$, and $\text{S}^{6+} = 2.60 \text{ \AA}^{-2}$. Accordingly, mullite in contact with SO_x gas implies a higher ΔF_s and thus a higher tendency of new phase formation between Al^{3+} and S^{6+} (1.76) than between Si^{4+} and S^{6+} (1.04). This confirms the strong affinity between aluminium and sulphur which consequently results in the formation of the observed aluminium sulphate. As silicon within the mullite has a lower affinity for sulphur it remains as SiO_2 relics (e.g., Figure 4f).

Figure 7.

(a) computed phase stabilities of 1 mole $\text{Al}_2(\text{SO}_4)_3$ over the temperature range of 300–1000 °C. (b) delta G^0 calculations for the reactions $\text{Al}_2(\text{SO}_4)_3 \rightarrow \text{Al}_2\text{O}_3 + 3 \text{SO}_3$ and $\text{Al}_2(\text{SO}_4)_3 \rightarrow \text{Al}_2\text{O}_3 + 3 \text{SO}_2 + 1.5 \text{O}_2$ from 300–1000 °C. (c) computed phase stabilities of 1 mole $\text{Al}_6\text{Si}_2\text{O}_{13}$ and 9 mole SO_3 over the temperature range of 300–1000 °C. (d) delta G^0 calculations for the reactions $\text{Al}_6\text{Si}_2\text{O}_{13} + 9 \text{SO}_3 \rightarrow 3 \text{Al}_2(\text{SO}_4)_3 + 2 \text{SiO}_2$ and $\text{Al}_6\text{Si}_2\text{O}_{13} + 9 \text{SO}_2 + 4.5 \text{O}_2 \rightarrow 3 \text{Al}_2(\text{SO}_4)_3 + 2 \text{SiO}_2$ from 300–1000 °C.



Conclusion

During calcination of hydrated TiO₂ at about 850–950 °C, fireclay bricks in the rotary kiln are affected by a pronounced thermochemical load. Acidic gaseous SO_x attack induces microtextural alteration of the brick matrix up to a depth of ~28 mm from the immediate hot face. This leads to a weakening of the brick bonding structure and enables subsequent discontinuous material loss at the refractory hot face by abrasive wear during the feed material transport through the rotary kiln. Weakening of the brick bonding structure is caused by a two-step corrosion that can be summarised as follows:

- Initially, the supply of gaseous SO₂ and SO₃ into the hot face of the Al₂O₃-SiO₂ brick alters the mullite dominated matrix up to a depth of ~28 mm through equations 7 and 8. Based on thermochemical calculations, mullite in the matrix decomposes to form aluminium sulphate and quartz at temperatures between 760–440 °C. SiO₂ is totally displaced from the matrix and concentrates on the rim areas of large fireclay grains through diffusional processes.
- In a second step, the newly formed aluminium sulphate within the altered brick matrix at the very hot face, up to ~10 mm depth, decomposes at a minimum of 720–780 °C through SO_x gas generation (equations 5 and 6). This temperature estimation is obtained by the combined application of thermochemical phase equilibrium and reaction delta G^0 calculations. Consequently, a very porous and fragile corundum dominated brick matrix is formed that increases the refractory vulnerability against discontinuous material loss by abrasive wear.

The detailed microtextural observations in combination with phase equilibrium modelling and application of the Dietzel's field strength provide evidence that Al₂O₃ in the mullite of the used fireclay bricks strongly interacts with SO_x gas that leads to a significant alteration and weakening of the matrix bonding structure and consequent wear. In contrast, the more acidic SiO₂ species in the brick is widely unaffected by the presence of SO_x gas. Thus, it is recommended to impregnate the bricks with a special silica sol to improve the resistance of the brick matrix against volatile acidic SO_x gas attack.

References

- [1] Dietzel, A. Die Kationenfeldstärke und ihre Beziehungen zu Entglasungsvorgängen, zur Verbindungsbildung und zu den Schmelzpunkten von Silikaten. *Zeitschrift für Elektrochemie und angewandte physikalische Chemie*. 1942, 48, 9–23.
- [2] Baxter, J.L. Heavy Mineral Sand Deposits of Western Australia. *M.R. Bulletin. Geological Survey of Australia*. 1977, 10, 147.
- [3] Chernet, T. Applied Mineralogical Studies on Australian Sand Ilmenite Concentrate With Special Reference to its Behaviour in the Sulphate Process. *Minerals Engineering*. 1999, 12, 485–495.
- [4] Lynd, L.E. and Lefond, S.J. *Titanium Minerals*. In: *Industrial Minerals and Rocks*; Society of Mining Engineers: New York, 1983, 1303–1362.
- [5] Stanaway, K.J. Overview of Titanium Dioxide Feedstocks. *Mining Engineering*. 1994, 46, 1367–1370.
- [6] Bale, C.W., Béllisle, E., Chartrand, P., Decterov, S.A., Eriksson, G., Gheribi, A.E., Hack, K., Jung, I.-H., Kang, Y.-B., Melançon, J., Pelton, A.D., Petersen, S., Robelin C., Sangster, J., Spencer, P. and Van Ende, M-A. FactSage Thermochemical Software and Databases, 2010–2016. *Calphad*. 2016, 54, 35–53.
- [7] Bale, C.W., Chartrand, P., Decterov, S.A., Eriksson, G., Hack, K., Ben Mahfoud, R., Melançon, J., Pelton, A.D. and Petersen, S. FactSage Thermochemical Software and Databases. *Calphad*. 2002, 26, 189–228.
- [8] Dietzel, A. Glasstruktur und Glaseigenschaften. *Glastechnische Berichte*. 1948, 22, 41–50, 81–86, 212–224.

Authors

Philip Schantl, RHI Magnesita, Leoben, Austria.

Christian Majcenovic, RHI Magnesita, Leoben, Austria.

Corresponding author: Philip Schantl, Philip.Schantl@rhimagresita.com



Aloísio Simões Ribeiro, Bruno Filipe Guimarães, Lucas de Brito Nascimento, Victor Luiz Cruz Morais and Vitor Guarnier Domiciano

Trends and Advances in Blast Furnace Casthouse Technologies with a Focus on Refractory Lining Performance, Operational Safety and Decarbonisation

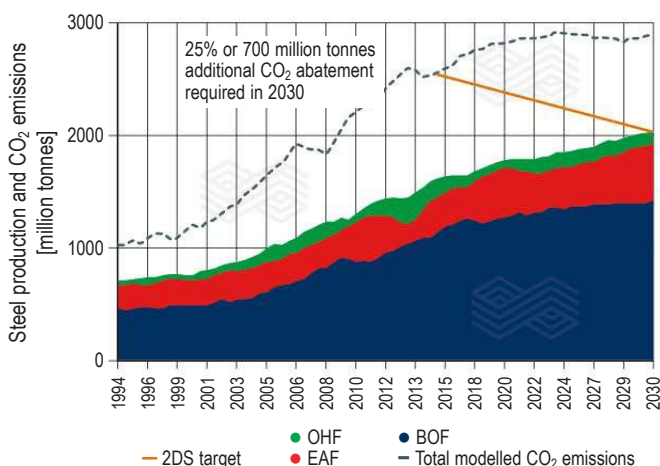
The blast furnace is the most used route for iron and steel production due to the numerous advantages it provides, such as low cost and high productivity. However, this process is very energy intensive, in addition to emitting large amounts of CO₂ and other pollutants into the atmosphere. In this context, the refractory industry plays an important role in the decarbonisation process through the implementation of safe, integrated, and innovative solutions that enable customers to reduce their CO₂ footprint without compromising operational performance. This paper aims to present the latest advances in refractory technologies for blast furnace runner maintenance practices in South America and to share some of the superior results achieved using digital integrated solutions, as well as their impact on the performance, safety, and process stability.

Introduction

In steelmaking, the blast furnace (BF) is the most widespread globally used route to produce hot metal as it offers several advantages, such as high productivity, continuous operation for long periods of time, and fuel consumption optimisation [1]. Nevertheless, with the intense growth of steel production, the level of associated CO₂ emissions has increased dramatically, imposing a series of challenges for this sector, including the transformation of its process conditions and the use of hydrogen as a fuel. Figure 1 presents the relationship between the increase in steel production and the emissions produced, with the blast furnace-basic oxygen furnace route leading the ranking. Consequently, a 25% reduction of CO₂ emissions is required based on current global projections relative to a 2-degree warming scenario (i.e., 2DS target), which corresponds to limiting temperature growth to avoid significant and potentially catastrophic changes due to global warming [2].

Figure 1.

Global CO₂ emissions in the steel industry and reductions required to achieve the 2DS target: Crude steel production (million tonnes) for basic oxygen furnaces (BOF), open hearth furnaces (OHF), and electric arc furnaces (EAF) plotted with the total modelled emissions (million tonnes CO₂) [2].



The refractory industry plays an important role in this decarbonisation process by reducing scope 1, 2, and 3 emissions, through incorporating recycled materials into products (i.e., circular economy), and by developing and implementing safe, integrated, and innovative solutions that enable customers to reduce their CO₂ footprint without compromising operational performance [3].

This article addresses the latest refractory technologies, maintenance practices, and project improvements recently implemented in South America's BF casthouse area that contribute to the current demands regarding energy efficiency, CO₂ emission reductions, and safety.

Materials and Methods

In order to address the most recent trends and advances in the BF casthouse, different refractory technologies were characterised in the laboratory (e.g., physical, mechanical, thermomechanical, and chemical properties) and further validated in the field. The first approach focused on comparing two castables, namely a conventional castable used for major BF runner maintenance (CARSIT) and a monolithic used to produce precast blocks (CARSITAL K31C-19-BR). The BF runner ultra-low cement castable (Al₂O₃-SiC-C) and the precast block monolithic were wet mixed in a planetary mixer for 5 minutes. Although both refractories have the same formulation, different water contents were used due to the differences in processing. Prismatic specimens of 160 x 40 x 40 mm were cast, air cured for 24 hours, then dried at 110 °C for 24 hours, 350 °C for 12 hours, and fired at 1400 °C for 5 hours prior to characterisation.

The properties and performance of a ramming mix (CARSIT RAM B14C-8-BR), currently used during minor repairs and emergency shutdowns, were also evaluated in comparison to a sol-bonded gunning mix (CARSIT SOL M10G-5-BR). For the latter mix, gunning panels were prepared during a field refractory installation and prismatic specimens

(160 x 40 x 40mm) were cut out, dried at 110 °C for 24 hours, and fired at 1400 °C for 5 hours before characterisation. The ramming mix samples were prepared in the laboratory and heat treated using the same conditions as the sol-bonded mix.

Comparison of Refractory Castable Installation and Precast Blocks

The main physical and mechanical property results for CARSIT and CARSITAL K31C-19-BR samples are presented in Table I. Firstly, it is important to note that even though both refractories have the same formulation, there is a difference in water content due to the type of installation and processing requirements. Water is a key ingredient in such processes and plays a major role by wetting the ceramic particle surfaces, generating strong capillarity forces between large and fine particles (i.e., wall effect), and acting as a crucial component of binding systems [4]. Nevertheless, the increase in porosity associated with the higher water content also promotes a reduction in the mechanical properties besides influencing corrosion resistance. In this context, better mechanical strength levels for the precast block grade were observed as a result of its lower porosity, higher density, and optimised water content.

Table I.

Main physical and mechanical properties of CARSIT (castable) and CARSITAL K31C-19-BR (precast block). Abbreviations include bulk density (BD), apparent porosity (AP), cold crushing strength (CCS), modulus of rupture (MoR), hot modulus of rupture (HMoR), permanent linear change (PLC), and ultra-low cement castable (ULCC).

Main properties		CARSIT	CARSITAL K31C-19-BR
Main raw materials		Brown fused alumina, silicon carbide, and carbon (ULCC)	Brown fused alumina, silicon carbide, and carbon precast shape
Water content [%]		5.50	4.50
110 °C	BD [g/cm ³]	2.85	2.86
	AP [%]	13.07	10.53
	CCS [MPa]	20.30	37.55
	MoR [MPa]	3.60	3.40
	PLC [%]	-0.16	-0.06
350 °C	BD [g/cm ³]	2.83	2.84
	AP [%]	15.01	13.23
	CCS [MPa]	25.70	40.91
	MoR [MPa]	3.10	3.20
1400 °C	BD [g/cm ³]	2.81	2.83
	AP [%]	16.33	14.20
	CCS [MPa]	40.24	60.21
	MoR [MPa]	3.20	5.40
	PLC [%]	-0.09	-0.04
HMoR (MPa) 1485 °C/3 hours		0.70	1.10

Although a significant amount of water reacts with the cement to form hydraulic bonding phases, a residual unreacted part facilitates proper installation of the refractory castable, generating porosity after firing [5] and a lower hot modulus of rupture.

During operation, the refractory applied in BF runners is subjected to extreme temperature conditions (1490–1530 °C) inherent to the steelmaking process. For example, when in contact with hot metal and slag at high temperatures, the lining is exposed to combined wear mechanisms such as corrosion and thermal shock [6]. In order to assess the materials' corrosion resistance, tests were performed using both an induction and rotary furnace. The results (Figure 2) revealed similar refractory wear for both materials in the induction furnace—a test used to evaluate the wear at the hot metal/slag interface. However, in the rotary test (widely used to evaluate the wear due to slag chemical attack and its erosive effect on the lining), a higher wear was obtained for the castable product. This result is in accordance with the higher apparent porosity observed (i.e., 16.33% at 1400 °C), which would increase the slag penetration rate, and the lower hot strength (0.70 MPa) that could be associated with decreased erosion resistance.

The thermal shock resistance of both refractories was also evaluated by measuring the elastic modulus (E) after successive cycles of thermal shock (i.e., 1400 °C for 30 minutes). The results showed a lower decrease of E for the monolithic block grade in comparison to the refractory castable (Figure 3), which confirms a superior thermal shock resistance of the CARSITAL K31C-19-BR.

Figure 2.

CARSIT (castable) and CARSITAL K31C-19-BR (precast block) wear after the induction furnace (IF) and rotary furnace (RF) tests.

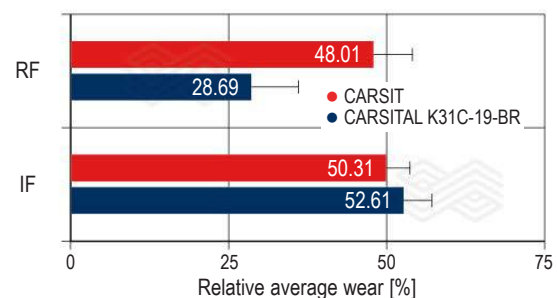
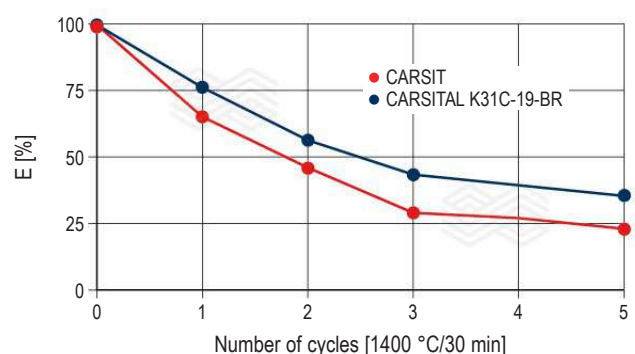


Figure 3.

Thermal shock resistance: The change in elastic modulus (E) was measured after successive cycles of thermal shock (i.e., 1400 °C for 30 minutes) for CARSIT (castable) and CARSITAL K31C-19-BR (precast block).



In addition to the beneficial material properties of CARSITAL K31C-19-BR, the refractory secondary runner maintenance schedule is significantly shorter when using precast blocks. This is illustrated by the following real case scenario for a South American customer where a typical runner wear lining installation with castables requires a 36-hour mould assembly stage before the application starts. This step is time consuming because the secondary runner borders are irregular, with no anchoring points to install the moulds. Another important stage when installing castables is the curing (10 hours), which needs to be completed before removing the moulds as the hydration process that takes place during this period is responsible for the castable's green mechanical strength development. In contrast, no mould assembly is required for precast blocks and only ~2 hours are needed to remove assembly parts after installation of the blocks. Moreover, as the refractory block has already been cured and dried (350 °C/12 hours) during its production, these processing steps are not necessary. Nevertheless, a heating up curve is required for both technologies as the refractory needs to reach a minimal temperature to minimise the thermal shock while ensuring suitable flowability of the slag and hot metal. Table II summarises the overall time requirement for each stage, comparing the installation of 8 blocks (~20 tonnes) with applying a castable in the secondary runners.

Regarding performance, independent of the refractory technology used, a typical secondary runner campaign can last up to 12 months with only minor (hot) repairs required during this time. However, when installing precast blocks in secondary runners, the amount of maintenance material used for repairs is ~20% lower when compared with that required for repairing castables. Therefore, due to its superior properties, the precast block technology can optimise the overall refractory maintenance time and increase the secondary runners' availability.

Comparison of Ramming and Sol-Bonded Gunning Mixes

The main physical and mechanical property results for the ramming (CARSIT RAM B14C-8-BR) and sol-bonded gunning (CARSIT SOL M10G-5-BR) mixes are presented in Table III.

Table II.

Typical stages and time requirement for refractory installation in the secondary runners using CARSIT (castable) and CARSITAL K31C-19-BR (precast block).

Stages	Time requirement using castables	Time requirement using precast blocks
Mould assembly	36 hours	
Refractory installation	2 hours	8 hours
Curing and mould removal	10 hours	2 hours
Heating up	24 hours	12 hours
Total	72 hours	22 hours

Both these materials were used in the same region of a secondary slag runner for hot repairs (between major campaigns) under similar conditions. In both situations, the total repair duration at a customer was about 7 days, but the installation time was optimised (almost 50% less time) using the gunning material. Moreover, this new repair method increased the safety standards due to the fact that an employee's presence was no longer required inside the slag runner. Figure 4 depicts the stages of a gunning application in a secondary runner as well as the thickness profile before and after the refractory hot installation.

The advantages of using a sol-bonded gunning mix have also been observed during emergency shutdowns or campaign extensions. For instance, when there is a requirement for a main runner drainage, gunning can increase the planned hot metal production by over 30000 tonnes without impacting the operation. Another benefit is that the sol-bonded technology, due to its optimised drying behaviour, can be installed in extreme temperature conditions.

Digital Solutions for the Casthouse: Benefits of Using a 3D Laser Scanner and Optical Pyrometer

Although BFs have been the most effective route to produce iron for over 200 years, several issues can affect their efficiency and stability, such as the runners' lining condition. Among the main digital solutions implemented, 3D laser scanning has proved to be one of the most effective methods to measure the lining thickness throughout the campaigns, providing a large amount of discrete data points in a very short time. To accomplish this, the scanning equipment is positioned next to the runner and a reference measurement of the original refractory lining is taken.

Table III.

Main physical and mechanical properties of CARSIT RAM B14C-8-BR (ramming) and CARSIT SOL M10G-5-BR (gunning) mixes. Abbreviations include bulk density (BD), apparent porosity (AP), cold crushing strength (CCS), modulus of rupture (MoR), and hot modulus of rupture (HMoR).

Main properties	CARSIT RAM B14C-8-BR	CARSIT SOL M10G-5-BR
Main raw materials	Bauxite, silicon carbide and carbon	Bauxite, silicon carbide and carbon
110 °C	BD [g/cm ³]	2.82
	AP [%]	17.97
	CCS [MPa]	10.16
	MoR [MPa]	1.30
1400 °C	BD [g/cm ³]	2.79
	AP [%]	19.01
	CCS [MPa]	32.00
	MoR [MPa]	3.50
HMoR (MPa) 1485 °C/3 hours	0.48	0.70

Once the runner reaches at least half of the planned production, a new inspection is performed to assess the remaining refractory lining thickness and establish a new production target. Additionally, in steel plants where the slag line determines the campaign, there is no need for full runner drainage.

Figure 4.

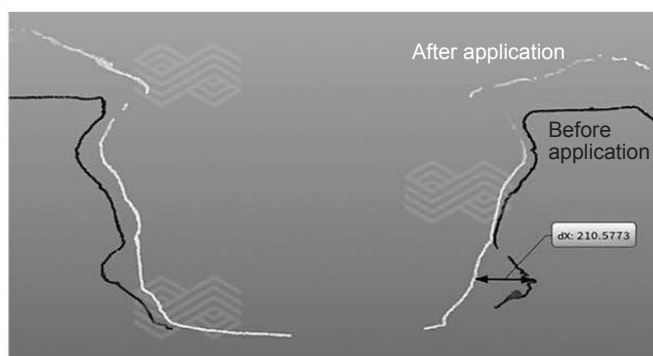
Secondary runner (a) before repair, (b) after the sol-bonded gunning mix application, and (c) the thickness profile (black and white lines) for each stage.



(a)



(b)



(c)

The result is a mobile-friendly report automatically generated in about 20 minutes, enabling the operator to have all the data on only one platform called Steel Lining Evaluation Scan (LES), which leads to fast decision making [7]. Figure 5 shows an example of measurements taken for the residual refractory lining in the slag line between tapping.

In a real case scenario, the scanner was successfully used to safely extend a main runner's campaign following hot inspection of the slag line. Through the implementation of this new technology in a BF with two tapholes and a daily hot metal production of 4200 tonnes, it was possible to increase the campaign by 5 days without draining the runner although the refractory thickness had decreased from 150 mm to 80 mm, taking into consideration the reliability of the data acquired. Furthermore, in a situation where the equipment had an average hot metal production of 90000 tonnes, the 3D laser solution enabled refractory maintenance to be postponed until the hot metal production had reached 108732 tonnes (an increase of 20% in comparison to the original planned campaign). Moreover, the refractory specific consumption (kg of refractory/tonne of hot metal) decreased by 10%, leading to increased annual productivity due to better maintenance practices [7].

It is also important to highlight that by decreasing the number of inspection drainages, a reduction in the CO₂ emissions during hot metal production is expected. As a reference, for each tonne of hot metal produced, 2 tonnes of CO₂ are released [8]. This means that considering a coke BF with four main runners (operating in pairs) and a campaign of 28 days, eliminating drainage for inspection would represent up to a 3120-tonne CO₂ reduction of the annual emissions (26 drainages of a main runner with a hot metal capacity of 60 tonnes were considered for the calculation).

Another digital solution implemented in South American BFs is improved thermal control through integrating continuous hot metal temperature measurements. By replacing the conventional thermocouple procedure (i.e., manual measurements are taken by immersing the thermocouple in the molten bath) with the novel optical pyrometer methodology, it was possible to continuously measure the temperature, improve data reliability, eliminate manual measurements that are a high safety hazard, and to have better control of the BF operation by anticipating necessary actions for process stability [7].

Figure 5.

Full runner inspection results (front view) generated by 3D laser scanning [7].



Figure 6 shows a pyrometer being used in the BF casthouse during high-temperature hot metal tapping.

By implementing these digital technologies, it is possible to increase productivity and achieve higher operational stability of casthouse processes. Furthermore, the online hot metal monitoring process associated with the precise control of runner refractory wear are part of the key initiatives that will make the construction of reliable prediction models possible and ultimately the creation of a fully integrated systemic analysis of BF runner campaigns.

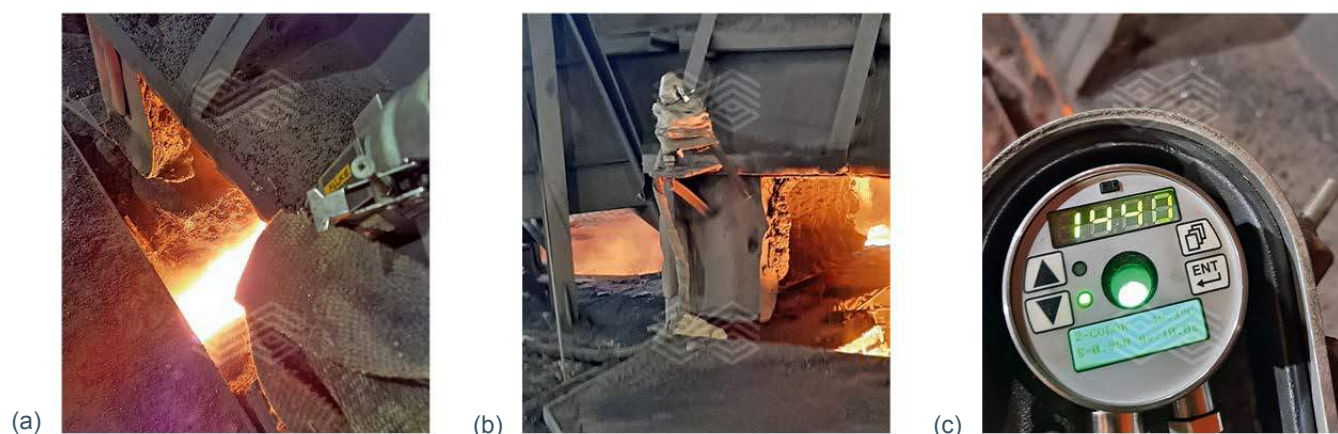
Results/Conclusion

The latest trends and advances in BF casthouse technologies have been outlined in this article with a focus on refractory lining performance, operational safety, and environmental considerations.

Replacing in-situ installed castables with preshaped blocks and ramming mixes with sol-bonded gunning mixes, in combination with the use of digital solutions (3D scanning and an optical pyrometer) in a runner's lining design results in increased performance, higher production, longer campaign life, and superior safety standards. Additionally, a decrease in the specific refractory consumption (10%) has been observed as well as an optimised number of inspection drainages, which result in lower CO₂ emission levels during hot metal production. Taking these aspects into consideration, through the use of integrated solutions safer casthouse operations with higher levels of productivity and stability can be expected.

Figure 6.

Pyrometer measurements in the BF casthouse: (a) monitoring the temperature during tapping, (b) positioning for continuous temperature measurement, and (c) recorded temperature.



References

- [1] Mourao, M.B., Yokoji, A., Malynowskyj, A., Leandro, C.A., Takano, C., Quites, E.E., Gentile, E.F., Silva, G., Bolota, J.R., Goncalves, M. and Faco, R.J. Introdução à siderurgia. ABM, São Paulo, 2007.
- [2] The Immense Decarbonisation Challenge Facing the Steel Industry. CRU International Limited. <https://www.crugroup.com/knowledge-and-insights/insights/2020/the-immense-decarbonisation-challenge-facing-the-steel-industry/>
- [3] Schnalzer, M., Janssen, T., Lückhoff, J., Ospino, E.E. and Spreij, M. Decarbonisation of the Steel Industry. 4. Freiburger Feuerfest-Symposium 2022, Freiberg, Germany, April 25–27, 2022.
- [4] Ramal, F.T., Salomão, R. and Pandolfelli, V.C. Water Content and its Effect on the Drying Behavior of Refractory Castables. *Ref. Appl. News*. 2005, 10, 10–13.
- [5] Lee, W.E., Vieira, W., Zhang, S., Ahari, K.G., Sarpoolaky, H. and Parr, C. Castable Refractory Concretes. *Int. Mater. Rev.* 2001, 46, 145–167. <http://dx.doi.org/10.1179/095066001101528439>.
- [6] Domiciano, V.G., Ollmann, A.R., Clemente, E.I., Duarte, A.K. and Brito, M.A. Desafios da Ala de Corrida de Altos-Fornos: Análise de Falha de Concreto Refratário para Canal de Corrida. In: 43º Seminário de Redução de Minério de Ferro e Matérias-Primas e o 14º Simpósio Brasileiro de Minério de Ferro. São Paulo, Brazil, 2013, 43, 784–793.
- [7] Macedo, J.F., Ribeiro, A.S., Nonaka, F., Guimarães, B.F., Morais, V.L. and Ávila, H.C. How 3D Laser Scan is Adding Value and Performance to Refractory Lining Inside Steel Industry. AISTech Technology Conference. Pittsburgh, USA, 2022.
- [8] Wang, P., Ryberg, M., Yang, Y., Feng, K., Kara, S., Hauschild, M. and Chen, W.Q. Efficiency Stagnation in Global Steel Production Urges Joint Supply- and Demand-Side Mitigation Efforts. *Nature Communications*. 2021, 12, 2066. <https://doi.org/10.1038/s41467-021-22245-6>

Authors

Aloísio Simões Ribeiro, RHI Magnesita, Belo Horizonte, Brazil.

Bruno Filipe Guimarães, RHI Magnesita, Belo Horizonte, Brazil.

Lucas de Brito Nascimento, RHI Magnesita, Leoben, Austria.

Victor Luiz Cruz Morais, RHI Magnesita, Belo Horizonte, Brazil.

Vitor Guarnier Domiciano, RHI Magnesita, Belo Horizonte, Brazil.

Corresponding author: Aloísio Simões Ribeiro, Aloisio.Ribeiro@rhimagnesita.com



bulletin

2023

Copyright notice:

The texts, photographs and graphic design contained in this publication are protected by copyright. Unless indicated otherwise, the related rights of use, especially the rights of reproduction, dissemination, provision and editing, are held exclusively by RHI Magnesita N.V. Usage of this publication shall only be permitted for personal information purposes. Any type of use going beyond that, especially reproduction, editing, other usage or commercial use is subject to explicit prior written approval by RHI Magnesita N.V.

